A Comprehensive Review of Continuum Constitutive Models for Thermoplastic Polymers

José L. P. Vila-Chã[a], A. Francisca Carvalho Alves[b], Mohsen Mirkhalaf[c,*], F.M. Andrade Pires[a]

[a] *DEMec - Department of Mechanical Engineering, Faculty of Engineering, University of Porto, Rua Dr. Roberto Frias, 4200-465 Porto, Portugal*
[b] *INEGI - Institute of Science and Innovation in Mechanical and Industrial Engineering, University of Porto, Rua Dr. Roberto Frias, 4200-465 Porto, Portugal*
[c] *Department of Physics, University of Gothenburg, Origovägen 6B, 41296 Gothenburg, Sweden*

Abstract

Thermoplastic polymers exhibit complex mechanical behavior characterized by nonlinear visco-elasticity, visco-plasticity, strain-rate sensitivity, temperature dependence, and distinct deformation mechanisms such as shear yielding, crazing, and internal particle cavitation. Understanding and accurately modeling their response is crucial for various engineering applications. Within this setting, this contribution provides a comprehensive review of continuum constitutive modeling approaches for thermoplastic polymers. To contextualize these models, an overview of continuum, micro-mechanical, and multi-scale modeling frameworks is provided. Emphasis is placed on continuum models, highlighting in particular their interpretation based on rheological elements originating from linear viscoelasticity, and adaptability through the selection of appropriate nonlinear functions for the different elements. The increasing complexity of these models often results in a high number of material parameters, necessitating extensive experimental characterization. To address this challenge, recent advancements in optimization techniques for parameter identification are briefly discussed, with a focus on Bayesian optimization strategies that enhance efficiency while reducing experimental costs.

Keywords: Thermoplastic polymers, Constitutive modeling, Continuum mechanics, Material behavior, BPA model, EGP model

*Email: mohsen.mirkhalaf@physics.gu.se

Contents

1. Introduction

In recent years, the global polymer market has experienced significant growth, reaching a value of 713 billion dollars in 2021 and projected to grow to 1078.5 billion by 2030 [1]. By type, the thermoplastics segment accounted for 43% market share in 2021, which generally includes both glassy amorphous and semicrystalline polymers. Thermoplastic polymers have gained significant traction due to their outstanding mechanical, thermal, optical, and chemical properties. Moreover, they can be easily tailored through suitable manufacturing processes at low production costs, making them highly attractive for material and structural design in a wide range of applications, comprising the military, automotive, aerospace, and consumer electronics industries [2]. Examples of thermoplastic amorphous polymers include polycarbonate (PC), poly(methyl methacrylate) (PMMA), polystyrene (PS), and polyamideimide (PAI), among others. In particular, PC and PMMA are widely used in high-performance military applications, such as protective glasses and machine guards, where their transparency, strength, and lightweight features meet advanced engineering requirements. Thermoplastic semicrystalline polymers, such as polyethylene (PE), polytetrafluoroethylene (PTFE), polyamide (PA), and polyether ether ketone (PEEK), are also extensively employed in various industries due to their excellent mechanical properties, chemical resistance, and thermal stability [3].

Thermoplastic polymers are also central to the development of new materials, particularly in the form of polymer blends, with more than 600 new grades entering the market annually [4]. A notable example of this blending technique is rubber-toughened amorphous polymers, where rubber particles are added to an amorphous polymer matrix to improve toughness, such as in high-impact polystyrene (HIPS) and acrylonitrile-butadiene-styrene (ABS). Furthermore, polymers are widely used in fiber reinforced composites, such as car-

bon fiber reinforced thermoplastics (CFRTP), which offer high specific strength, corrosion resistance, fatigue resistance, dimensional stability, and high design flexibility [5].

Polymers exhibit versatile mechanical behavior, which is a result of their complex microstructures and intrinsic deformation mechanisms, such as shear yielding and crazing. Their behavior is also influenced by extrinsic factors, including temperature, strain rate, hydrostatic pressure, and the chemical environment (e.g., exposure to water, oxygen, or organic solvents). Accurate modeling, while not straightforward, is essential for understanding the structure-property relationship, where the microstructure of the polymer dictates its macroscopic properties and performance. This approach aligns with the principles of Integrated Computational Materials Engineering (ICME), as highlighted by Olson [6], which links processing, structure, properties, and performance across multiple scales.

To address the complexities of accurately modeling the mechanical behavior of thermoplastic polymers, different modeling approaches have been developed, including continuum, micro-mechanical, and multi-scale frameworks. Continuum models offer a macroscopic perspective by employing constitutive equations that capture the overall stress-strain response of polymers under various loading and environmental conditions. While these models are computationally efficient and widely applicable, they often require extensive calibration to account for the material's dependence on factors such as strain rate, temperature, and pressure [7, 8]. Micro-mechanical models, on the other hand, delve into the material's internal structure, explicitly representing the interactions between phases or constituents, such as rubber inclusions in blends like ABS or PC/ABS or the crystalline and amorphous phases in semicrystalline polymers. These models provide insights into the local mechanisms driving macroscopic behavior but can be computationally expensive [9, 10]. Multiscale modeling bridges the gap between these approaches by linking microstructural details to continuum-level predictions, enabling a more comprehensive understanding of how structure influences the material's macroscopic properties [11].

Despite the vast number of constitutive models available in the literature, most of these models face significant challenges. Within this setting, some models (i) fail to account for the full range of phenomena that are characteristic of polymer behavior, (ii) involve a large number of material parameters whose identification is not straightforward, (iii) pose

difficulties in numerical implementation, and (iv) may have limitations in their range of applicability. These constraints highlight the need for a comprehensive understanding of the various modeling techniques and their respective trade-offs.

In this context, this work aims to provide a thorough overview of the different modeling approaches and tools available to predict the mechanical behavior of amorphous polymers. To this end, in Section 2, a brief discussion is presented regarding various categories of thermoplastic polymers and their morphologies, while Section 3 outlines the main deformation mechanisms that govern their mechanical response. Section 4 collects some of the most relevant experimental observations regarding the thermomechanical behavior of thermoplastic polymers, providing the motivation for the development of the wide range of constitutive models available in the literature. Section 5 provides a brief outline of continuum, micro-mechanical, and multi-scale modeling as the main approaches available to model the mechanical behavior of polymers. Special attention is given to the continuum modeling approach, with Section 6 collecting the main nonlinear rheological elements used in the literature to model the different nonlinear phenomena observed in thermoplastic polymers. Section 7 presents a review of the main continuum constitutive models for thermoplastic polymers, employing as the organizing principle the arrangement of the rheological elements in its one-dimensional visco-elastic representation. The main focus is on the adaptability and extensibility of these models, such as the BPA and EGP models. Finally, Section 8 summarizes the main findings of this review and outlines potential future research directions in the field of constitutive modeling for amorphous polymers.

2. Categories of Solid Polymers

Polymers are macromolecules composed of repeating units linked together to form long chains, primarily made up of carbon and hydrogen atoms. These so-called monomers are held together by strong covalent bonds within the polymer chain, while weaker intermolecular forces, such as van der Waals interactions or hydrogen bonds, act between chains. Each polymer chain may string together from a few hundred to several thousand monomer units. The distribution of molecular weights is generally characterized by parameters such as the number-average molecular weight, the weight-average molecular weight, the polydis-

persity index, and the degree of polymerization. Yet another aspect of polymer structure at the individual chain level is the distinct stereoisomerisms, such as tacticity, which play an important role in determining the properties of polymers, such as their ability to crystallize.

Of special importance to the spatial configuration of polymer chains is their molecular structure. The structure or topology of the polymer concerns the way the different monomers are connected, which is commonly categorized as linear, branched, crosslinked, or network structures, as illustrated in Fig. 1. The molecular structure significantly influences the flexibility of polymer chains and their ability to respond to thermal vibrations. Linear polymers have more chain mobility due to the absence of rigid crosslinks, making them more flexible and responsive to temperature changes. In contrast, crosslinked and network polymers contain bonds between chains that restrict movement, resulting in higher rigidity and reduced thermal response. This diversity in molecular structures allows polymers to exhibit a wide range of mechanical and thermal properties. Of particular interest, is the distinction between thermoplastic and thermosetting polymers, tightly linked to their molecular structure. Typically linear or branched in structure, thermoplastic polymers soften or melt when heated and solidify when cooled in a reversible and repeatable manner. In contrast, thermosetting polymers do not melt or soften upon heating. Instead, they become permanently rigid after undergoing a curing process that forms extensive crosslinks or networks of covalent bonds between molecular chains. This distinction is further elaborated in Section 4 concerning experimental results of polymer behavior to thermomechanical loading.

If the chains are regular enough, and thermomechanical conditions are favorable, they may arrange themselves into highly ordered structures, forming crystalline regions. Otherwise, the chains will assume a more disordered arrangement, forming amorphous regions. The differences in the morphology of semicrystalline and amorphous polymers are schematically illustrated in Fig. 2. This state of affairs leads to possibly the most relevant classification of solid polymers, i.e., between those that are completely amorphous and those that are semicrystalline.

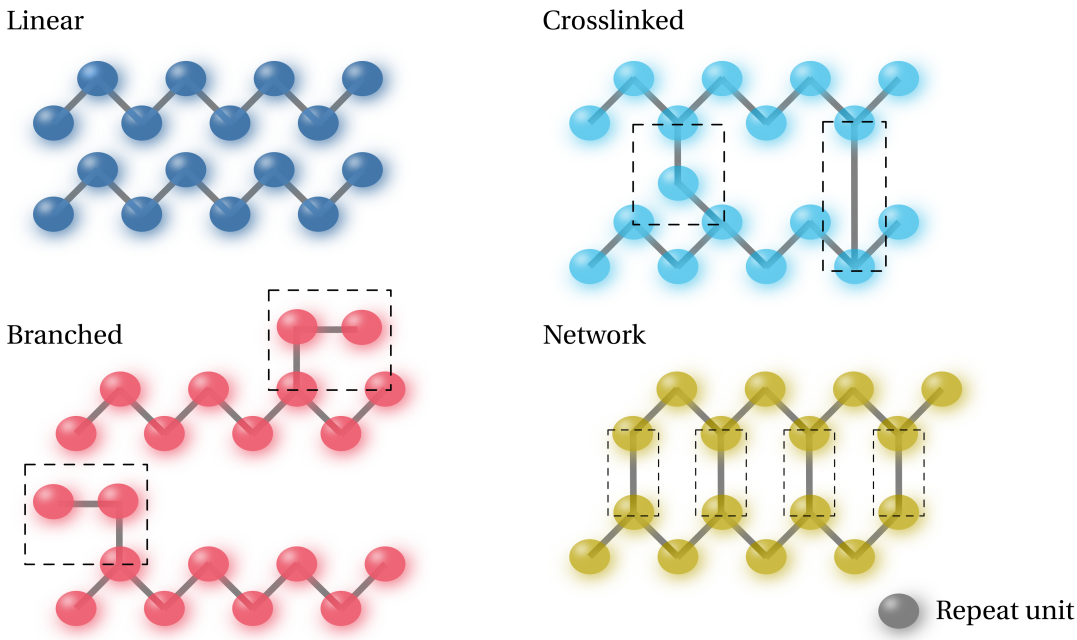

Figure 1: Schematic representation of different types of polymer molecular structures.

2.1. Amorphous polymers

Focusing first on amorphous polymers, these consist solely of disordered arrangements of polymer chains, where often the end-to-end distance of the chains is much smaller than their contour length. This spatial arrangement, where entanglements between chains abound, constrains the global motion of the chains, allowing primarily for local movements of chain segments. That said, features such as a comparatively high density relative to a hypothetically fully disordered state show that the packing cannot be completely random. In particular, under mechanical loading, amorphous polymers may develop some degree of orientation of the polymer chains in the loading direction [12].

2.2. Semicrystalline polymers

If in some domains of the polymer, the molecular orientation is sufficiently regular, crystalline regions may form. These regions are characterized by the constituent chains packing parallel to one another in an orderly fashion into lamellae. This picture is, in fact, an idealization, with reality resembling more a switchboard model, with the chains reentering through loose folds at non-adjacent sites or even forming tie-chains with neighboring lamellae [13]. The thickness of the lamellae in semicrystalline polymers is of the order of

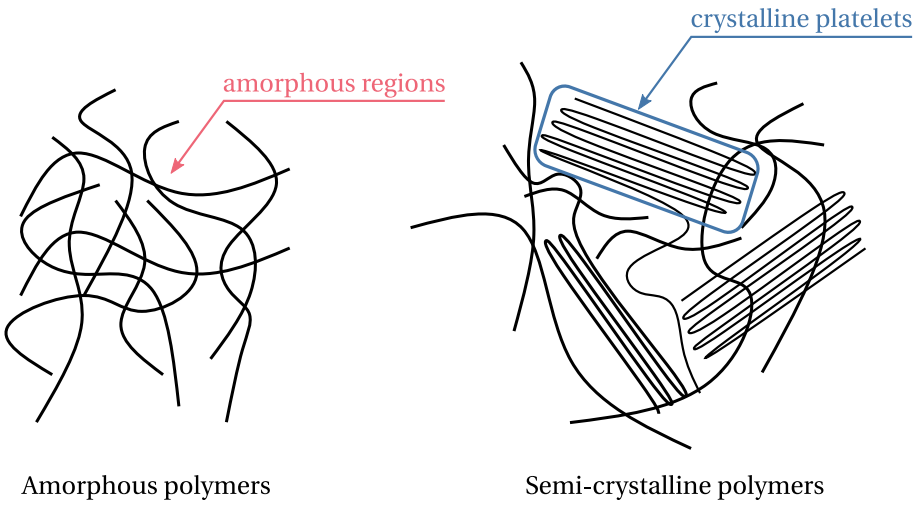

Figure 2: Representation of amorphous and semicrystalline polymers' structure.

nanometers, e.g., 10 nm to 15 nm for PE samples [14]. The crystalline structure depends on the particular polymer. PE often possesses orthorhombic symmetry [15], while polytetrafluoroethylene (PTFE) at temperatures above 19 °C is hexagonal, with individual molecules arranged in helical conformations [16].

The main parameters influencing the degree of crystallinity are the molecular structure of the polymer, its molecular weight, the presence of plasticizers, and especially the thermomechanical history of the polymer [17, 18]. Because of the way polymer crystals form, polymer chains must have a linear structure; the more branches/dependent side groups, the lower the degree of crystallinity. However, even linear polymers must have sufficient regularity to crystallize [17]. Polyethylenes of different crystallinities have been achieved through the manipulation of the degree of branching and the introduction of various amounts of defects in the main chains of the polymer [19]. In addition, a high molecular weight tends to suppress a high degree of crystallinity [20], as seen when comparing high-density polyethylene (HDPE) and ultra-high molecular weight polyethylene (UHWPE) [21]. The particular stereoisomer under consideration also plays a role, with isotactic polymers tending to crystallize more easily than atactic ones, as is the case with polypropylene (PP) [3].

Since crystallization is a kinetic process, the crystallized fraction is a function of time, with the crystallization rate in polymers depending on the temperature difference relative to the melting temperature and the glass transition temperature [3]. The mechanical load-

ing of a polymer may also induce changes in crystallinity, e.g., through the phenomenon of strain-induced crystallization [22]. Accordingly, the most frequent approach to achieve different degrees of crystallinity is through the control of crystallization temperatures and crystallization times, be it when crystallizing from the melt or through annealing treatments [19, 23, 24]. However, preparing samples with different degrees of crystallinity is challenging for polymers such as HDPE, whose crystallization rate is very high [19].

The crystallinity of a semicrystalline polymer can be specified by the degree of crystallinity. It may range from completely amorphous to almost entirely crystalline. Commercially available semicrystalline polymers range from 10 to 90% degree of crystallinity [25]. The degree of crystallinity by weight may be determined from accurate density measurements according to

$$\chi = \%\ \text{crystallinity} = \frac{(\rho_s - \rho_a)/\rho_s}{(\rho_c - \rho_a)/\rho_c} \times 100 \tag{1}$$

where ρ_s is the density of a specimen for which the percent crystallinity is to be determined, ρ_a is the density of the completely amorphous polymer, and ρ_c is the density of the perfect polymer crystallite. In addition to this method based on density, other experimental techniques employed to determine the crystallinity along with the lamellar thickness of the polymer crystallites include wide (WAXS) and small (SAXS) angle X-ray scattering [23, 26], differential scanning calorimetry (DSC) [27], and, electron microscopy, e.g., transmission electron microscopy (TEM) [28].

Mesostructure. According to the processing, thermal, and mechanical history, as well as its degree of crystallinity, molecular weight, and polydispersity, a semicrystalline polymer can display different mesoscopic structures [18, 29]. When the polymer crystallizes from the melt, the two most commonly reported types of mesoscopic structures for semicrystalline polymers are the spherulitic structure [30], obtained from quiescent crystallization, and the shish-kebab structure, obtained from crystallization under shear stress [31].

The spherulitic structure is composed of spherulites, an aggregate of ribbon-like chain-folded crystallites that radiate outward from a single nucleation site in the center, with their diameter in the order of 10 µm for PE, and 6 µm for polyamide 6 (PA6), for example. Between them, there are amorphous regions, crossed by tie-chain molecules that act as

connecting links between adjacent lamellae [32, 3, 17, 33, 13]. The lamellae are generally twisted about their long axis [34]. A sheaf-like structure is also possible under suitable conditions [31], as are so-called hedrites, lamellae joined together along a common line or, more often, along a common plane [35]. Mandelkern [29] warns, however, that spherulites, and other types of supermolecular structures, are not universally observed in homopolymers.

Mechanical loading will also lead to changes in the mesoscopic structure of the polymer. Regarding higher crystallinity polymers such as HDPE, it usually destroys the crystallites of the original morphology, followed by reordering to form new crystallites. For materials such as PET, in which the crystalline and amorphous components are intermixed, the most noticeable effect may be strain-induced crystallization due to macromolecular texture [12].

All these properties and characteristics significantly influence the thermomechanical behavior of solid polymers, which we describe in the following section.

3. Deformation Mechanisms

Understanding and accurately modeling the behavior of thermoplastic polymers, including their role in blends and composites, requires careful consideration of the deformation mechanisms involved. Phenomena such as shear yielding, crazing, and internal particle cavitation significantly influence the material's response and should be accounted for to ensure predictive reliability in engineering applications. In this setting, a brief overview of the main deformation mechanisms of thermoplastic polymers is provided below.

3.1. Shear yielding

In metals, the shear deformation is well established by the slip theory [36]. For polymers, however, there is some uncertainty about molecular-level shear deformation. Nevertheless, two different theories are typically considered. The first of these theories is the metals' slip theory, and the second one is a theory based on viscous mechanisms.

Haward and Young [2] stated that the applied stress converts the molecular structure from one metastable state to another, which persists after the stress is removed. This requires that the interatomic or intermolecular bonds be overcome and replaced by other equivalent bonds in the deformed state. The transition from one state to another occurs

via molecular chain slip. As a consequence, for temperatures below the glass transition temperature, T_g, shear becomes localized, resulting in accentuated shear bands. In contrast, as the glass transition temperature is approached, the shear bands become smoother and may even become unobservable.

The formation of shear yielding is often associated with strain-softening behavior, although there are cases where strain hardening or no significant softening occurs. This behavior is commonly modeled by Eyring's viscosity theory [37], but other models may also be used depending on the specific material and conditions.

In the case of semicrystalline polymers, the amorphous domain is further restrained in its movement by the presence of the crystalline regions. In the crystalline regions, the molecular chains are tightly packed in an ordered structure, and their motion can be explained by the slip theory, with the caveat that normal to the chain direction, the slip is highly restricted [38, 39].

3.2. Crazing

Crazes are localized regions of plastic deformation in polymers, characterized by the formation of microvoids and fibrils under tensile stress. They have been observed in most amorphous thermoplastics and some semicrystalline polymers, such as polypropylene [40]. Crazes typically originate from flaws in the material—like microcracks—that may not be initially visible but develop under loading. Their structure consists of a dense array of fibrils separated by voids, as schematically illustrated in Fig. 3. These fibrils, formed from aligned molecular chains, contribute to increased tensile modulus and mechanical strength, promoting strain hardening. The regions just ahead of craze tips, known as pre-crazes [41], are zones of high stress concentration.

The morphology of crazes is usually observed using optical techniques, such as transmission electron microscopy (TEM), scanning electron microscopy (SEM), and high voltage electron microscopy (HVEM) [41]. While crazes share some similarities with cracks, they are distinct due to their distinct formation processes and behaviors. Crazes are often described as microcracks, but unlike cracks, they typically form under lower stress and have a high load-bearing capacity due to the fibrillar structure that develops during their forma-

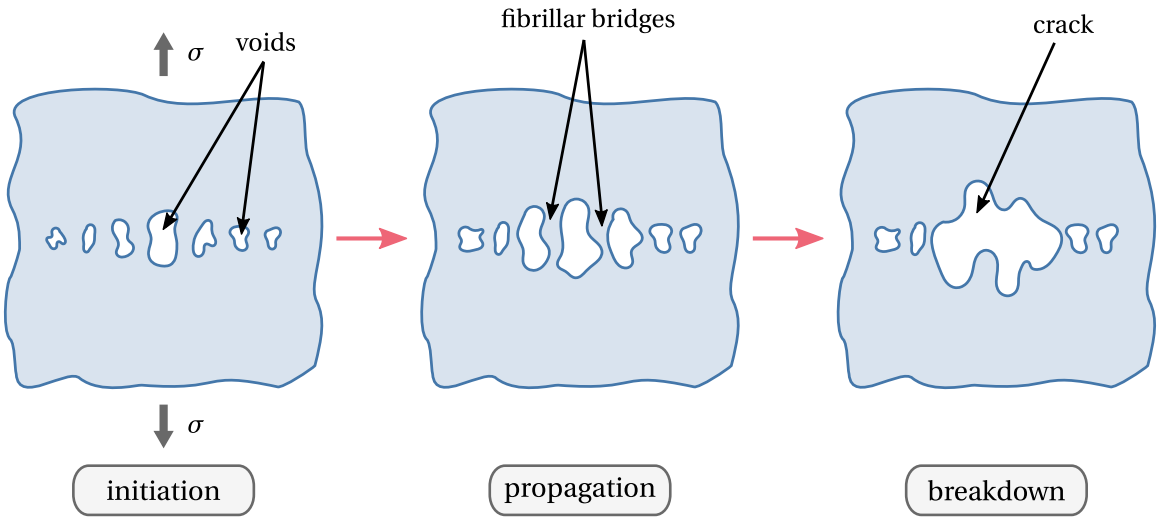

Figure 3: Schematic representation of the crazing deformation mechanism.

tion. This fibrillar structure enables crazes to absorb significant stress before propagating, making them fundamentally different from cracks, which generally fail suddenly with little deformation [37].

Understanding each phase of the crazing process (initiation, propagation, and breakdown) is essential to predict the behavior of amorphous polymers and, consequently, their failure. The initiation phase is still not fully understood, despite efforts to model it [37, 40]. The lack of a criterion accepted by the scientific community is due to the lack of reliable data on the crazing phenomenon across a wide range of triaxial tensile stresses. Nevertheless, it is accepted that, for craze initiation to occur, there must be a local high-stress state, followed by the nucleation of voids and the strain hardening of the polymer ligaments as the molecular chains align with the maximum loading direction. Moreover, it is accepted that the crazing envelope is asymptotic to the pure shear line, as schematically represented in Fig. 4. Moreover, the crazing envelope lies below the shear yielding envelope in the tensile quadrant and over the two neighbouring quadrants. As a result, fracture occurs without yielding for these stress states [40].

Craze propagation may occur by growing in width or length. The width growth is explained by drawing in more polymeric material from the craze surfaces to the fibrils. In contrast, the length growth is related to the propagation of the craze tip, which moves

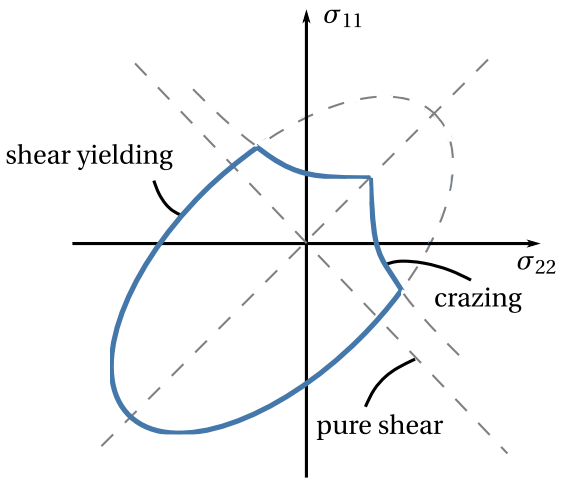

Figure 4: Failure envelope for poly(methyl methacrylate) (PMMA) under biaxial stress at room-temperature, adapted from [40].

outwards normal to the maximum tensile direction. The formation of a new plastic deformation zone at the pre-craze region also characterizes the growth in length. The most common approach to describing the crack-tip advance is based on the Dugdale model [42]. Dugdale's assumption of constant stress along the entire craze length is not verified at the craze tip, but overall it is a reasonable assumption [2]. In addition, it is now accepted that the craze-tip advance is modeled by the Taylor meniscus instability mechanism [43]. Experimental observations at the tip of the crazes revealed that no isolated voids are nucleated in the pre-craze region. Instead, a series of finger-like interfaces are observed [44].

The crazing fracture mechanism is more typical in amorphous brittle polymers and polymers with low entanglement density, as the formation of the void-fibril structure requires a loss of entanglement. This loss can occur either by chain scission (i.e., chain breaking) or disentanglement (i.e., relative motion between chains) [37]. Scission is generally assumed to be the dominant mechanism in crazing. Crazing failure occurs through crack initiation and propagation within the crazes, leading to brittle fracture with minimal energy absorption [41]. In some cases, the fibrils inside the crazes undergo plastic deformation and break due to local stress concentrations, typically around 200 MPa [40]. Failure often originates at the edge of the crazes, where new material is still being drawn. One of the major limitations of polymers in engineering applications is their tendency to fracture by crazing due

to absorbed liquids and vapours. When in contact with an aggressive liquid, the polymer's surface is very susceptible to crazing, and once crazing has initiated, the liquid is pushed into the voids and proceeds to the craze-tip, promoting craze growth [40].

Many polymers, such as polystyrene-acrylonitrile, present both shear and crazing deformation modes simultaneously [45]. The intersection between crazes and shear bands may even be favorable and may stop a craze from growing; that is, a craze may be stopped if it meets a pre-existing craze or a shear band. The competition between crazing and shear yielding is present in most amorphous polymers and, therefore, should be considered when modeling their behavior.

3.3. Internal particle cavitation

A common strategy to improve the toughness of amorphous polymers is to incorporate rubber particles into the bulk material. The presence of rubber particles facilitates the transition from brittle to ductile fracture by promoting extensive plastic deformation, allowing the material to dissipate large amounts of energy through mechanisms such as crazing or shear yielding. The primary role of these particles is to cavitate (as schematically represented in Fig. 5), either internally or through debonding, which alters the local stress state and initiates the plastic response of the polymer matrix. In general, if the craze initiation stress of the matrix is lower than the yield stress, then the predominant fracture mechanism is by crazing, and rubber toughening is mainly achieved by the dispersed rubber particles acting as craze initiators. In contrast, if the craze initiation stress is higher than the yield stress, failure occurs by shear yielding, and the dispersed rubber particles act as initiators of shear bands.

The rubber particles act as craze initiators, since they are responsible for concentrating stress, and hence, initiate crazing, typically near their equator [37]. As a result, the number of crazes in the polymer is strongly dependent on the number of rubber particles in the amorphous matrix. This phenomenon is called *multiple crazing*. Further, rubber particles may act not only as craze initiators, but also as craze controllers. The craze growth is blunted when a rubber particle is encountered, therefore, preventing the growth of large crazes, which are more likely to break. The multiple crazing phenomenon also promotes toughness, as

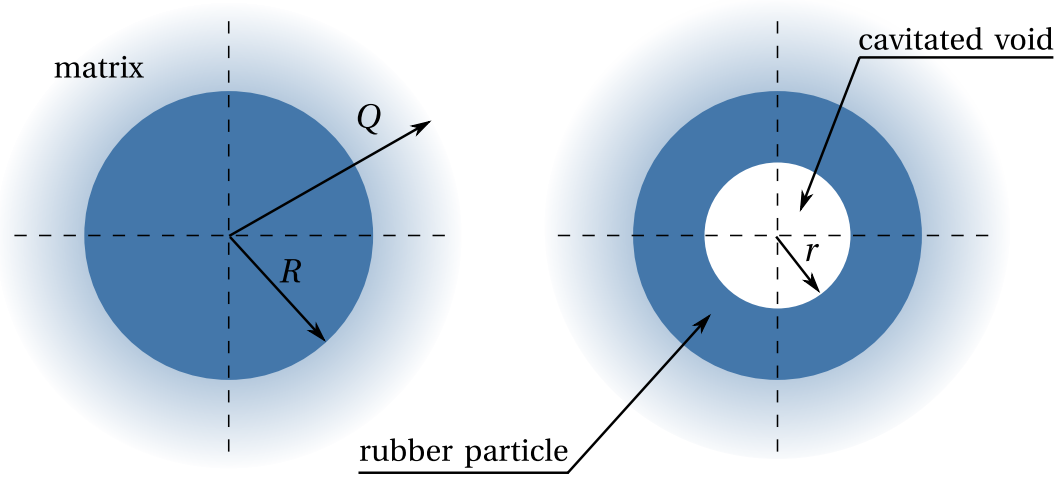

Figure 5: Schematic representation of the rubber particle internal cavitation phenomenon in rubber-toughened amorphous polymers.

crazes remain load-bearing until a certain deformation is reached. Furthermore, debonding at the particle-craze interface may appear as a result of the contraction between the crazes and the solid rubber particles when they intersect. This debonding promotes the formation of voids, which may yield premature craze breakdown.

The mechanism of shear yielding in rubber-toughened amorphous polymers is intrinsically related to cavitation of the rubber particles (see Fig. 5), followed by extensive shear yielding throughout the matrix (which in the end is the primary energy absorbing mechanism). The rubber particles dissipate the bulk strain energy through cavitation, reducing local hydrostatic stress and lowering the material's yield stress.

4. Thermomechanical Properties of Polymers

This section collects and discusses experimental results available in the characterization of solid polymers. It includes several relevant thermomechanical loading conditions and aims to highlight the typical nonlinear constitutive behavior of these materials, which advanced constitutive models should capture. For a refresher on the thermomechanical problem, thermodynamically consistent modeling and linear thermo-viscoelasticity, the reader is referred to Appendix A.

4.1. Isothermic stress relaxation, creep and dynamic mechanical analysis experiments

Stress-relaxation, creep, and dynamic mechanical analysis experiments are all pertinent for characterizing a material's time-dependent behavior. In particular, solid polymers exhibit time-dependent behavior that distinguishes them from metals at temperatures well below their melting points. This section will first focus on isothermal measurements, followed in the next section by isochronal measurements. It highlights the nonlinearities observed in these experiments, which infinitesimal linear viscoelasticity fails to model.

Ferry [46] collects some experimental results illustrating the nonlinear behavior of semicrystalline polymers. In a stress-relaxation experiment, linear behavior implies coincident curves in a plot of the relaxation modulus divided by the strain at different strain levels. However, for tensile stress relaxation of PE single crystal mats, the ratio of stress to strain decreases more rapidly with time at higher extensions, in the range of $\epsilon = 3 \times 10^{-4}$ to 3×10^{-3}; the degree of nonlinearity increases markedly with decreasing temperature in the range of 40 °C to 10 °C. Nonlinear creep recovery of polyethylene has also been reported. It is shown that, after partial stress relaxation at constant strain for various times and strain magnitudes, recovery is much slower at large strains but somewhat faster for shorter initial strain durations. In this context, strains less than 10^{-4} appear to be required for a linear behavior. Nonlinear behavior under large-amplitude harmonic loadings has also been investigated. Finally, Ben Hadj Hamouda and coworkers [47] report the existence of two regimes of creep deformation for medium-density ethylene-butene copolymers (MDPE). The recovery may also display nonlinear features: the recovered strain ε_r depends on the initial strain ε_0 and on how long the sample is strained, t_0, yielding completely different $\varepsilon/\varepsilon_0$ versus $\log t/t_0$ curves [46].

4.2. Isochronal stress relaxation, creep, and dynamic mechanical analysis experiments

The results previously discussed were obtained at a constant temperature and are thus isothermal. Isochronal results are obtained when the mechanical experiments described in the previous section are performed at different temperatures and plotted at the same time or frequency. These are, in fact, the most common type of available data on semicrystalline polymers [46].

In Fig. 6, the evolution of the relaxation modulus with temperature is shown for various types of polymers, including linear and crosslinked amorphous polymers with different crosslinking densities, as well as semicrystalline polymers with varying degrees of crystallinity. Five regions of distinct mechanical behavior are identified in the figure, illustrated specifically for the linear amorphous polymer:

Glassy region: At low temperatures, the material behaves as a rigid and brittle solid. Its mechanical response is elastic, exhibiting time-independent, fully reversible deformations, with the relaxation modulus equal to the (time-independent) tensile modulus. In this regime, molecular mobility is minimal, confined primarily to vibrational and short-range rotational movements.

Glassy transition (or leathery) region: The material undergoes a transition from a rigid solid state to a rubbery solid state. The deformation behavior becomes time-dependent, as the viscous characteristics become increasingly prominent with rising temperature. This transition is marked by a sharp decrease in the relaxation modulus, driven by the initiation of long-range coordinated molecular motion. The glass transition temperature is commonly defined as the temperature at which the rate of decrease in the relaxation modulus is maximum.

Rubbery (or plateau) region: The material is in a rubbery, ductile state. Its mechanical behavior is viscoelastic, showing a combination of elastic and viscous responses, with the relaxation modulus remaining relatively stable.

Rubbery flow region: The material undergoes a transition from a rubbery solid state to a viscous liquid state. In this region, the mechanical response resembles that of a highly viscous liquid, while still retaining some elastic characteristics. The relaxation modulus begins to decrease once more.

Viscous flow region: The material behaves as a viscous liquid, where, at the molecular level, thermal rotational motions of the polymer chains become so pronounced that their movements occur largely independently. The relaxation modulus decreases sharply up to the melting temperature, and the deformation is predominantly viscous.

Beyond the melting point, the material's resistance to flow is governed primarily by its viscosity.

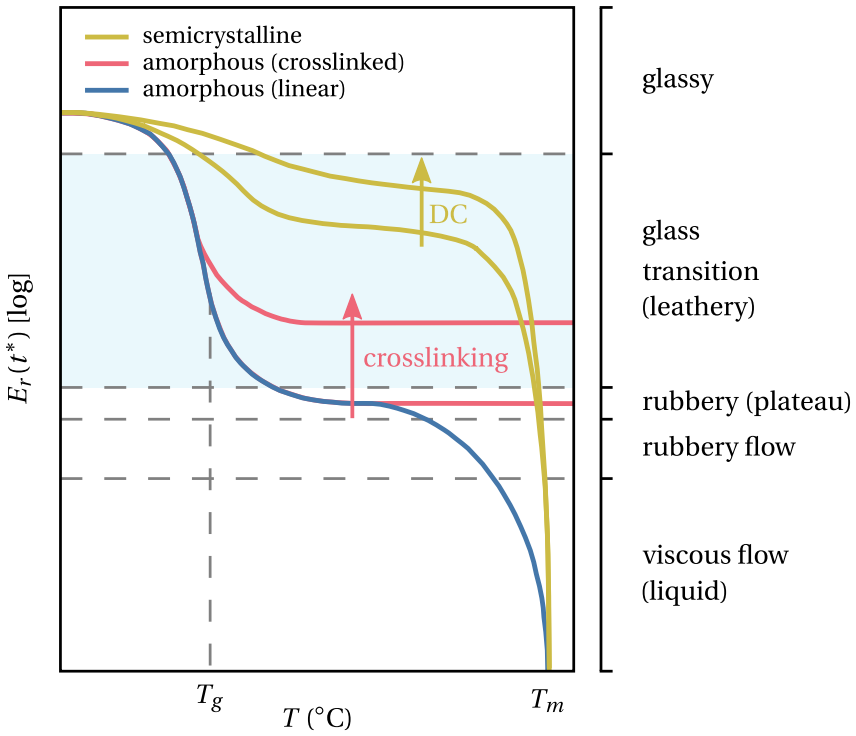

Figure 6: Evolution of the relaxation modulus, for a given instant of time t^*, with the temperature, for different types of polymers: linear amorphous polymers, crosslinked amorphous polymers with different crosslinking degrees, and semicrystalline with different degrees of crystallinity (DC). Regions of distinct mechanical behavior are presented for the amorphous linear polymer.

Glass transition and melting temperatures

The *de Gennes Reptation theory* is the most accepted theory for explaining the movement of molecular chains [37]. According to this theory, polymer chains exhibit a snake-like motion, termed *reptation*, within an invisible confining tube. This tube imposes constraints on the chains' movement, significantly slowing their dynamics. At temperatures above the melting temperature, T_m, the molecular chains are highly disordered, freely moving within this tube in random orientations. However, as the temperature drops below the melting temperature, the chains lose mobility and begin to either align into organized crystalline regions in semicrystalline polymers or become kinetically trapped in a disordered glassy

state in amorphous polymers. The degree of crystallinity achieved depends on the cooling rate. Under slow cooling, chains have sufficient time to rearrange into ordered crystalline structures, resulting in a semicrystalline polymer. Conversely, rapid cooling prevents extensive crystallization, producing a glassy or amorphous polymer as the material transitions abruptly into the glassy state. In this rigid, disordered state, molecular mobility is severely restricted. It should be noted that all polymers exhibit a glass transition temperature, T_g, marking the transition from a rubbery to a glassy state. Only crystallizable polymers possess a melting temperature, T_m, where the polymer undergoes a transition from solid to liquid. Amorphous polymers do not undergo this type of melting; instead, they soften as they approach and pass through their glass transition temperature.

Thermoplastic vs thermosetting polymers

Polymers are often categorized based on their response to heat and mechanical forces, leading to two primary classifications: (i) thermoplastic and (ii) thermosetting polymers. These categories reflect distinct thermal and mechanical behaviors governed by their molecular structures.

Thermoplastic polymers are characterized by their ability to soften or melt when heated and solidify when cooled in a reversible and repeatable manner. This behavior arises because heat increases the thermal motion of polymer chains, reducing the intermolecular van der Waals forces that hold the chains together. This reduction in bonding strength allows adjacent chains to slide past each other more easily under applied stress. Most linear polymers are thermoplastics, as their relatively simple molecular structures enable significant chain mobility. Some branched polymers with flexible chains also exhibit thermoplastic behavior due to their structural flexibility. However, excessive temperatures can cause irreversible degradation, limiting their thermal stability. Examples of thermoplastics include polyethylene (PE), polypropylene (PP), polyvinyl chloride (PVC), polystyrene (PS), and polycarbonate (PC).

In contrast, thermosetting polymers do not melt or soften upon heating. Instead, they become permanently rigid after undergoing a curing process that forms extensive crosslinks or networks of covalent bonds between molecular chains. These covalent bonds act as

anchors, restricting molecular motion even as temperature rises, preventing the sliding of chains under stress. As a result, thermosets maintain their shape and structural integrity at high temperatures, making them ideal for high-performance applications. This class primarily includes highly crosslinked or networked polymers such as epoxy resins, phenolic resins, polyurethanes, and melamine formaldehyde.

Shifting from isochronal relaxation and creep experiments to isochronal DMA experiments, the focus turns to the identification of relaxation transitions in solid polymers at a given frequency. They can be identified as peaks in the loss modulus, and as drops in the storage modulus (see Eq. (A.40)). Starting with low-crystallinity polymers helps clarify the discussion of relaxation transitions in semicrystalline polymers. In fact, for a completely amorphous polymer glass, there will be two important transitions: the alpha and beta transitions. For semicrystalline polymers, these transitions will still be present in the amorphous domains of the polymer, but other transitions may appear due to the presence of the crystalline phase [48]. The results in Fig. 7 illustrate the effect of crystallinity on the DMA results for polyethylene terephthalate (PET) and polyethylene (PE) samples, both sets including samples with different degrees of crystallinity.

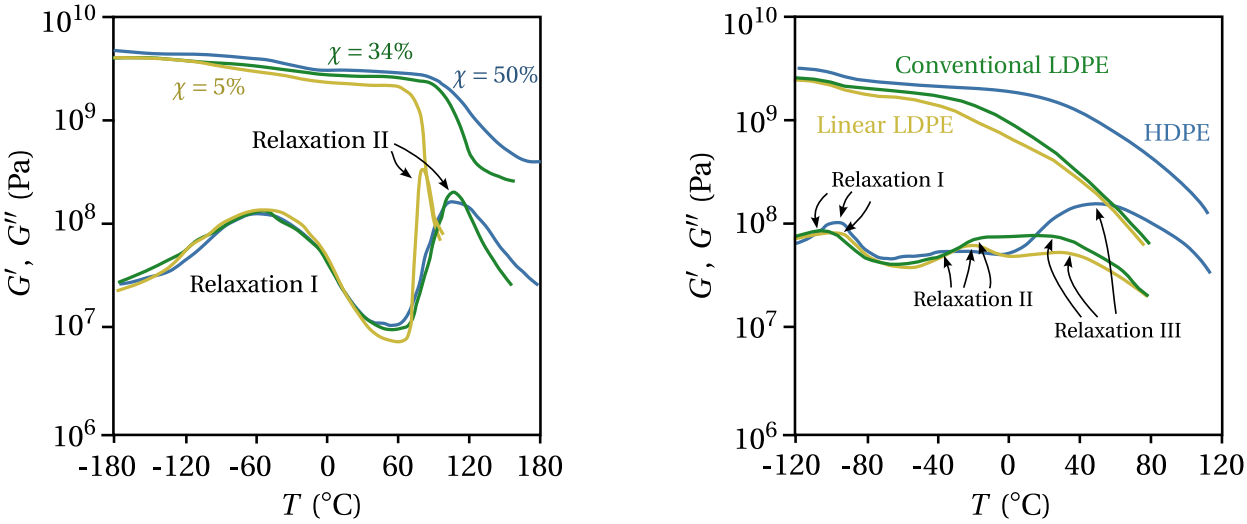

Figure 7: Dynamic mechanical analysis results for a PET with degrees of crystallinity of 5%, 34% and 50% at 138 Hz, obtained by Takayanagi [12], and for b PE samples, linear LDPE (∼45%), conventional LDPE (∼48%), and HDPE (∼67%), at 1 Hz, obtained by Khanna and coworkers [49].

Note that a linear behavior as described by linear thermoviscoelasticity would imply no dependence of relaxation or creep modulus on temperature. This is not the case, as has been discussed. Indeed, there are similarities in the dependence of the relaxation modulus on temperature and time, which motivate the use of time-temperature superposition principles to build master curves and model these relations [50].

4.3. Constant strain rate experiments

Another set of mechanical experiments useful for characterizing solid polymers are the constant strain rate experiments, in particular, the uniaxial tensile and compression tests. Typically, three distinct responses may be observed in these experiments (see Fig. 8): (i) brittle (low ductility), (ii) plastic (extensive post-yielding), and (iii) elastomeric (highly elastic reversible deformation) [3]. In general, these responses are governed by two primary sources of resistance: intermolecular resistance, linked to the polymer's internal energy, and entropic resistance. At low strains, the behavior of amorphous polymers is dominated by a visco-elastic region (stage (A) in Fig. 8), which arises from intermolecular interactions between the polymer chains, particularly van der Waals forces [51]. During this phase, the polymer chains undergo partial, reversible rotations and translations relative to one another due to these molecular interactions. As stress increases and overcomes these secondary intermolecular forces, localized regions form, and the chains reorient into new configurations. This leads the polymer to reach its yield point, marked by a maximum on the stress-strain curve. Following yield, the material experiences strain-softening (stage (B)), where the stress required to deform the polymer further decreases. Strain-softening indicates that the resistance to rotation of chain segments has decreased due to deformation, suggesting that deformation leads to local changes in the material's structure. These changes facilitate easier rotation of the polymer chains, requiring less stress to induce further rotation. As the deformation progresses, the entropic resistance becomes increasingly influential in the material's response [52]. The polymer chains rotate towards the direction of maximum elongation, thereby decreasing the system's entropy. This entropic change, which becomes more pronounced as the chains align and approach their maximum extension, contributes to strain hardening (stage (C)) and ultimately increases the material's resistance to further

deformation. After yielding, the polymer undergoes some plastic deformation until fracture. Fracture in an amorphous polymer involves breaking both the strong covalent and secondary bonds, and is often the result of shear yielding or crazing.

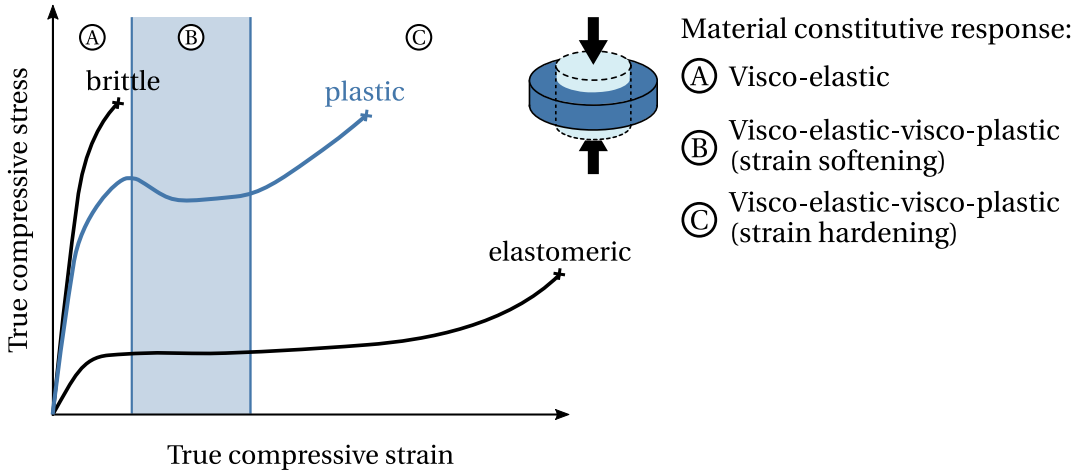

Figure 8: Characteristic true Cauchy stress-true logarithmic strain constitutive behavior of amorphous polymers when subjected to uniaxial compression loading at constant strain rate. Three typical material responses are represented: brittle, plastic, and elastomeric. The three characteristic regions of deformation — (A), (B), and (C) — are highlighted specifically for the plastic response.

Moreover, these responses are highly dependent upon temperature, strain rate, aging history (i.e., the accumulated effects of time, temperature, and environmental factors on the material's properties), molecular entanglements, type of loading, and hydrostatic pressure.

Regarding the response of a solid polymer pre-yield, an increase in temperature will lead to a more compliant response and a lower yield strength, as shown in Fig. 9 for nylon 101 [53], and in the results reported in [21] and [26] for PEs. In fact, temperature is possibly the single most influential parameter dictating a polymer's mechanical response. Some polymers may exhibit brittle fracture to necking or even homogeneous rupture during a uniaxial tension test, depending on the temperature [12]. Moreover, whether the polymer is below or above its glass transition temperature results in markedly different behaviors in the case of amorphous polymers (see Fig. 9, adapted from [54]). An amorphous polymer in its glassy state behaves as a plastic polymer, whereas in its rubbery state, it exhibits a much more compliant response, with large deformations and no clear yield point. On

the other hand, even if the temperature of a semicrystalline polymer is much higher than its glass transition temperature, the crystalline phase causes the polymer's response to be qualitatively similar to that of a plastic polymer, although less stiff than it would be at a lower temperature (see Fig. 9).

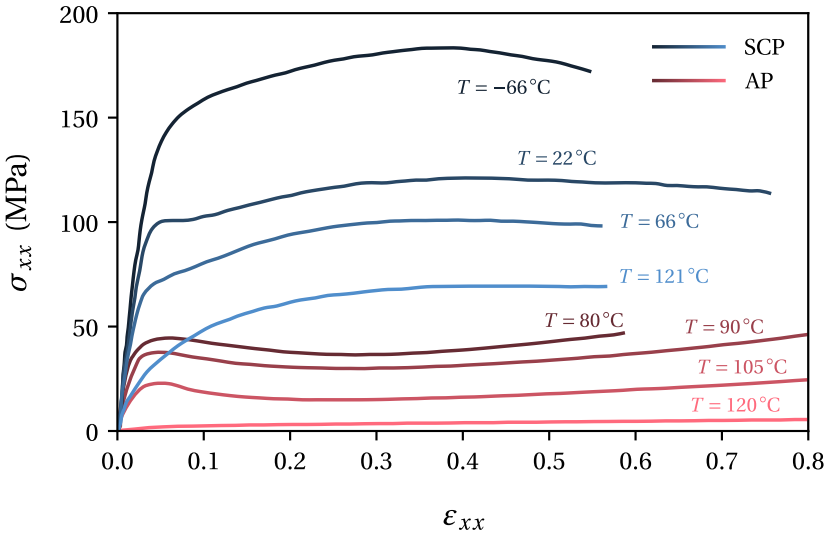

Figure 9: Stress-strain curves for a semicrystalline polymer (SCP), nylon 101 [53], and an amorphous polymer (AP), poly(methyl methacrylate) [54]. Above and below their glass transition temperatures, 60 °C and 118 °C, respectively.

The strain rate and the hydrostatic pressure have the opposite effect, such that their increase will lead to a stiffer response and higher yield stresses, as gathered from the results in [55] (uniaxial tension) and [56] (torsion). Bauwens-Crowet [57] compiles an extensive set of experimental results regarding the relationship between the strain rate, the temperature, and the yield strength of amorphous polymers. Based on these results, a schematic representation of the ratio between the compressive yield stress and temperature as a function of the logarithm of the strain rate is presented in Fig. 10a. El-Qoubaa and Othman [58] also provide a similar set of results regarding the relationship between the strain rate, the temperature, and the yield strength of semicrystalline PEEK, shown in Fig. 10b. Both figures illustrate the nonlinear relationship between the yield stress and the strain rate.

In addition to the previously discussed factors, mechanical pre-deformation significantly influences the mechanical response of polymers. This term refers to the material's prior

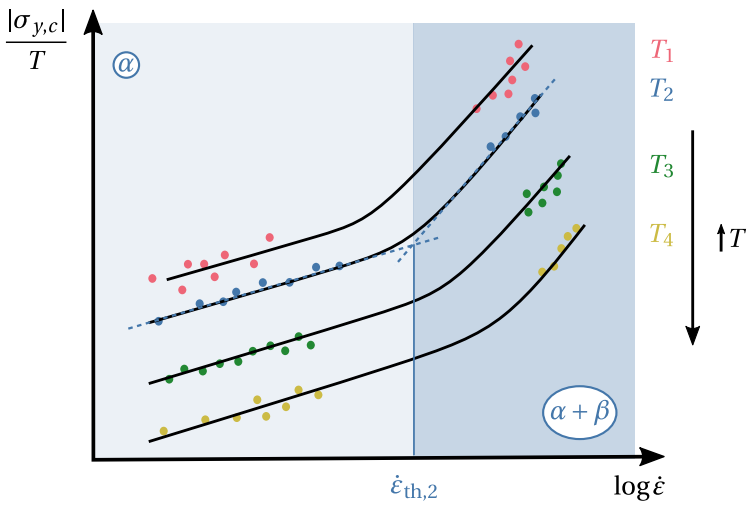

(a)

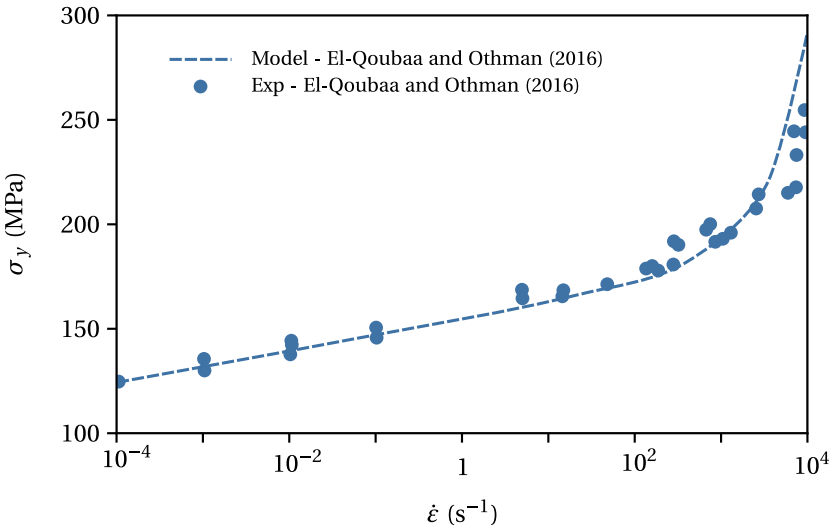

(b)

Figure 10: a Schematic representation of the ratio between the compressive yield stress and temperature as a function of the logarithm of the strain rate, according to the experimental results of Bauwens-Crowet [57]. The transition strain rate, $\dot{\varepsilon}_{\mathrm{th}}$, depicts the shift between the low, α-transition, and high, $\alpha + \beta$-transition, strain rate sensitivity of amorphous polymers. b Yield stress, σ_y, as a function of the strain rate, $\dot{\varepsilon}$, for PEEK at room temperature. Model and experimental results are taken from the work of El-Qoubaa and Othman [58].

deformation history, which can induce molecular orientation, residual stresses, and localized structural changes. Such alterations affect subsequent mechanical behavior, potentially enhancing stiffness, modifying yield behavior, or reducing ductility [59].

Nevertheless, another relevant aspect is the polymer's crystallinity. An increase in bulk crystallinity will lead to a stiffer response and increased yield strength [27, 60, 61, 23]. However, the relationship between stiffness and crystallinity appears to be nonlinear as depicted in Fig. 11. It has also been observed that an increase in lamellar thickness is

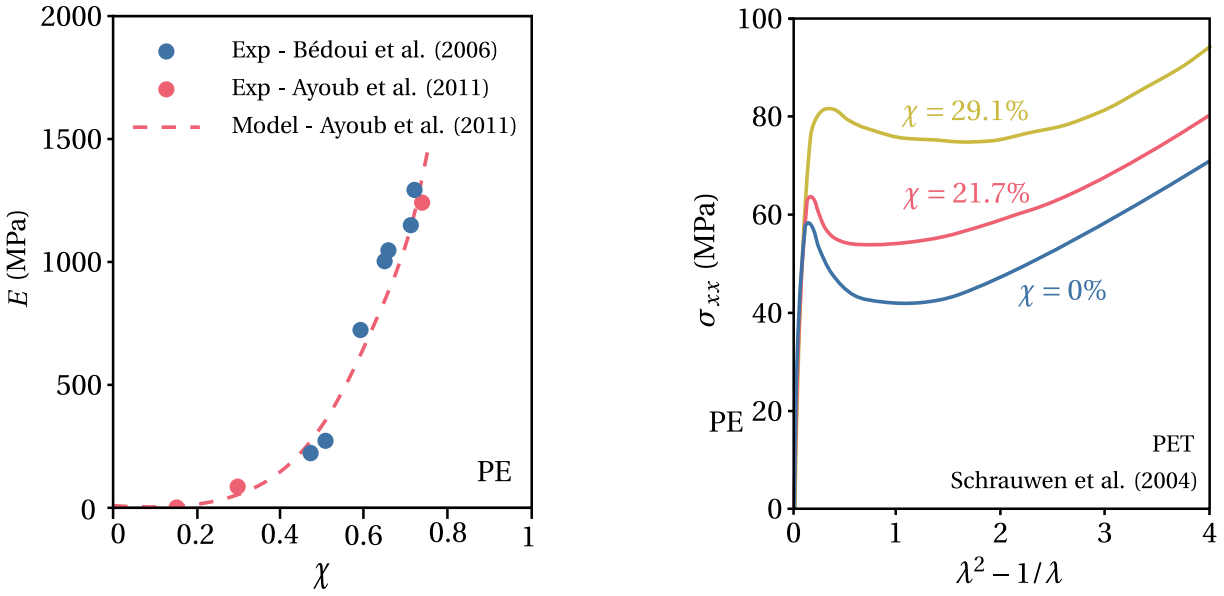

(a) (b)

Figure 11: Effect of the bulk crystallinity on a the Young modulus, E, and on the b yield strength of a semicrystalline polymer.

correlated to a higher yield strength [23, 14]. Regarding the effect of the mesostructure on the response of a semicrystalline polymer, one can compare the behavior of isotropic (spherulitic) and oriented (fibrilar) PE when subject to uniaxial tension. As shown in [62], the latter possesses a higher yield strength and begins to strain harden immediately after yielding, while the former resists at approximately constant stress.

A common strategy to enhance the toughness of amorphous polymers is the incorporation of rubber particles, which significantly improve their ductility while sacrificing some material strength [37, 2, 63, 64]. Examples of such rubber-toughened polymer blends include

high-impact polystyrene (HIPS) and acrylonitrile-butadiene-styrene (ABS). While rubber-toughened polymers are widely used for impact-resistant applications, the concept extends beyond these specific blends. Amorphous polymers also serve as critical components in various polymer blends and composites aimed at achieving a broader range of tailored properties, such as improved processability, thermal stability, or strength. For instance, their use as matrices in fiber-reinforced composites highlights their versatility in creating lightweight materials with enhanced impact resistance, fatigue life, and structural integrity.

There may be some intrinsic strain softening after yielding, i.e., a decrease in stress with strain. The results in [23] show that after yield is reached, there is a sharp decrease in stress for completely amorphous PET above its glass transition temperature. The drop becomes broader and less pronounced as crystallinity increases to values of 21.7% and 29.1%. The same authors report PE results showing no strain softening at a degree of crystallinity of 76.6%. Minor strain softening is visible at lower crystallinity values for the same polymer. PP softens mildly as well, despite having a crystallinity of around 70% in the samples studied. These results were obtained under uniaxial compression. However, no softening is visible after yielding in the results of Truss and coworkers [56] obtained for PE in torsion. G'sell and coworkers [65] present results of pure shear experiments in which HDPE exhibits mild strain softening at 23 °C while PP and PA66 show none.

Despite the presence of intrinsic strain softening, its experimental observation is complicated by two phenomena: thermal softening and plastic instabilities. The results presented thus far were obtained at strain rates slow enough to allow for isothermal evolution. However, as the strain rate increases, a phenomenon known as 'temperature softening' occurs, leading to a similar decrease in stress with strain due to increased temperature. This temperature rise is due to the difficulty of removing the heat generated by the plastic work in such a short time, which makes the process adiabatic. According to Furmanski and coworkers [66], this effect should be considered at strain rates greater than $0.01\,\mathrm{s}^{-1}$ and strains greater than 15%. Plastic instabilities, i.e., the growth of a locally thinned region in a material upon application of stresses, must also be considered when the intrinsic response of the material is sought. They are a function of the geometry and loading conditions of the loaded body, in addition to its intrinsic constitutive behavior [12]. There are, nonetheless, experimental

methods that allow the use of uniaxial tensile tests to determine intrinsic material behavior. The video-controlled technique in [67] is one example, as is the SEÉ method [68, 69], which uses full-field data from digital correlation measurements of heterogeneous displacement fields.

Another important aspect of the plasticity of semicrystalline polymers is that, unlike metals, permanent volumetric strains can be detected in addition to elasticity-related volumetric strains. These effects, found both in tension and compression, cannot be explained by Hooke's elasticity and correspond to an irreversible contraction or dilation of the material [18, 70]. Cangemi and Meimon [18] report the existence of plastic dilation in compression for semicrystalline polymers. In contrast, glassy polymers show a very weak contraction. Damage, or void growth, is one of the mechanisms responsible for these observations. However, according to Polanco-Loria and coworkers [70], an increase in volume in semicrystalline polymers may also be associated with crystalline deformation. This happens because the molecules are densely packed in the crystalline phase. Thus, the specific volume is likely to increase when the crystalline lamellae break up. In fact, after a compression test in which the specimens showed net plastic expansion for the majority of the test, Kitagawa and Yoneyama [71] made thin cuttings of semicrystalline polymer samples (PP, POM, and PE) for observations in a polarized light microscope. No cracks or crazes were found. This point expresses the peculiarity of plastic volume expansion in semicrystalline polymers, which may be related to the complexity of their microstructures as well as their two-phase nature [18].

The decomposition of the deformation of semicrystalline polymers into elastic and plastic portions remains to be discussed. When applied to metals at temperatures far from their melting points, an elastic deformation pertains to the seemingly instantaneous part of the deformation that is recovered upon unloading. If the metal yields, it undergoes irreversible plastic deformation that persists after unloading. This decomposition is less evident in time-dependent materials, such as polymers, because deformation may not be fully recovered upon unloading but instead recovers over time. It yields a definition of the irreversible part of the deformation, which depends on the observation time; i.e., some deformation may be irreversible during the experiment but potentially reversible if the observation were extended in time.

Strobl and coworkers [72, 26, 73, 62] performed a very detailed study on polyethylenes, which includes the results of both free shrinkage, where, after loading, the load is immediately released, and step cycle experiments, where unloading is carried out at the same strain rate as the loading phase. The decomposition of the constant-strain-rate stress-strain curve is based on the reversible and irreversible parts of deformation, as determined from these experiments. For very small strains, the deformation is almost completely recovered immediately. As the strain increases, some deformation will not be immediately recovered, and the proportion of irreversible deformation, i.e., deformation that is never recovered, increases as well. However, the results also show that even after the load is completely removed, some deformation is recovered over time. Bartczak and coworkers [28] also report that HDPE samples deformed under uniaxial compression exhibit significant strain recovery upon unloading. They are partly instantaneous and partly over a few hours ($< 24\,\mathrm{h}$).

4.4. Thermal analysis techniques

To fully characterize the thermomechanical behavior of semicrystalline polymers, information about their thermal behavior must be gathered. To model the thermomechanical response of polymers, it is necessary to know their thermal expansion or stress coefficient, $\boldsymbol{\alpha_F}$ or $\boldsymbol{\beta_P}$, as well as their specific heat capacity, $C_{\boldsymbol{F}}$ and thermal conductivity, k_0. For a brief overview of the thermomechanical problem, please refer to Appendix A. The glass transition temperature, T_g, and melting temperature, T_m, are also indispensable bits of information to decide on the appropriate constitutive model to employ. This information can be obtained from experiments such as dilatometry [74], pressure volume temperature (PVT) experiments [75], differential scanning [76, 77, 78, 79] and laser flash tests [74].

The thermal expansion coefficients of polymers reported in the literature are in the hundreds to thousands (µm/m)/K, at least an order of magnitude larger than metals and ceramics, varying linearly with temperature [74]. That said, in general, thermal stresses, $\Delta\sigma$, are not as significant in polymers as large as in metals, since for polymers $\Delta\sigma = \alpha E \approx 0.1$, while for metals $\Delta\sigma = \alpha E \approx 1$ [80].

Regarding the experimental determination of the specific heat capacity of semicrystalline polymers employing DSC, Blumm and coworkers [74] report an almost constant value, which

ranges from around $1000\,\mathrm{J\,kg^{-1}\,K^{-1}}$ at $0\,^{\circ}\mathrm{C}$ to $1500\,\mathrm{J\,kg^{-1}\,K^{-1}}$ at $300\,^{\circ}\mathrm{C}$ for PTFE. This agrees with the value of $\rho C_p \approx 3 \times 10^6\,\mathrm{J\,m^{-3}\,K^{-1}}$, which, according to Ashby [80], is true for all solids, employing considerations from statistical mechanics.

Finally, the thermal conductivity of polymers is generally low when compared to metals and ceramics, ranging from $0.1\,\mathrm{W\,m^{-1}\,K^{-1}}$ to $0.5\,\mathrm{W\,m^{-1}\,K^{-1}}$ [80]. Blumm and coworkers [74] report $0.31\,\mathrm{W\,m^{-1}\,K^{-1}}$ for PTFE, for example. Given their relatively high linear thermal expansion and low thermal conductivity, polymers are more prone to heat distortion than, for example, metals. This is because they combine a longer time to reach a uniform temperature with larger size changes due to temperature differences.

5. Modeling approaches

As discussed above, the mechanical behavior of thermoplastic polymers is complex and governed by a range of deformation mechanisms operating at different scales. Accurately modeling these behaviors requires understanding both localized phenomena, such as shear yielding, crazing, and internal particle cavitation, as well as their dependence on loading conditions, namely temperature, pressure, and strain rate. Given these requirements, this section discusses briefly the three most common approaches to constitutive modeling for thermoplastic polymers, *continuum modeling* (Section 5.1), *micro-mechanical modeling* (Section 5.2), and *multi-scale modeling* (Section 5.3). The next two sections (Sections 6 and 7) place special focus on the very diverse class of continuum models, which are the most widely used in engineering applications, and reviews the most recent developments in this area.

5.1. Continuum models

Continuum models embody a macroscopic perspective towards constitutive modeling, capturing the stress-strain responses of materials without resolving microstructural details. This approach is particularly well-suited for describing the behavior of homogeneous amorphous polymers, in which the material can be treated as a continuous medium, neglecting its molecular structure and microstructural discontinuities. By treating the material as a continuum, it becomes possible to develop constitutive models that fall under the

broader category of single-scale approaches. These include both phenomenological models and micro-mechanically inspired continuum models. Phenomenological models describe material behavior based on empirical observations, without directly referencing the underlying microscopic mechanisms. Micro-mechanically inspired continuum models, on the other hand, incorporate knowledge of microstructural effects, such as internal variables, phase interactions, and damage mechanisms, into the macroscopic response while still operating at the continuum level without explicitly resolving the microstructure's geometry. Notably, these two categories are not mutually exclusive: many micro-mechanically inspired models retain a phenomenological character, relying on fitted parameters and empirical assumptions.

Phenomenological models typically span length scales ranging from 10^{-5} to 10^{2} meters and time scales greater than 10^{-6} seconds [81]. A key subgroup within this class is the thermodynamics-based continuum framework with internal variables, which incorporates thermodynamic principles to track the evolution of internal state variables. These models often employ closed-form analytical expressions or numerical solutions of complex constitutive equations, making them versatile tools for predicting the mechanical behavior of amorphous polymers.

Despite their practicality and efficiency, continuum phenomenological models may struggle to capture the highly nonlinear behavior of multiphase materials with complex microstructures. Such models often require a large number of parameters calibrated using extensive experimental data. They may not adequately describe local interactions — such as stress concentrations, strain localization, or phase-specific mechanisms — that can significantly influence macroscopic behavior.

To address these limitations, explicit micro-mechanical models provide a complementary approach by directly accounting for the material's microstructure. For instance, rubber-toughened amorphous polymers can be modeled at the macro-scale using continuum formulations that account for phenomena like particle cavitation and void growth [82, 83, 84, 85], or through explicit micro-mechanical simulations that resolve the internal microstructure [63, 86, 87]. These explicit micro-mechanical models are discussed in the following section.

5.2. Micro-mechanical modeling

Micro-mechanical models provide a means to incorporate details of a material's underlying microstructure into the constitutive response. These approaches are particularly useful for amorphous polymers exhibiting microstructural heterogeneities, such as rubber-toughening phases, fillers, or voids. In contrast, for neat and structurally homogeneous polymers, macroscopic continuum models often offer a more practical and sufficiently accurate description of their mechanical behavior.

In this context, as an alternative to the continuum models discussed in the previous section, rubber-toughened amorphous polymers can also be characterized using micro-mechanical approaches. In these cases, a Representative Volume Element (RVE), which explicitly accounts for the discrete rubber particles in an amorphous polymer matrix is considered. Consequently, it is possible to study the deformation mechanisms at a micro level, where the interaction between particles is explicitly considered [63, 86, 87]. In Fig. 12 a scheme of an RVE with different material phases is provided.

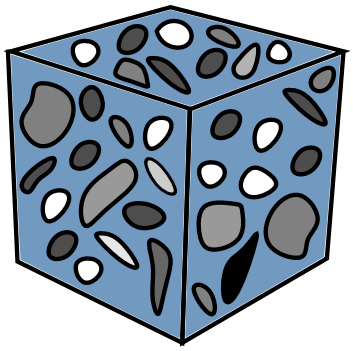

Figure 12: Scheme of a Representative Volume Element with different material phases.

Micro-mechanical modeling techniques can generally be categorized into two main approaches: mean-field and full-field models. Mean-field models estimate the macroscopic behavior of heterogeneous materials by averaging the responses of the constituent phases, without explicitly resolving the microstructural geometry [38, 88]. These models are computationally efficient and particularly useful when the microstructure is relatively uniform or when only overall trends are of interest. In contrast, full-field models explicitly resolve the microstructural morphology, typically by defining an RVE that captures the spatial dis-

tribution and interaction of different phases [89, 90]. This allows for a more detailed and accurate prediction of local fields, but at the expense of higher computational cost. In the work developed by Mirkhalaf et al. [10], several micro-mechanical approaches used to model semicrystalline polymers, including both mean-field and full-field strategies, are reviewed.

When full-field simulations are used to extract the macroscopic behavior from detailed microstructural models, the process is often referred to as computational homogenization. In this context, the RVE serves as the fundamental micro-scale domain over which boundary value problems are solved, and its averaged response is used to inform or define a macro-scale constitutive law. Depending on the application, this homogenization may be carried out offline to calibrate continuum models, or online in multi-scale frameworks such as FE^2, where micro- and macro-scales are coupled during the simulation process [91, 92].

Note that the success of the full-field models relies on the accurate generation of RVEs to describe the material's microstructure. In this setting, different microstructure generation techniques have been proposed [93, 94, 95, 96, 97]. For instance, Vila Chã et al. [97] developed a robust and flexible geometrical method based on an adaptive multi-temperature isokinetic time-driven molecular dynamics scheme for particle-reinforced materials. Salnikov et al. [94] introduced a stochastic generation algorithm that resolves initial particle overlaps using repulsive forces, enabling the generation of statistically representative configurations. Similarly, Herráez et al. [95] presented VIPER, a tool for efficiently generating microstructures of hybrid composites with non-circular fibers at high volume fractions. In a different approach, Bostanabad [96] developed a deep learning-based framework that reconstructs 3D microstructures from 2D images, providing a data-driven alternative when experimental data is limited.

5.3. Multi-scale modeling

Multi-scale modeling has emerged as an essential tool to address the limitations of single-scale models. In contrast to traditional micro-mechanical models, where RVEs are typically used to estimate effective material properties in a decoupled or offline manner, multi-scale frameworks such as Coupled Multi-scale Finite Element Analysis (FE^2) embed an RVE directly at each integration point of the macro-scale simulation. This enables a fully cou-

pled, on-the-fly computation of the stress–strain response, directly informed by the evolving microstructure. As a result, the heterogeneity of the material's microstructure is not just represented, but dynamically linked to the global response, making FE^2 particularly valuable for the design of new materials and structures requiring high fidelity and predictive accuracy.

In Fig. 13, a schematic of this coupled analysis framework is provided. Each integration point $\boldsymbol{x}$ of the continuum macroscopic body has an RVE linked to it, being the solution at each point given by volume averaging the response over the deformed RVE's domain. The macro-scale deformation gradient, $\boldsymbol{F}$, drives the disturbance to the RVE equilibrium, being the equilibrium problem then solved according to the micro-scale boundary conditions. Once the solution to the equilibrium problem is found, the macro-scale stress tensor, $\boldsymbol{P}$, and the consistent tangent modulus, $\mathbf{A}$, are computed by computational homogenization.

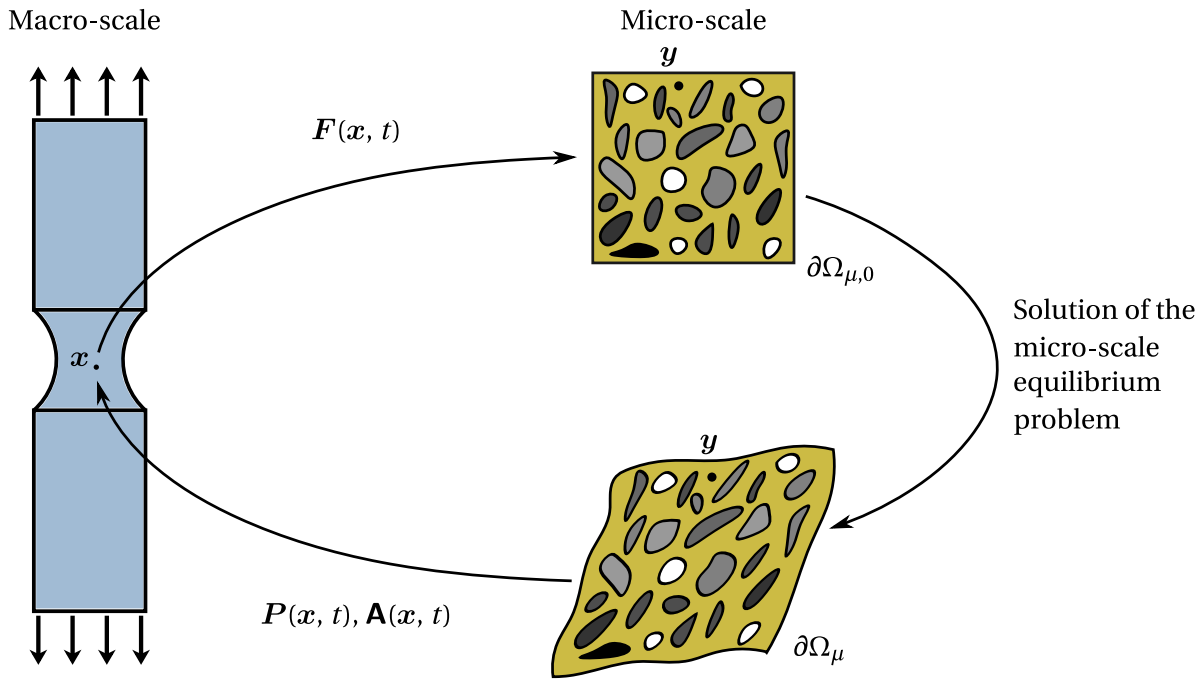

Figure 13: Scheme of a multi-scale finite element analysis based on a first-order homogenization model.

A rigorous variational formulation of this approach was developed by de Souza Neto et al. [92, 98], based on the Method of Multi-Scale Virtual Power. This ensures variational consistency across scales. The formulation rests on two core procedures: (i) kinematic

insertion, which transfers macro-scale deformation measures to the micro-scale, and (ii) kinematic homogenization, which upscales micro-scale fields back to the macro-scale. The scale coupling is governed by the Principle of Multi-scale Virtual Power — a generalization of the Hill-Mandel principle — ensuring energetic consistency between scales. This principle yields the governing equations for the micro-scale domain and defines admissible boundary conditions for the RVE, along with the stress homogenization process.

6. Nonlinear rheological elements

In this section, we collect foundational continuum constitutive models widely used to describe the behavior of thermoplastic polymers. The choice of a constitutive model implies the choice of appropriate functions relating stress to strain, temperature, with the addition of internal variables and their corresponding evolution equations to capture history dependent beahvior (for a brief overview on constitutive modeling see Appendix A). Perhaps, the most used approach to model thermoplastic polymers is to consider a rheological one-dimensional originating from infinitesimal viscoelasticity and choose appropriate nonlinear functions describing the behavior of the different elements, guided by the experimental results discussed in Section 4. Although not all authors adopt this rheological interpretation, almost all constitutive models for thermoplastic polymers can be rationalized within this framework. Accordingly, in this section, we first collect the different models used in the literature for both viscous and elastic elements. We discuss the different flow rules and yield criteria for the viscous elements, as well as the different free energies used for the elastic elements. Then since the rheological interpretation concerns a small strain one-dimensional setting, we discuss how different authors have generalized these models to three-dimensional finite deformations. We also discuss how the polymer's thermal behavior may be incorporated into the constitutive models.

6.1. Viscous elements or flow rules

In this section, we focus on the one-dimensional laws relating the strain rate $\dot{\gamma}$ to the applied stress τ. They are first collected in this simplified form for clarity, and later in the section, the different approaches for extending them to three dimensions are discussed.

As pointed out by Frost and Ashby [99], plastic flow is a kinetic process. Therefore, the strength of a solid depends on both strain and strain rate, in addition to the temperature. The temperature dependence follows from the assistance provided by thermal fluctuations to the kinetic units responsible for plastic flow in overcoming energy barriers that hinder their motion. Following the procedure outlined by Eyring [100], the flow rule for thermally activated viscous flow can be derived as

$$\dot{\gamma} = \dot{\gamma}_0 \exp\left(-\frac{\Delta H}{k_B T}\right) \sinh\left(\frac{v\tau}{k_B T}\right), \tag{2}$$

where v is the so-called activation volume, and it can be identified with the product of the area swept out by the mobile unit in moving from one local free energy minimum to the next, and the resolved component of the distance moved by the kinetic unit in the direction of the applied stress. $\dot{\gamma}_0$ is a reference strain rate, ΔH is the activation energy for flow when no stress is applied, k_B is the Boltzmann constant, and T is the absolute temperature.

According to the same author, $v\tau$ is much smaller than $k_B T$ in an ordinary flow. Thus, the expression for Newtonian viscous flow is recovered from Eq. (2) as

$$\dot{\gamma} = \frac{\dot{\gamma}_0 v}{k_B T} \exp\left(-\frac{\Delta H}{k_B T}\right) \tau = \frac{1}{\eta}\tau, \tag{3}$$

where η is the viscosity, keeping only the first term in the Taylor expansion of the hyperbolic sine function. On the other hand, for plastic flow, where τ is large, the flow rule is

$$\dot{\gamma} = \dot{\gamma}_0 \exp\left(-\frac{\Delta H - v\tau}{k_B T}\right) = \dot{\gamma}_0 \exp\left(-\frac{\Delta G(\tau)}{k_B T}\right), \tag{4}$$

since $\sinh(x) \approx \frac{1}{2}\exp(x)$ for large x, implying a negligible rate in the backward direction, and where $v\tau$ is identified with the activation work such that $\Delta G = \Delta H - v\tau$. The contribution of the hydrostatic pressure can also be accounted for in this framework in a similar way to the shearing force, i.e.,

$$\dot{\gamma} = \dot{\gamma}_0 \exp\left(-\frac{\Delta H - v\tau + \Omega p}{k_B T}\right), \tag{5}$$

where Ω is the activation volume corresponding to the hydrostatic pressure. This relationship can be justified in terms of experimental results, where the stress response of polymers shows a pressure dependence, in part due to the low bulk moduli of polymers ($\approx$5 GPa, compared with metals $\approx$100 GPa). Thus, a suitable expression for the effective stress on the

kinetic units is a linear combination of shear stress and hydrostatic pressure, similar to the Mohr-Coloumb yield criterion [12]. The expressions above show that higher shear stresses lead to higher flow rates, while higher hydrostatic pressures produce the reverse effect. The reader can find more general rate equations for thermally activated flow in [101] or [102].

Roberston [103] presents an alternative to the Eyring model applicable to glassy polymers. The author considers a molecular model in which the shear-stress field is introduced as a bias on the rotational conformation of backbone bonds. The temperature at which the maximum fraction of flexed bonds is observed is estimated and inserted into the Williams-Landel-Ferry (WLF) equation to compute the corresponding viscosity, and hence the equation for the strain rate. See [12, Section 6.3.2] for more details on the WLF equation. Comparisons with results for PS and PMMA are provided. Duckett and coworkers [104] also employ this model to fit the responses of PMMA and PET.

El-Qoubaa and Othman [58] provide an implicit flow rule while seeking to model the yield stress of PEEK as a function of the strain rate and the temperature. The equation proposed is

$$\dot{\gamma} = \dot{\gamma}_0 \exp\left(\frac{\tau v(\dot{\gamma}, T)}{k_B T}\right), \tag{6}$$

where the activation volume, v, depends on the strain rate and the temperature according to

$$v(\dot{\gamma}, T) = v_0(T) \exp\left(-\sqrt{\frac{\dot{\gamma}}{\dot{\gamma}_c(T)}}\right), \tag{7}$$

$$v_0(T) = v_1 + v_2 \left(\frac{T}{T_g}\right)^n, \tag{8}$$

$$\dot{\gamma}_c(T) = \dot{\gamma}_1 \exp(qT), \tag{9}$$

T_g is the glass transition temperature, and τ_1, m, r, v_0, v_1, n, $\dot{\gamma}_1$ and q are material constants. The authors find a good agreement between the model and experimental data.

The models described so far are often termed velocity-controlled, as they assume that yield occurs when the strain rate of the viscous element, identified with the movement of kinetic units, equals the impressed rate of deformation [105]. These models can also be thought of as specifying that the presence of stress causes an increase in pre-existing flow processes in the material, such that the stress corresponding to their flow equals the loading

stress [12]. Notice that despite mentioning the existence of deformation mechanisms corresponding to the motion of kinetic units, the models presented in the previous paragraphs do not attempt to model the specific physical events directly. Alternatively, in the case of nucleation-controlled models for polymer plastic flow, the free energy is directly modeled to determine the energy required in the nucleation and motion of the kinetic units [105, 12].

Argon [106] proposes a model for the plastic deformation of glassy polymers where the deformation mechanism is the buckling of the polymer chains via the action of a pair of opposed kinks. The expression found for the free energy is

$$\Delta G(\tau) = \frac{3\pi G\omega^2 a^3}{16(1-\nu)}\left[1 - \left(\frac{\tau}{\hat{\tau}}\right)^{5/6}\right], \tag{10}$$

where G and ν are the shear modulus and Poisson coefficient, respectively, $\hat{\tau}$ is the athermal strength defined as

$$\hat{\tau} = \frac{0.077G}{1-\nu}, \tag{11}$$

ω is the net angle of rotation of the molecular segment between the initial and activated configurations, and a is the mean molecular radius. The relationship between the athermal strength and the shear modulus in Eq. (11) can be used to establish the temperature dependence of the athermal strength [107]. In the case of amorphous polymers, however, Ward and Sweeney [12] mention that computer simulations of polymer chains at the atomic level on both glassy atactic polypropylene and polycarbonate did not yield a dominant deformation mechanism that should be the target of modeling.

Turning to semicrystalline polymers, the picture changes in the sense that, as reviewed in Section 3, the plastic behavior of the material is clearly linked to deformation mechanisms in the crystalline phase. There is extensive modeling of plastic behavior in polycrystalline solids with direct identification of the kinetic units as dislocations in the crystal[1]. According to Kocks, Argon and Ashby [102], their motion can be modeled as in Eq. (4), with the pre-exponential factor given by

$$\dot{\gamma}_0 = b\rho_m L\nu_G, \tag{12}$$

[1]A dislocation loop can be defined as the demarcation line, in one slip plane, between an area that has slipped and a surrounding area that has not [102].

where b is the Burgers vector[2] with dimensions of length, ρ_m is the mobile dislocation density with dimensions of dislocation length per unit volume, L the mean path of a mobile dislocation between inception and arrest at an obstacle and ν_G the frequency factor associated with the attempt rate of the nucleation process. At still moderate stresses, the average velocity is mainly controlled by thermally activated processes in which dislocations wait until a thermal fluctuation allows them to overcome the obstacle.

Argon [14] presents the three relevant modes of dislocation nucleation in polymer lamellae as the nucleation of a monolithic straight screw-dislocation line from the edge of a lamella (mode A), nucleation of a screw-dislocation half loop from the narrow edge of a lamella (mode B), and nucleation of an edge-dislocation half loop from the wide face of a lamella (mode C). The respective free energies for each mode are

$$\Delta G_A(\tau) = \frac{\mu b^2}{4\pi} \ln\left(\frac{\hat{\tau}}{\tau}\right), \tag{13}$$

$$\Delta G_B(\tau) = \frac{\mu b^2}{4\pi} \frac{1-(\tau/\hat{\tau})^{2/3}}{(\tau/\hat{\tau})^{1.25}}, \tag{14}$$

$$\Delta G_C(\tau) = \frac{\mu b^3}{1-v} \frac{1-(\tau/\hat{\tau})^{1/3}}{(\tau/\hat{\tau})^{1.15}}. \tag{15}$$

The same author also presents expressions for the mobile dislocation density as

$$\rho_m = \frac{\chi p N \lambda}{\lambda \Lambda^2}, \tag{16}$$

where λ is the length of the dislocation produced, p the probability of a successful nucleation event at a site, χ is the degree of crystallinity, and $N = 2\Lambda/h$ is the number of possible nucleation sites in the representative volume $\lambda\Lambda^2$ allocated to a lamella, and h is the interplanar spacing. The mobile dislocation density, ρ_m, or the ideal shear force, $\hat{\tau}$, can also be taken as an internal variable and made to evolve according to a rate equation. See [108] and [102] for thorough discussions on modeling the deformation mechanisms in crystalline solids.

For an amorphous or semicrystalline polymer, Eq. (4) and (12) can still be employed, with a slightly different interpretation for the quantities involved and keeping in mind that

[2]The Burgers vector is a vector that represents the magnitude and direction of the lattice distortion resulting from a dislocation in a crystal lattice.

the kinetic units are not as precisely defined as in the case of crystalline solids. Thus, the strain rate is still given by

$$\dot{\gamma} = b\rho_m \bar{v}_m, \tag{17}$$

i.e., by the product of the density of kinetic units responsible for the deformation, ρ_m, the amount of displacement per kinetic unit, b, and their average velocity, $\bar{v}_m$. This velocity is approximately given by

$$\bar{v}_m = L\nu_G \exp\left(-\frac{\Delta G(\tau)}{k_B T}\right), \tag{18}$$

where L is the mean free path of the kinetic unit, ν_G is the rate of attempts to move over the obstacle impeding its motion, and the Arrhenius term is the probability that the thermal fluctuations will supply the energy necessary to overcome the obstacle [109, 110]. Finally, one must keep in mind that both the nucleation and velocity-controlled models produce similar expressions, but their interpretations differ [105].

The motion of several different kinetic units contributes to the material's flow behavior, as discussed in Section 3. Ree and Eyring [111] assume that they can be classified based on an average relaxation time that varies significantly between them. A single group is also composed of many kinetic units with different relaxation times, yet can be adequately described by an average value for the group. Assuming that each group behaves according to the previously described Eyring model, the shear stress is expressed as follows

$$\tau = \sum_{k=1}^{n} x_k \tau_k = \sum_{k=1}^{n} x_k \frac{k_B T}{v_k} \sinh^{-1}\left(\frac{\dot{\gamma}}{\dot{\gamma}_0} \exp\left(\frac{\Delta H}{k_B T}\right)\right), \tag{19}$$

where x_k is the area fraction swept by the kth kinetic unit during its movement.

Roetling mentions that the Ree-Eyring model with two flow groups describes the tensile yield strength of PMMA, below the glass transition temperature [112], and isotactic polypropylene (iPP), above the glass transition temperature [113], well in the strain rate range of $10^{-5}\,\mathrm{s}^{-1}$ to $1\,\mathrm{s}^{-1}$. The author suggests a connection between the α and β relaxation transitions and these two flow groups. Other authors have successfully captured the strain rate and temperature dependence of the yield strength of glassy polymers using the Ree-Eyring model and variations thereof [114, 115, 57, 116].

Ree and Eyring's approach allows the inclusion of different deformation mechanisms in the model. In particular, Bauwens, Bauwens-Crowet and collaborators [114, 115, 57]

relate the two flow groups to the α and β relaxation processes, associating the former to the rotations of the main-chain segments of the polymer, and the latter to rotations of side groups. It can be interpreted as a rheological model in which parallel dashpots materialize distinct deformation mechanisms. Furthermore, using the fraction of area swept by each kinetic unit to weight their contribution to the total stress is analogous to popular approaches in semicrystalline polymer modeling, where crystallinity is similarly incorporated (see Section 7.5).

As already noted, kinetic processes are cooperative, occurring only when several kinetic units act in unison. In fact, Cherry and Holmes [117] mention that the fitted values to the activation volume in Eyring's model are too large to agree with their corresponding physical interpretation (see Eq. (2).) As an alternative to the Ree-Eyring model with multiple flow groups, Fotheringham and Cherry [118, 105] assume that n kinetic units, all following the Eyring model, are needed to substantiate a deformation mechanism. The expression found for the flow rate is

$$\dot{\gamma} = \dot{\gamma}_0 \sinh^n \left(\frac{v\tau}{2kT} \right) \exp \left(-\frac{n\Delta H}{kT} \right), \tag{20}$$

where the notation employed retains its meaning from the previous paragraphs, and a temperature below the glass transition temperature is assumed. Richeton and coworkers [119, 120, 121] seek to model the yield stress of amorphous polymers, extending the cooperative model to temperatures through the glass transition temperature. They achieve this by proposing

$$\dot{\gamma} = \dot{\gamma}_0 \exp \left(\frac{\ln 10 \cdot c_1^g (T - T_g)}{c_2^g + T - T_g} \right) \sinh^n \left(\frac{v\tau}{2kT} \right) \exp \left(-\frac{\Delta H}{kT_g} \right), \tag{21}$$

for temperatures above T_g, where c_1^g and c_2^g are the WLF parameters. These authors [122] also compare the models of Eyring (see Eq. (2)), Argon (see Eq. (10)), and their cooperative model in predicting the yield stress of PMMA and PC.

Other models, however, do not fit neatly into the scheme outlined above. Power laws are fairly common empirical laws for the flow rule [123]. They are given, for example, as [16]

$$\dot{\gamma} = \dot{\gamma}_0 \left(\frac{\tau}{\hat{\tau}} \right)^m, \tag{22}$$

where m is a material parameter and $\hat{\tau}$ a reference stress. Perzyna [124], e.g., proposes

$$\dot{\gamma} = \frac{1}{\mu}\left(\frac{\langle \tau - \hat{\tau}\rangle}{\hat{\tau}}\right)^{1/\varepsilon}, \tag{23}$$

to describe the rate sensitivity of plastic materials, where $\langle \bullet \rangle$ denotes the ramp function, defined as $\langle x \rangle = (|x| + x)/2$, and μ and ϵ are material parameters. Another law available for the strain rate is [125, 126]

$$\dot{\gamma} = \dot{\gamma}_0 \exp\left(-\left(\frac{\hat{\tau}}{\tau}\right)^n\right), \tag{24}$$

where n is a material parameter. According to Bodner and Partom [126], this last set of laws is suggested by both direct measurements and theoretical considerations of the average velocity of mobile dislocations as a function of the applied stress in polycrystalline solids (see Eq. (12)).

Yet another model available in the literature, based on reptation [127], is described by Bergström and Boyce [128, 129]. The flow is due in part to the Brownian motion of the polymer chains, in addition to thermally activated events, yielding the following flow rule

$$\dot{\gamma} = C_1(\overline{\lambda} - 1)^{C_2}\left(\frac{\tau}{\hat{\tau}}\right)^m, \tag{25}$$

where $\overline{\lambda}$ is an effective stretch and C_1, C_2, m and $\hat{\tau}$ are material parameters. Bergström and Hilbert [130] later extend this flow adding pressure sensitivity and temperature dependence, as

$$\dot{\gamma} = C_1(\overline{\lambda} - 1)^{C_2}\left(\frac{\tau}{\hat{\tau} + \alpha p}\right)^m \left(\frac{T}{\hat{T}}\right)^n, \tag{26}$$

where $\hat{T}$ is a reference temperature and n a material parameter.

Finally, in the same contribution [130], the authors present yet another flow rule, now of the phenomenological type, given by

$$\dot{\gamma} = ab\,(\varepsilon - \varepsilon_0)^{b-1}\,\dot{\varepsilon} \tag{27}$$

where ε is an effective strain and $\dot{\varepsilon}$ its rate, $a > 0$, $b > 0$. The authors apply this flow rule paired with a yield criterion identical to the von Mises yield function.

According to de Souza Neto and coworkers [131], more flow rules can be generated by multiplying several simpler laws, including those already provided. For example, assuming

that $\dot{\gamma}$ is a function of the stress, time, and temperature, one can write

$$\dot{\gamma} = \dot{\gamma}(\tau, t, T) = f_\sigma(\tau) f_t(t) f_T(T), \tag{28}$$

where f_τ, f_t and f_T are possibly experimentally defined functions.

Internal variables. So far, all constitutive descriptions of the strain rate neglect the material's thermomechanical history. As discussed in more detail in Appendix A, a set of appropriate internal variables is employed to capture the contribution of the material's history to its thermomechanical response [102, 99]. Thus, the implicit assumption so far is either that the structure remains constant during flow, ($\boldsymbol{\alpha} = \boldsymbol{\alpha}_0$), or that it has reached a steady state, ($\dot{\boldsymbol{\alpha}} =$ constant). Either of these hypotheses is often unreasonable and fails to explain the nonlinear behavior of polymers. This shortcoming is evident in the ability to capture the shape of the transient during a constant-strain-rate test, whether the characteristic strain softening of many glassy polymers or the double yield of various semicrystalline polymers. The most common targets of modeling are the athermal strength, $\hat{\tau}$, and the mobile dislocation density, ρ_m, (see Eq. (11) and (12)).

Regarding the athermal strength $\hat{\tau}$, two natural assumptions are that it may depend on the plastic strain γ and time. Thus, by the chain rule, one finds

$$\dot{\hat{\tau}} = h\dot{\gamma} - r, \tag{29}$$

where $h \equiv \partial\hat{\tau}/\partial\gamma|_t$ corresponds to a hardening rate and $r \equiv -\partial\hat{\tau}/\partial t|_\gamma$ denotes a recovery or, in the case of polymers, also an aging rate. Hardening is expected if there is an increase in the number of obstacles to the motion of the kinetic unit [102, 132]. The minus sign in the recovery/aging rate definition is introduced to enforce a decrease in the athermal strength connected to either recovery or aging. That said, Boyce and coworkers [133] conclude that aging in PVC may increase its strength.

Bodner and Partom [134] propose

$$\hat{\tau} = \hat{\tau}_1 + (\hat{\tau}_0 - \hat{\tau}_1) \exp\left(-\frac{m}{\hat{\tau}_0} w^p\right), \tag{30}$$

where $\hat{\tau}_0$ and $\hat{\tau}_1$ are the initial and final athermal strengths, respectively, and m is a material property. Compared with the original text, a multiplicative factor $((n+1)/n)^{1/n}$ is neglected

as it tends to 1 for large n. In the one-dimensional case, the plastic work, w^p, is defined as $\int \tau\dot{\gamma}\ dt$. The corresponding rate equation can be written as [135]

$$\dot{\hat{\tau}} = m\left(\frac{\hat{\tau}_1 - \hat{\tau}}{\hat{\tau}_0}\right)\dot{w}^p. \tag{31}$$

Zaïri and coworkers [135] propose similar rate equations for partial contributions, $\hat{\tau}^{(1)}$ and $\hat{\tau}^{(2)}$, to the athermal strength, $\hat{\tau}$, when modeling glassy polymers. The former concerns the hardening effect of the network alignment, such that the corresponding rate equation is defined as

$$\dot{\hat{\tau}}^{(1)} = m\left(\frac{\hat{\tau}^{(1)} - (1-\alpha)\hat{\tau}_0^{(1)}}{\hat{\tau}_0^{(1)}}\right)\dot{w}^p, \tag{32}$$

where m is material parameter, $\hat{\tau}_0^{(1)}$ is the initial athermal strength and α a hardening parameter. In turn, the latter accounts for the effect of strain softening, with the corresponding rate equation given as

$$\dot{\hat{\tau}}^{(2)} = p\left(\frac{\hat{\tau}_1^{(2)} - \hat{\tau}^{(2)}}{\hat{\tau}_1^{(2)}}\right)\dot{w}^p, \tag{33}$$

where p is a material parameter and $\hat{\tau}_1^{(2)}$ is a final partial athermal strength, such that

$$\dot{\hat{\tau}} = \dot{\hat{\tau}}^{(1)} + \dot{\hat{\tau}}^{(2)}. \tag{34}$$

The solution to both equations can be found by substituting the appropriate values into Eq. (31).

Note that the use of plastic work instead of the plastic strain in the definition of the rate equations just discussed is often equivalent. This is because the mapping between the two can be made one-to-one such that $\hat{\tau}(\gamma) = \tilde{\hat{\tau}}(w^p) \equiv \hat{\tau}(w^p(\gamma))$. See [131] for the complete derivation.

Boyce, Parks and Argon [133] propose an entirely similar rate equation for the athermal strength in a glassy polymer. The corresponding strain softening is described as

$$\dot{\hat{\tau}} = h\left(1 - \frac{\hat{\tau}}{\hat{\tau}_1\left(T, \dot{\gamma}\right)}\right)\dot{\gamma}, \tag{35}$$

employing, however, the strain rate as the 'driving force' behind its change. The initial structure is represented by the value of $\hat{\tau}$ at the upper yield point, $\hat{\tau}_0$, given by Eq. (11), h is the slope of the yield drop with respect to the strain, $\hat{\tau}_1$ is the value of $\hat{\tau}$ reached at the steady state, i.e., the 'preferred' structure, and, as indicated, $\hat{\tau}_1$ may depend on temperature

and strain rate. This choice for the rate equation of the athermal strength enables modeling the distinctive glassy polymer strain softening. They also account for pressure sensitivity by replacing $\hat{\tau}$ by $\hat{\tau} + \alpha p$, where α is a material parameter in Eq. (10).

Hasan et al. [136] propose the use of the softening parameter, D, that evolves to a saturation level, D_∞, according to an identical law, i.e.,

$$\dot{D} = h \left(1 - \frac{D}{D_\infty}\right) \dot{\gamma}, \tag{36}$$

where h is the softening slope. Subtracting D from the argument of the exponential function in Eq. (2), allows the modeling of strain softening.

In their attempt to model semicrystalline polymers, Ahzi and coworkers [137] propose

$$\dot{\hat{\tau}} = \frac{\hat{\tau}}{n} \left(\frac{\hat{\tau}_0}{\hat{\tau}}\right)^n \dot{\gamma}, \tag{37}$$

as the rate equation for the athermal strength $\hat{\tau}$, where $\hat{\tau}_0$ is the corresponding initial value and n is a hardening coefficient.

Seeking to model the effect of manufacturing-induced voids in polymer-based composites, Chowdhury and coworkers [138] present an extension of Eq. (35). It describes the transition from a pre-defined initial yield stress, $\hat{\tau}_0$, to a peak yield stress, $\hat{\tau}_1$, followed by strain softening to a saturated state, $\hat{\tau}_2$. The corresponding rate equation is

$$\dot{\hat{\tau}} = H_1(\gamma) \left(1 - \frac{\hat{\tau}}{\hat{\tau}_1}\right) \dot{\gamma} + H_2(\gamma) \left(1 - \frac{\hat{\tau}}{\hat{\tau}_2}\right) \dot{\gamma}, \tag{38}$$

with the smooth Heaviside-like functions H_i, $i = 1, 2$ given by

$$H_1(\gamma) = -h_1 \left(\tanh\left(\frac{\gamma - \gamma^p}{f\gamma^p}\right) - 1\right); \quad H_2(\gamma) = h_2 \left(\tanh\left(\frac{\gamma - \gamma^p}{f\gamma^p}\right) + 1\right), \tag{39}$$

where h_1 and h_2 are the hardening (softening) parameters, f the smoothing factor and γ^p the plastic strain at the peak yielding point. This approach is also pursued by Hao and coworkers [107], where a fourth athermal shear stress $\hat{\tau}_3$ is considered, connected to the yield of the crystalline phase in a semicrystalline polymer. According to the authors, this property can depend on temperature, strain rate, crystallinity, and humidity. The rate equation for the athermal strength $\hat{\tau}$ is given similarly to Eq. (38) as

$$\dot{\hat{\tau}} = H_1(\gamma) \left(1 - \frac{\hat{\tau}}{\hat{\tau}_1}\right) \dot{\gamma} + H_2(\gamma) \left(1 - \frac{\hat{\tau}}{\hat{\tau}_2}\right) \dot{\gamma} + H_3(\gamma) \left(1 - \frac{\hat{\tau}}{\hat{\tau}_3}\right) \dot{\gamma}, \tag{40}$$

The corresponding smooth functions, H_i, $i = 1, 2, 3$, are given by

$$H_1(\gamma) = -h_1 \left(\tanh \left(\frac{\gamma - \gamma^{p,1}}{f\gamma^{p,1}} \right) - 1 \right), \tag{41}$$

$$H_2(\gamma) = h_2 \left(-\tanh \left(\frac{\gamma - \gamma^{p,1}}{f\gamma^{p,1}} \right) \tanh \left(\frac{\gamma - \gamma^{p,2}}{f\gamma^{p,2}} \right) + 1 \right), \tag{42}$$

$$H_3(\gamma) = h_3 \left(\tanh \left(\frac{\gamma - \gamma^{p,2}}{f\gamma^{p,2}} \right) + 1 \right), \tag{43}$$

where h_1, h_2 and h_3 are the hardening (softening) parameters, f is the smoothing factor, (chosen as 0.3), $\gamma^{p,1}$ is the plastic strains at the peak yielding point, and $\gamma^{p,2}$ is the low yield point just before the yielding of the crystal structure takes place. This last parameter may depend on both the strain rate and the temperature, according to the authors.

Anand and Gurtin [139] propose adding to the athermal strength $\hat{\tau}$ in the power law of Eq. (22) a term αp to account for the influence of pressure, where α is a material parameter and p is the hydrostatic pressure. Additionaly, they take η to be an internal variable in addition to the athermal strength $\hat{\tau}$ following an evolution law

$$\dot{\hat{\tau}} = h_0 \left(1 - \frac{\hat{\tau}}{\hat{\tau}^*(\eta)} \right) \dot{\gamma}, \tag{44}$$

$$\dot{\eta} = g_0 \left(\frac{\hat{\tau}}{\hat{\tau}_{cv}} - 1 \right) \dot{\gamma}, \tag{45}$$

with

$$\hat{\tau}^*(\eta) = \hat{\tau}_{cv}(1 + b(\eta_{cv} - \eta)), \tag{46}$$

where h_0, g_0, b, $\hat{\tau}_{cv}$ and η_{cv} are material parameters. Note the similarities of Eq. (44) with Eq. (35). The authors point out that this differential system has a stable fixed point at $(\hat{\tau}, \eta) = (\hat{\tau}_{cv}, \eta_{cv})$, which corresponds to the steady-state flow condition. Moreover, the phase portrait of the system shows that for initial conditions $\hat{\tau} = \hat{\tau}_0$ and $\eta = 0$, with $\hat{\tau}_0 \leq \hat{\tau} \leq \hat{\tau}_{cv}(1 + b\eta_{cv})$, η increases monotonically to its equilibrium value η_{cv}, while $\hat{\tau}$ first increases to a peak value before decreasing to $\hat{\tau}_{cv}$, capturing the strain-softening behavior of glassy polymers.

Anand and coworkers [140, 141] adopt an expression identical to Eq. (20) describing a cooperative thermally activated motion, where the stress τ is replaced by an effective stress, τ_{eff}, defined as

$$\tau_{\text{eff}} = \tau - (\tau_1 + \tau_2 + \alpha_p p), \tag{47}$$

where τ_1 and τ_2 are internal variables with dimensions of stress, α_p is a material parameter and p is the hydrostatic pressure. Another dimensionless internal variable, η, is also introduced. According to the authors, the variables η and τ_1 are included in the model to capture the 'yield-peak' of glassy polymers. A key microstructural feature controlling the strain-softening associated with the "yield-peak" is the deformation-induced disordering of glassy polymers. The variable η, a positive-valued dimensionless 'order'-parameter, is introduced to represent such deformation-induced disordering; and τ_1, a stress-dimensioned internal variable, represents the corresponding transient resistance to plastic flow accompanying the microstructural disordering. Their evolution equations are coupled similar to those in Eqs. (44) and (45). Their evolution is given by

$$\dot{\tau}_1 = h_1(\tau_1^*(\dot{\gamma}, T, \eta) - \tau_1)\dot{\gamma}, \tag{48}$$

$$\dot{\eta} = g_1(\eta^*(\dot{\gamma}, T) - \eta)\dot{\gamma}, \tag{49}$$

where h_1 and g_1 are material constants, and $\eta^*(\dot{\gamma}, T)$ and $\tau_1^*(\dot{\gamma}, T, \eta)$ are material parameter functions defined as

$$\eta^*(\dot{\gamma}, T) = \begin{cases} \eta_r \left(1 + \left(\dfrac{T_c - T}{k}\right)^r\right) \left(\dfrac{\dot{\gamma}}{\dot{\gamma}_r}\right)^s, & T < T_c, \\ 0, & T > T_c, \end{cases} \tag{50}$$

with

$$T_c = \begin{cases} T_g + n \ln\left(\dfrac{\dot{\gamma}}{\dot{\gamma}_r}\right), & \dot{\gamma} > \dot{\gamma}_r, \\ T_g, & \dot{\gamma} \leq \dot{\gamma}_r, \end{cases} \tag{51}$$

and

$$\tau_1^*(\dot{\gamma}, T, \eta) = b(\eta^*(\dot{\gamma}, T) - \eta). \tag{52}$$

In these expressions, η_r, k, r, s, n, b, and $\dot{\gamma}_r$ are material parameters, and T_g is the glass transition temperature.

The parameter τ_2, is another positive-valued stress-dimensioned internal variable, introduced to capture additional 'isotropic'-hardening aspects of the stress-strain response of these material as the chainsare pulled taut between entanglements at large strains. It evolves according to

$$\dot{\tau}_2 = h_2(\bar{\lambda} - 1)(\tau_2^*(T) - \tau_2)\dot{\gamma}, \tag{53}$$

where h_2 is a material constant, and $\tau_2^*(T)$ a material parameter function of the temperature, such that the resistance τ_2 increases and the material hardens as long as $\tau_2 < \tau_2^*(T)$. $\bar{\lambda}$ is the effective stretch computed from the strain associated with the viscous element described by this flow rule.

In an attempt to model the temperature and rate-dependent response of an incompressible semicrystalline polymer, Okereke and Akpoyomare [142] propose a flow rule

$$\dot{\gamma} = \frac{\tau}{\eta(\tau, p, T, T_f)} = \frac{\tau}{2G\theta(\tau, p, T, T_f)},, \tag{54}$$

where the relaxation time θ is given by

$$\theta(\tau, p, T, T_f) = a_T(T)a_S(T_f)a_\sigma(\tau, p, T)\theta_0^*, \tag{55}$$

with θ_0^* being a reference relaxation time. The influence of temperature is captured through the shift factor a_T as

$$a_T(T) = \exp\left(\frac{\Delta H}{R}\left(\frac{1}{T} - \frac{1}{T^*}\right)\right), \tag{56}$$

where R is the universal gas constant, and the superscript $*$ denotes a reference value. The effect of pressure and shear stress is taken into account through the shift factor a_σ as

$$a_\sigma(\tau, p, T) = \frac{v_s\tau}{2\sqrt{3}RT}\exp\left(-\frac{v_p p}{RT}\right)\left(\sinh\left(\frac{v_s\tau}{2\sqrt{3}RT}\right)\right)^{-1}, \tag{57}$$

where v_s and v_p are material parameters, according to Eyring's theory (see Equations (2) and (5)). The influence of the structure is taken into account through a fictive temperature, T_f, and the corresponding shift factor a_S is given by

$$a_S(T_f) = \exp\left(\frac{\Delta H}{R}\left(\frac{C}{T_f - T_\infty} - \frac{C}{T_f^* - T_\infty}\right)\right), \tag{58}$$

where C is the Cohen-Turnbull constant and T_∞ is the Vogel temperature. The rate equation for the fictive temperature is given by

$$\dot{T}_f = \frac{T - T_f}{a_S(T_f)a_T(T)\theta_0^*} + \frac{\kappa}{\sqrt{2}}\dot{\gamma}, \tag{59}$$

where κ is a material parameter. According to the authors, this choice of the rate equation for the fictive temperature incorporates significant post-yield strain-softening observed in high-rate compression of propylene into the model.

Particle cavitation and void growth. As previously described, a straightforward technique to improve the toughness of amorphous polymers is to incorporate rubber particles into the amorphous polymer matrix. As a result, phenomena such as internal particle cavitation and void growth must be accounted for when modeling the response of these materials. The continuum model approach to this phenomenon usually involves coupling continuum models for amorphous polymers with the well-established Gurson potential [143]. This potential implicitly assumes the presence of two scales: (i) the macroscale, where the material is a continuum, and (ii) the microscale, explicitly accounting for the discrete rubber particles in the polymer matrix and some (potential) initial porosity. To clearly distinguish quantities associated with both scales, the subscript $(\bullet)_\mu$ is adopted to denote microscale fields. Nonetheless, this theory has some limitations, such as the assumption that the voids remain spherical irrespective of the stress state, and it does not predict the evolution of microstructural damage unless an initial non-zero void volume fraction is prescribed. To overcome these limitations, Chu and Needleman [144] proposed a nucleation law, and Tvergaard [145] introduced three heuristic parameters in Gurson's potential to account for the interaction between voids and their growth. The model accounting for both these extensions is known as Gurson-Tvergaard-Needleman (GTN) model, and has been extensively used to predict the behavior of rubber-toughened materials [82, 83, 84].

The GTN potential is defined as

$$\Phi = (\tau^{\text{eq}})^2 + 2 f q_1 (\tau_\mu^{\text{eq}})^2 \cosh\left(\frac{q_2 \tau}{2\sqrt{3}\tau_\mu^{\text{eq}}}\right) - (\tau_\mu^{\text{eq}})^2 (1 + q_3 f^2) = 0\,, \tag{60}$$

where q_1, q_2 and q_3 are the three heuristic parameters, f is the void volume fraction defined as

$$f = \frac{V_\mu^v}{V_\mu}\,, \tag{61}$$

being V_μ^v and V_μ the void and RVE volumes, respectively, τ^{eq} and τ_μ^{eq} are the macroscopic and microscopic equivalent stresses, respectively, and τ is the macroscopic stress.

The evolution of the void volume fraction, $\dot{f}$, is taken to account for both the evolution of the void volume fraction associated with existing voids, $\dot{f}_G$, and the rate of nucleation of new voids, $\dot{f}_{\text{N}}$, as

$$\dot{f} = \dot{f}_G + \dot{f}_N\,. \tag{62}$$

The former evolves with the rate of plastic strain, $\dot{\varepsilon}^p$, as

$$\dot{f}_G = (1 - f)\dot{\varepsilon}^p \,, \tag{63}$$

and the latter as

$$\dot{f}_N = \frac{f_N}{s_N\sqrt{2\pi}} \exp\left[-\frac{1}{2}\left(\frac{\varepsilon^p - \varepsilon_N}{s_N}\right)^2\right]\dot{\varepsilon}^p \,, \tag{64}$$

where f_N is the volume fraction of nucleated voids, and ε_N and s_N are the mean and standard deviation of the plastic nucleation strain.

Since the heuristic parameters introduced by Tvergaard [145] do not account for the evolution of the voids shape explicitly, some studies [146, 82, 147] have modified these parameters to consider the evolution in the geometry of the voids during their growth. Yan et al. [147] proposed a constitutive model for semicrystalline polymers, which accounts for the cavitation damage accumulation associated with the nucleation and growth of voids in the amorphous phase. Building on these developments, Carvalho Alves et al. [85] proposed a constitutive model to predict the nonlinear behavior of neat, porous and rubber-toughened amorphous polymers, accounting for nucleation of the rubber particles as well as the interaction and growth of voids. This model results from a suitable coupling between the extended EGP model [148] with a modified version of the well-established Gurson's potential [143]. Moreover, the model establishes a nucleation law to predict the cavitation of voids in rubber particles under volumetric strains and is combined with the nucleation criterion proposed by Bucknall et al. [149] to identify the material parameters.

Crazing. Crazing is also an important deformation mechanism in amorphous polymers, as it typically precedes brittle fracture. Due to its significance, several authors have focused on characterizing the initiation, growth, and impact of crazing on the overall mechanical behavior and fracture resistance of these materials [150, 84]. In general, two different approaches are employed to describe crazing: (i) using cohesive zone models and (ii) continuum-based models. The former introduces a set of cohesive interface elements in the Finite Element Method discretization, which define the nonlinear behavior in the interface of the craze-amorphous polymer [151, 152, 153, 154]. The latter approach does not explicitly represent individual crazes. Instead, it employs a continuum constitutive relation, where the inelastic

deformation due to crazing is modeled as the averaged response of a Representative Volume Element (RVE) containing plate-like craze structures [155].

Gearing and Anand [155] pioneered the continuum modeling of crazing to avoid the need to represent each craze with special interface elements, which becomes prohibitive when dealing with multiple crazing, as is present in rubber-toughened polymer blends. In their model, once craze initiation occurs[3], the average macroscopic flow becomes oriented in the direction of maximum principal stress, which is characterized by a transition from shear-flow, $\chi = 0$, to craze-flow, $\chi = 1$, by a change in the flow rule, i.e.,

$$\dot{\varepsilon}^p = \begin{cases} \dot{\varepsilon}^p_s \,, & \text{if} \quad \chi = 0 \\ \dot{\xi}^p \,, & \text{if} \quad \chi = 1 \,\text{and}\, \sigma \geq 0 \end{cases} \tag{65}$$

where $\dot{\varepsilon}^p$ is the flow rule, $\dot{\varepsilon}^p_s$ stands for shear-flow rule and $\dot{\xi}^p$ is the macroscopic averaged tensile plastic strain rate, defined by Argon [156] as kinematically related to the lateral transition of a given volume fraction of active craze borders:

$$\dot{\xi}^p = \frac{\dot{\delta}}{h} \,, \tag{66}$$

where $\dot{\delta}$ is the thickening average rate and h is the average spacing of the planar crazes, as schematically illustrated in Fig. 14.

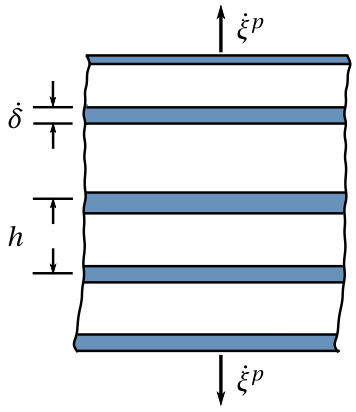

Figure 14: Idealization of craze-plasticity, adapted from [155].

[3]Craze initiation occurs as a consequence of satisfying a given craze initiation criterion.

The macroscopic averaged tensile plastic strain rate, $\dot{\xi}^p$, has been expressed as [155]

$$\dot{\xi}^p = \dot{\xi}_0 \left(\frac{\sigma_1}{s_{\text{craze}}} \right)^{1/m}, \tag{67}$$

where $\dot{\xi}_0$ is a reference craze strain rate, and s_{craze} is a material parameter associated to the resistance to craze-flow, m is the strain-rate sensitivity parameter for craze-flow. The variable $\dot{\xi}_0$ is chosen to ensure continuity of the magnitude of the plastic stretching $|\dot{\varepsilon}^p|$ at the transition from shear-flow to craze-flow. This model has been successfully implemented by several authors [84, 157, 158, 159].

Following this approach, Holopainen [84] proposed a constitutive model for rubber-toughened amorphous polymers that simultaneously accounts for the internal cavitation of rubber particles, the growth of voids, and crazing. The author observed that excessive porosity growth is predicted when crazing evolves in simultaneous with the void volume fraction. As a result, the growth of voids is inhibited once the craze initiation-criterion is satisfied.

Generalization to three-dimensions. The models discussed so far concern one-dimensional flow, i.e., laws for the scalar strain rate $\dot{\gamma}$. For three-dimensional models capable of describing large deformations, it is necessary to provide a macroscopic flow rule, i.e., a law prescribing the spatial velocity gradient $\boldsymbol{L}$.

Consider the flow rule for the Newtonian fluid without the pressure term to see how this might be accomplished for isotropic materials,

$$\boldsymbol{D} = \mathbf{S} : \boldsymbol{\sigma}, \quad \boldsymbol{W} = \mathbf{0}, \tag{68}$$

where $\mathbf{S}$ is the appropriate compliance tensor, defined as

$$\mathbf{S} = \frac{1}{2\eta} \left(\mathbf{I}_S - \frac{1}{3} \boldsymbol{I} \otimes \boldsymbol{I} \right) + \frac{1}{9\kappa} \boldsymbol{I} \otimes \boldsymbol{I}, \tag{69}$$

η and κ are the dynamic and bulk viscosity, and $\mathbf{I}_S$ is the fourth-order symmetric identity tensor. Eq. (68) can be rewritten as

$$\boldsymbol{D} = \frac{\|\boldsymbol{\sigma}_{\text{dev}}\|}{2\eta} \frac{\boldsymbol{\sigma}_{\text{dev}}}{\|\boldsymbol{\sigma}_{\text{dev}}\|} + \frac{\sigma_m}{3\kappa} \boldsymbol{I}. \tag{70}$$

To establish the connection with the one-dimensional flow rules already presented, consider a pure shear flow with a strain rate equal to $\dot{\gamma}$. The shear stress found from Eq. (70) is

$$\tau = \eta\dot{\gamma}. \tag{71}$$

τ is identified with $\|\boldsymbol{\sigma}_{\text{dev}}\|$ to generalize from pure shear to a three-dimensional stress state. Some authors choose this quantitiy to be the octahedral shear stress, defined as $\tau_{\text{oct}} = \frac{1}{\sqrt{3}}\|\boldsymbol{\sigma}_{\text{dev}}\|$, instead [142]. Thus one can substitute $\|\boldsymbol{\sigma}_{\text{dev}}\|/\eta = \dot{\gamma}_{\text{dev}}$, and $\sigma_m/\kappa = \dot{\gamma}_{\text{vol}}$, found employing a similar logic, yielding

$$\boldsymbol{D} = \frac{\dot{\gamma}_{\text{dev}}}{2}\boldsymbol{N}_{\text{dev}} + \frac{\dot{\gamma}_{\text{vol}}}{3}\boldsymbol{N}_{\text{vol}}, \tag{72}$$

where

$$\boldsymbol{N}_{\text{dev}} = \frac{\boldsymbol{\sigma}_{\text{dev}}}{\|\boldsymbol{\sigma}_{\text{dev}}\|}, \quad \boldsymbol{N}_{\text{vol}} = \boldsymbol{I}, \tag{73}$$

Note that τ and p are computed from the Cauchy stress tensor, $\boldsymbol{\sigma}$, acting as the driving force on the viscous element. Other stress measures can also be employed, such as the Kirchhoff stress tensor, $\boldsymbol{\tau}$, or the Mandel stress tensor, $\boldsymbol{M}$ [140, 141].

In the literature, there is not much focus on nonlinear laws for the volumetric strain rate, $\dot{\gamma}_{\text{vol}}$. When included, they are often chosen to coincide with the Newtonian fluid (see Eq. (70)). Most often, the factors 1/2 and 1/3 in Eq. (68) are neglected, perhaps because the flow rule contains a leading term that absorbs the missing elements during calibration.

For constitutive models based on potentials, such as the GTN model described in Eq. (60), the flow rule is given by

$$\tilde{\boldsymbol{D}}^p = \Lambda\frac{\partial\Phi}{\partial\boldsymbol{\tau}}\,, \tag{74}$$

where Λ is a positive scalar function and Φ is the flow potential. In this case, the scalar multiplier, Λ, is determined from the equivalence between the macroscopic plastic power, $\dot{W}^p$,

$$\dot{W}^p = \boldsymbol{\tau} : \tilde{\boldsymbol{D}}^p = \boldsymbol{\tau} : \Lambda\frac{\partial\Phi}{\partial\boldsymbol{\tau}}\,, \tag{75}$$

and the microscopic plastic power, $\dot{W}^p_\mu$, dissipated in the polymer matrix,

$$\dot{W}^p_\mu = (1-f)\boldsymbol{\tau}_\mu : \tilde{\boldsymbol{D}}^p_\mu = (1-f)\tau^{\text{eq}}_\mu\dot{\gamma}_\mu\,, \tag{76}$$

where the viscous flow, $\dot{\gamma}_\mu$, is established based on an adequate flow rule, such as the Eyring flow rule. The equivalence between the macroscopic and microscopic plastic works is a necessary condition to ensure the coherence in the energy dissipation at the two scales.

For semicrystalline polymers, when modeling the plastic flow in the crystalline phase, crystal plasticity models are often employed [38]. In these models, the plastic deformation is assumed to occur by slip on a set of N crystallographic slip systems. The spatial velocity gradient is given by

$$\boldsymbol{L} = \sum_{i=1}^{N} \dot{\gamma}^{(i)} \boldsymbol{R}^{(i)}, \tag{77}$$

where $\dot{\gamma}^{(i)}$ is the shear rate on slip system i, and $\boldsymbol{R}^{(i)}$ is the Schmid tensor for slip system i defined as

$$\boldsymbol{R}^{(i)} = \boldsymbol{s}^{(i)} \otimes \boldsymbol{m}^{(i)}, \tag{78}$$

with $\boldsymbol{s}^{(i)}$ and $\boldsymbol{m}^{(i)}$ being the slip direction and slip plane normal, respectively. The shear rate is found from a flow rule such as Eq. (22), using expressions for the activation energies such as those in Eqs. (13) to (15). Note that this flow rule leads in general to a non-symmetric velocity gradient, or equivalently, a non-zero spin tensor, $\boldsymbol{W} \neq \boldsymbol{0}$.

6.2. Yield criteria

The yield stress is not as clearly defined in polymers as in metals, even far below their melting points. This difficulty in defining yield stress arises because, for many polymers, flow is observed at all stress levels and does not occur at a characteristic yield stress. Notwithstanding, a yield criterion, Φ, can still be used to set the flow rule, defining the flow potential Ψ appropriately. Choosing the flow potential equal to the yield surface, associative plasticity, $\Psi = \Phi$, the flow direction is computed as

$$\boldsymbol{D} = \dot{\gamma}\boldsymbol{N} = \dot{\gamma}\frac{\partial \Phi}{\partial \boldsymbol{\sigma}}, \tag{79}$$

being perpendicular to the yield surface in the stress domain. The choice of $\dot{\gamma}$ in rate-independent plasticity is made to satisfy the loading-unloading conditions

$$\dot{\gamma} \geq 0, \quad \Phi(\boldsymbol{\sigma}, \boldsymbol{A}) \leq 0, \quad \Phi(\boldsymbol{\sigma}, \boldsymbol{A})\dot{\gamma} = 0. \tag{80}$$

However, in the present context, an explicit expression for $\dot{\gamma}$, like the ones presented in Section 6.1, is the most common choice. Ghorbel [160] provides a detailed description of the yield criteria employed to describe polymers. The most common criteria are the von Mises, Mohr-Coloumb, Drucker, and Raghava yield [161] criteria.

6.3. Elastic elements or free energies

The elastic elements employed in the models under discussion typically fit into two classes: linear elasticity and rubber-like elasticity. The former is based on the energy for isotropic linear elasticity in small deformations, given by

$$\psi_{\text{lin}}(\boldsymbol{\varepsilon}) = \frac{1}{2}\boldsymbol{\varepsilon} : \mathbf{D} : \boldsymbol{\varepsilon}, \tag{81}$$

where $\mathbf{D}$ is the isotropic elastic modulus defined as

$$\mathbf{D} \equiv 2G\mathbf{I}_S + \left(K - \frac{2}{3}G\right)\boldsymbol{I} \otimes \boldsymbol{I}, \tag{82}$$

where G is the shear modulus, K is the bulk modulus, $\boldsymbol{I}$ is the second order identity tensor and $\mathbf{I}_S$ is the symmetric identity[4]. One way to extend this model to large deformations is to use finite-strain measures. In particular, one may employ logarithmic strains, $\boldsymbol{\varepsilon}^{(0)}$, finding the so-called Hencky model, whose free energy is given by

$$\psi_{\text{Hencky}}(\boldsymbol{\varepsilon}^{(0)}) = \frac{1}{2}\boldsymbol{\varepsilon}^{(0)} : \mathbf{D} : \boldsymbol{\varepsilon}^{(0)}, \tag{83}$$

or the Green-Lagrange strain tensor, $\boldsymbol{E}^{(2)}$, yielding the so-called Saint-Venant-Kirchhoff model, whose free energy is given by

$$\psi_{\text{SVK}}(\boldsymbol{E}^{(2)}) = \frac{1}{2}\boldsymbol{E}^{(2)} : \mathbf{D} : \boldsymbol{E}^{(2)}. \tag{84}$$

The stress is then found as the derivative of the free energy with respect to the deformation (see Eq. (A.23)). In modeling the intermolecular forces, generally connected with the initial stiffness of the polymer, these are the most common choices for elastic elements [133, 139].

[4]The symmetric identity $\mathbf{I}_S$ is defined as $(\mathbf{I}_S)_{ijkl} = \frac{1}{2}(\delta_{ik}\delta_{jl} + \delta_{il}\delta_{jk})$ where δ_{ij} is the Kronecker delta, such that $\mathbf{I}_S : \boldsymbol{A} = \boldsymbol{A} : \mathbf{I}_S = \text{sym}(\boldsymbol{A})$, with $\boldsymbol{A}$ being a second order tensor.

In modeling the hardening or large strain response of plastic polymers, models based on non-Gaussian statistical theory for rubber-like elasticity are the most common choice [16]. These models are based on the statistical mechanics of polymer chains, which consider the entropy change associated with the deformation of long-chain molecules. From an appropriate expression of the entropy as a function of the deformation, we can find the Helmholtz free energy, ψ, from Eq. (A.22) and derive the constitutive relation from Eq. (A.23). Assuming each chain has many links, $n \gg 1$, and that the end-to-end distance, r, is small compared to the contour length, $r \ll nl$, where l is the length of each link, yields the Gaussian chain model, i.e.,

$$s_{\text{Gaussian}}(\overline{\lambda}) = -\frac{3}{2} N k_B (\overline{\lambda})^2 + \text{const}, \tag{85}$$

where $\overline{\lambda}$ is the average chain stretch defined as $\overline{\lambda} = r/(\sqrt{n}l)$, where $\sqrt{n}l$ is the average end-to-end distance of the chain in the undeformed state, N is the number of chains per unit volume, and k_B is the Boltzmann constant.

When large deformations are being modeled, meaning that r is comparable to nl, non-Gaussian chain models must be employed. The corresponding entropy for a single chain is given by

$$s_{\text{Langevin}}\left(\overline{\lambda}\right) = N k_B \ln\left(\left(\frac{\sinh\beta}{\beta}\right)^n \exp\left(-\frac{\beta}{\lambda^{\text{lock}}}\right)\right), \tag{86}$$

where $\lambda^{\text{lock}} \equiv \sqrt{n}$, $\beta = \mathcal{L}^{-1}(\overline{\lambda}/\lambda^{\text{lock}})$, and the Langevin function is defined by

$$\mathcal{L}(\beta) = \coth\beta - \frac{1}{\beta}. \tag{87}$$

The choice of how the average chain stretch, $\overline{\lambda}$, depends on the deformation gradient varies between models. A three-chain model where a third of all the chains are assumed to be aligned with each of the principal stretches,

$$\overline{\lambda}(\boldsymbol{F}) = \lambda_i, \quad i = 1, 2, 3, \tag{88}$$

has been proposed by Wang and Guth [162].

However, the most widely used model is the eight-chain model of Arruda and Boyce [163, 164], which assumes that there are eight chains aligned with the diagonals of a unit cube in the principal stretch space. This implies that the average chain stretch is given by

$$\overline{\lambda}(\boldsymbol{F}) = \sqrt{\frac{\text{tr}(\boldsymbol{b})}{3}}. \tag{89}$$

As the chain stretch hits its limiting value, this choice for functional dependency results in an asymptotically increasing stress. This same choice when applied to the Gaussian chain model in Eq. (85) leads to the neo-Hookean model, valid for small to moderate deformations [139]. These models can also compute $\bar{\lambda}$ from the isochoric component of the deformation gradient to account for the incompressibility of rubber-like materials. In general, the volumetric response is included in the internal energy (see Eq. (A.22)) [16].

Another alternative of the same type that takes more interactions between the polymer chains is presented by Edward and Vilgis [165], postulating the free energy as

$$\psi_{EV}(\lambda_1,\lambda_2,\lambda_3) = \frac{1}{2}N_c\left\{\frac{\sum_{i=1}^{3}(1-\alpha^2)\,\lambda_i^2}{1-\alpha^2\bar{Z}\lambda_i^2} - \log\left(1-\alpha^2\sum_{i=1}^{3}\lambda_i^2\right)\right\} + \\ + \frac{1}{2}N_s\left[\sum_{i=1}^{3}\left\{\frac{\lambda_i^2(1+\eta)\,(1-\alpha^2)}{(1+\eta\lambda_i^2)\,(1-\alpha^2\sum_i\lambda_i^2)} + \log\left(1+\eta\lambda_i^2\right)\right\} - \log\left(1-\alpha^2\Sigma\lambda_i^2\right)\right], \quad (90)$$

where λ_i are the principal stretches, α is a measure of the inextensibility and η of the slippage, N_c is the number of crosslinks and N_s the number of slip links. The stress is found from the constitutive relation in Eq. (A.20).

6.4. Caveats regarding the generalization to three-dimensions and large deformations

Before proceeding, some comments on developing a fully three-dimensional large-strain model from a one-dimensional rheological model are in order. When considering only infinitesimal strains, the strain applied to elements in series is added together, whereas elements in parallel are subjected to the same strain. For example, for the model in Fig. 15, the strain across the elements on the first branch is decomposed additively, $\boldsymbol{\varepsilon} = \boldsymbol{\varepsilon}^e + \boldsymbol{\varepsilon}^p$, being the same across both branches. A suitable kinematic decomposition must be chosen to achieve an appropriate generalization to three dimensions and large deformations. The classical Lee multiplicative decomposition of the deformation gradient [166, 167] is the most common choice,

$$\boldsymbol{F} = \boldsymbol{F}^e\boldsymbol{F}^p, \quad (91)$$

where $\boldsymbol{F}$ is the deformation gradient and superscripts e and p correspond to the elastic and plastic parts. In practice, elements in parallel will experience the same strain gradient, whereas elements in series will divide the deformation using a multiplicative decomposition.

See Fig. 15 for reference. Since, in general, the deformation gradients do not commute, the choice of order is relevant.

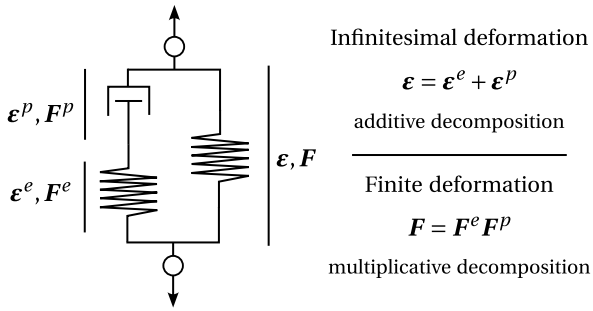

Figure 15: Additive and multiplicative strain decomposition corresponding to infinitesimal and finite deformations, respectively.

Focusing on a decomposition between an elastic, denoted here by e, and a viscous element, denoted here by p, the application of the decomposition in Eq. (91) to the definition of the spatial velocity gradient (see Appendix A.1) yields

$$\boldsymbol{L} = \boldsymbol{L}^e + \boldsymbol{F}^e \boldsymbol{L}^p (\boldsymbol{F}^e)^{-1}, \tag{92}$$

where $\boldsymbol{L}^e$ and $\boldsymbol{L}^p$ are defined as

$$\boldsymbol{L}^e = \boldsymbol{F}^e (\boldsymbol{F}^e)^{-1}, \tag{93}$$

$$\boldsymbol{L}^p = \boldsymbol{F}^p (\boldsymbol{F}^p)^{-1}. \tag{94}$$

The deformation gradient may also be expressed as the product of the elastic stretch, the rotation, and the plastic stretch, as

$$\boldsymbol{F} = \boldsymbol{V}^e \boldsymbol{R} \boldsymbol{U}^p \,, \tag{95}$$

where $\boldsymbol{R} = \boldsymbol{R}^e \boldsymbol{R}^p$.

The constitutive description is most often supplied as a law for $\boldsymbol{D}^p$ and $\boldsymbol{W}^p$, where

$$\boldsymbol{D}^p = \mathrm{sym}(\boldsymbol{L}^p), \quad \boldsymbol{W}^p = \mathrm{skew}(\boldsymbol{L}^p). \tag{96}$$

A common approach is [131]

$$\bar{\boldsymbol{D}}^p \equiv (\boldsymbol{R}^e)^T \boldsymbol{D}^p \boldsymbol{R}^e = \dot{\gamma}_{\mathrm{dev}} \boldsymbol{N}_{\mathrm{dev}} + \dot{\gamma}_{\mathrm{vol}} \boldsymbol{N}_{\mathrm{vol}}, \tag{97}$$

$$\bar{\boldsymbol{W}}^p \equiv (\boldsymbol{R}^e)^T \boldsymbol{W}^p \boldsymbol{R}^e = \boldsymbol{0}, \tag{98}$$

with $\boldsymbol{R}^e$ defined by the polar decomposition theorem as $\boldsymbol{F}^e = \boldsymbol{R}^e\boldsymbol{U}^e$, where $\boldsymbol{N}_{\text{dev}}$ and $\boldsymbol{N}_{\text{vol}}$ are given by Eq. (73) and $\dot{\gamma}_{\text{dev}}$ is found from the laws described in Section 6.1. This yields the plastic spatial velocity gradient as

$$\boldsymbol{L}^p = (\boldsymbol{R}^e)^T(\dot{\gamma}_{\text{dev}}\boldsymbol{N}_{\text{dev}} + \dot{\gamma}_{\text{vol}}\boldsymbol{N}_{\text{vol}})\boldsymbol{R}^e. \tag{99}$$

Assuming isotropic plasticity, allows us to remove the rotation from the flow rule [131], yielding for the plastic spatial velocity gradient

$$\boldsymbol{L}^p = \dot{\gamma}_{\text{dev}}\boldsymbol{N}_{\text{dev}} + \dot{\gamma}_{\text{vol}}\boldsymbol{N}_{\text{vol}}, \tag{100}$$

and, equivalently, for the elastic spatial velocity gradient we have

$$\boldsymbol{L}^e = \boldsymbol{L} - (\dot{\gamma}_{\text{dev}}\boldsymbol{N}_{\text{dev}} + \dot{\gamma}_{\text{vol}}\boldsymbol{N}_{\text{vol}}). \tag{101}$$

An alternative description can be given as

$$\frac{1}{2}\mathcal{L}_v\boldsymbol{b}^e = -(\dot{\gamma}_{\text{dev}}\boldsymbol{N}_{\text{dev}} + \dot{\gamma}_{\text{vol}}\boldsymbol{N}_{\text{vol}})\boldsymbol{b}^e, \tag{102}$$

where $\mathcal{L}_v\boldsymbol{b}^e$ is the Lie derivative of $\boldsymbol{b}^e$ with respect to the velocity field $\boldsymbol{v}$. In particular, Reese and Govindjee [168] explore isotropic finite viscoelasticity employing Newtonian viscous elements as given by Eq. (68) and Eq. (69). The same authors highlight that this approach implies truly finite viscoelasticity, i.e., valid for large deformations and large perturbations away from thermodynamic equilibrium. They point out that an intermediate description, allowing for large deformations but constrained to small deviations from thermodynamic equilibrium, is also possible. Thus linearizing Eq. (102) yields

$$\dot{\boldsymbol{C}}^p = \frac{1}{\theta}(\boldsymbol{C} - \boldsymbol{C}^p), \tag{103}$$

where θ is a relaxation time. Note the similarities with Eq. (A.43) describing the evolution of $\boldsymbol{\varepsilon}^p$ in infinitesimal viscoelasticity. Accordingly, the $\boldsymbol{C}^p$ is given by a convolution integral. This possibility had already been pointed out by Coleman and Noll [169]. A similar approach is pursued by Simo [170], where the internal variables are the nonequilibrium forces acting on the different arms of the rheological model.

One can also and prescribe a law for $\boldsymbol{D}^p$ directly [133],

$$\boldsymbol{D}^p = \dot{\gamma}_{\text{dev}} \boldsymbol{N}_{\text{dev}} + \dot{\gamma}_{\text{vol}} \boldsymbol{N}_{\text{vol}}, \tag{104}$$

$$\boldsymbol{W}^p = \boldsymbol{W} - \mathcal{W} : (\boldsymbol{D} - \boldsymbol{D}^p), \tag{105}$$

where $\mathcal{W}$ is a fourth-order spin tensor whose full description is given by Onat [171]. This is necessary because the authors assumed that the rotation tensor, $\boldsymbol{R}$, is entirely plastic, i.e., $\boldsymbol{R} = \boldsymbol{R}^p$. As a consequence, the model attributes all rotation effects to plastic deformation. This results in a symmetric, and therefore unique, elastic deformation gradient, $\boldsymbol{F}^e = (\boldsymbol{F}^e)^T$. The spin tensor, $\boldsymbol{W}^p$, is thus required to sustain the adopted symmetry of $\boldsymbol{F}^e$.

Finally, we can also follow Bergström [16]

$$\tilde{\boldsymbol{D}}^p \equiv \text{sym}((\boldsymbol{F}^e)^{-1} \boldsymbol{L}^p \boldsymbol{F}^e) = \dot{\gamma}_{\text{dev}} \boldsymbol{N}_{\text{dev}} + \dot{\gamma}_{\text{vol}} \boldsymbol{N}_{\text{vol}}, \tag{106}$$

$$\tilde{\boldsymbol{W}}^p \equiv \text{skew}((\boldsymbol{F}^e)^{-1} \boldsymbol{L}^p \boldsymbol{F}^e) = \boldsymbol{0}, \tag{107}$$

which is equivalent to Eq. (97) if elastoplastic isotropy [131] is assumed.

6.5. Inclusion of the thermal field

Including temperature-dependent material parameters is insufficient to account for the thermal field when using constitutive descriptions based on rheological models. The first missing feature of such a model is that a change in temperature with null stress would not lead to contraction or dilation. Similarly, a temperature change while preventing expansion/contraction would lead to zero stress. To fix this omission, an additional thermal configuration can be considered, e.g.,

$$\boldsymbol{F} = \boldsymbol{F}^{\text{mech}} \boldsymbol{F}^{\text{th}}, \tag{108}$$

where $\boldsymbol{F}^{\text{mech}}$ and $\boldsymbol{F}^{\text{th}}$ are the deformation gradients concerning only the mechanical and temperature fields, respectively. Note that the reverse order for the deformation gradients can be considered, as well as decompositions where the thermal deformation gradient is applied between elastic and plastic deformation gradients [164].

When employing the models described so far, consider that an increase in the temperature with no mechanical loading applied leads to a null stress response from the 'mechanical

part', thus, its corresponding deformation gradient will be unitary, making the total deformation gradient equal to the thermal deformation gradient, $\boldsymbol{F} = \boldsymbol{F}^{\text{th}}$. Taking inspiration from isotropic infinitesimal thermoelasticity theory, we can write

$$\boldsymbol{\varepsilon}^{\text{th}} = \alpha_{\boldsymbol{\varepsilon}} \Delta T \boldsymbol{I}. \tag{109}$$

Lu and Pister [172] suggest, however,

$$\boldsymbol{F}^{\text{th}} = \upsilon(T)\boldsymbol{I}, \tag{110}$$

where υ is a scalar-valued function of temperature, reflecting intrinsic thermal expansion characteristics of the material

$$\upsilon(T) = \exp\left[\int_{T_0}^{T} \alpha_{\boldsymbol{F}}(T^*)\, dT^*\right], \tag{111}$$

where α is the coefficient of thermal expansion, allowed to depend on the temperature. In particular, if $\alpha_{\boldsymbol{F}}$ is independent of temperature, Eq. (111) reduces to

$$\upsilon(\Delta T) = \exp(\alpha_{\boldsymbol{F}} \Delta T). \tag{112}$$

Further, if the conditions for infinitesimal thermal strain are satisfied, i.e., $\alpha_{\boldsymbol{F}} \Delta T \ll 1$, we recover Eq. (109).

Considering the energy balance equation (Eq. (A.28)), the internal dissipation and the Gough-Joule effect still need to be added to the present analysis. In the one-dimensional rheological model, the dissipation is due to the linear dashpots,

$$\mathcal{D}^i_{\text{int}} = \sigma^i \dot{\gamma}^i, \tag{113}$$

where $\dot{\gamma}^i$ and σ^i are the strain rate and stress in the dashpot i. In three dimensions, this rational yields

$$\mathcal{D}^i_{\text{int}} = \chi_{\text{d}} \boldsymbol{\sigma}_i : \boldsymbol{D}^i, \tag{114}$$

where $\boldsymbol{\sigma}^i$ is the Cauchy stress tensor across the ith viscous elements and $\boldsymbol{D}^i$ the corresponding rate of deformation tensor. $\chi_{\text{d}} \in [0, 1]$ is a constant dissipation factor, commonly chosen in the range $\chi_{\text{d}} \approx 0.85$ to 0.95 for metals [173] and equal to 1 for polymers [142, 174]. The

possibility of $\chi_d < 1$ materializes the fact that some plastic work may be stored in the material.

Concerning the temperature dependence of material parameters more broadly, several authors try to include it in their models, in general, through simple linear [148] or exponential dependencies [164, 130]

Remark 1 (Single integral models). *One approach that seeks to generalize the results of infinitesimal viscoelasticity is based on the integral constitutive equation for the stress as a function of the strain in Eq. (A.31). These models include nonlinear phenomena while considering only small strains [12]. For example, the model of Pipkin and Rogers is given by [12]*

$$\sigma(t) = \int_{-\infty}^{t} R(t-\tau, \varepsilon(\tau)) \frac{\partial \varepsilon}{\partial \tau} \, d\tau, \tag{115}$$

where R is a nonlinear stress relaxation modulus depending on time and strain, incorporating nonlinear effects into the material's infinitesimal viscoelastic constitutive description.

A list of models of this type, including Leaderman, Pipkin and Rogers; Schapery; and Bernstein, Kearsley and Zapas (BKZ), can be found in [12] and [175]. This class of models is not given much attention in this text since, due to their formulation in terms of convolution integrals with non-trivial kernels, they are not particularly appropriate for application in computational mechanics based on the FEM.

7. Continuum models for thermoplastic polymers

This section outlines the most common continuum models for the description of the mechanical behavior of polymers found in the literature. Given that much of the models' ability to describe the experimental behavior of the polymers relies on the structural arrangement of the its rheological elements, i.e., whether elements are arranged in series or in parallel, we bin the different models according to a classification based on the underlying linear model. The next set of models generalizes various infinitesimal viscoelastic models by using the previously described nonlinear elements in the corresponding rheological models.

7.1. Maxwell model

The Maxwell model is given as

$$\sigma + \frac{\eta}{E}\dot{\sigma} = \eta\dot{\varepsilon}, \tag{116}$$

corresponding to the rheological model in Fig. 16. It is able to model stress relaxation

Figure 16: Rheological model corresponding to the Maxwell model.

and creep, but not time-dependent recovery. In a constant-strain experiment, it attains a plateau stress and only captures hardening through internal variables in the description of the flow rule.

An early improvement to describe the large-strain behavior of elastomers is presented by Smith [176]. The Bodner-Partom material model [134] is another generalization of the same constitutive description. It can simulate the behavior of a visco-elastoplastic material under small strains and arbitrary loading history. The elastic element obeys Hooke's law, and the flow rule is given by Eqs. (24) and (104), with the athermal strength evolving according to Eq. (31). The model can describe a rate-sensitive response and hardening. However, it cannot display strain recovery. Based on this work, the rate equations in Eq. (34) for $\hat{\tau}$, in conjunction with a power law (see Eq. (22)), have been used in models describing poly(methyl methacrylate) (PMMA), a glassy polymer, by Zaïri and coworkers [177, 135, 82], to describe HDPE by Zhang and Moore [178], and to describe PC by Frank and Brockman [179]. It has also been used to model the behavior of metallic alloys at high temperatures [131].

In the same vein, Ben Hadj Hamouda and coworkers [47] employ a Double Inelastic Deformation (DID) model—whose background is described in detail by Cailletaud and Saï [180]. Formulated in small strains, an additive split is assumed between a linear strain and two viscoplastic strains, corresponding to the deformation mechanism in the amorphous and crystalline phases. Each viscoplastic strain follows a power law (see Eq. (22)) with a von

Mises yield criterion, accounting also for nonlinear kinematic hardening. The authors use it to model MDPE response in constant-strain-rate uniaxial tension experiments, as well as in stress-relaxation and dip tests. Balieu and coworkers [161] also present a model that can be interpreted as a nonlinear Maxwell model. It is formulated using hypoelasticity, with the plastic flow rule deduced from Raghava's criterion, modified to include an isotropic damage variable representing micro-voids and micro-cracks developed in the material. The law for the strain rate is a power law (see Eq. (22)), and the authors employ an integral-type nonlocal damage model to describe mineral-filled semicrystalline polymers.

In the work developed by Doghri et al. [181, 182, 183, 184], a constitutive model that couples viscoelasticity and viscoplasticity is also proposed. In their contributions, the elastic spring of the standard Maxwell model is replaced by a generalized Maxwell model, effectively allowing the modeling of viscoelasticity. The associated stress is expressed as a Boltzmann integral, and the visco-elastic relaxation moduli follow the general Prony series (Eq. (A.42)). In Krairi and Doghri [182], the visco-plastic response combines isotropic and nonlinear kinematic hardening. Moreover, a ductile damage evolution is implemented, with this variable linked to the visco-plastic strains. Krairi et al. [184] extended the model proposed by Miled et al. [181] by including the model into a thermo-mechanical coupled framework, such that it couples visco-elasticity and visco-plasticity under non-isothermal loading conditions.

7.2. Standard Linear Solid

The following set of models is a generalization of the so-called standard linear solid model. In the context of infinitesimal viscoelasticity, it can be expressed in equivalent ways in its Maxwell or its Kelvin-Voigt representation, as shown in Fig. 17 with the constitutive differential equations for the stress and the strain given as

$$\sigma + \frac{\eta}{E_2}\dot{\sigma} = E_1\varepsilon + \frac{\eta\,(E_1+E_2)}{E_2}\dot{\varepsilon}, \quad \text{(Maxwell representation)}, \tag{117}$$

$$\sigma + \frac{\eta}{E_1+E_2}\dot{\sigma} = \frac{E_1E_2}{E_1+E_2}\varepsilon + \frac{E_1\eta}{E_1+E_2}\dot{\varepsilon}, \quad \text{(Kelvin-Voigt representation)}, \tag{118}$$

where in both equations, the terms containing the strain, ε, are the stress response in equilibrium. For linear viscoelastic materials, both representations are equivalent. However, when nonlinear elements are introduced, the two representations generally yield different

results. That said, these models can display stress relaxation with a plateau value, creep with a plateau strain, and time-dependent full recovery. In a constant-strain experiment, no steady-state stress is reached, allowing hardening even without internal variables beyond the viscous strain.

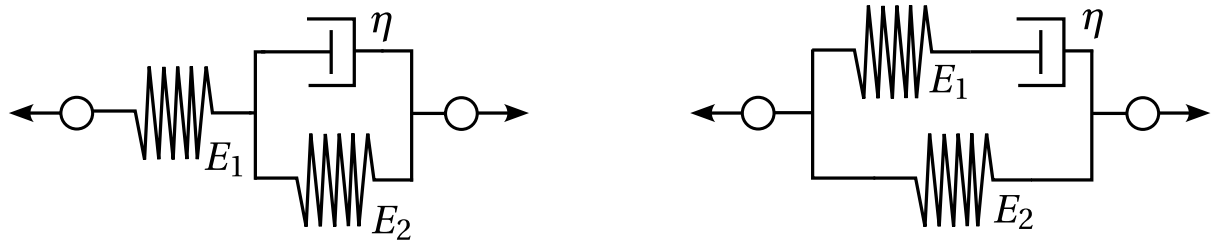

(a) (b)

Figure 17: Rheological model for the standard linear solid: a Maxwell representation; b Voigt representation.

The viscoplasticity theory based on overstress (VBO) was introduced by Cernocky and Krempl [185] and is based on the standard linear solid. The so-called overstress is the difference between the full stress and the equilibrium part, which is allowed to be a nonlinear function of the strain. Thus, Equations (117) and (118) can be written as

$$\sigma - f(\varepsilon) = M\dot{\varepsilon} - K\dot{\sigma}, \tag{119}$$

where f may be a nonlinear function of the strain, and M and K are general functions of the stress, the strain, and their derivatives. It has been used to successfully model metals [186, 187] as well as polymers, such as polypropylene [188], polyethylene [189], nylon 66, polyetherimide, poly(ether ether ketone) [190], and polyphenylene oxide (PPO) [191]. More advanced versions of this approach include kinematic and isotropic hardening and strain softening through appropriate internal variables [190, 192].

Polanco-Loria and coworkers [70] present a generalization that allows for a hyperelastic-viscoplastic response due to intermolecular resistance and an entropic hyperelastic response due to molecular chain reorientation. The stress in the Maxwell branch is determined from an isotropic compressible Neo-Hookean material (see Eq. (85)). At the same time, the flow in the dashpot is controlled by Raghava's yield criterion, which is pressure sensitive (see Section 6.2). A non-associative viscoplastic flow potential is employed, allowing for

volumetric plastic strain. Finally, the eight-chain model provides the deviatoric part of the stress on the other branches, including a volumetric part similar to that shown in Eq. (73) for the Neo-Hookean model. The authors validated their models against experimental results obtained for polypropylene samples.

That said, the most popular thermoplastic models are generalizations of the Voigt version of the standard solid. Halsey and coworkers [193] present one of the earliest contributions considering an Eyring dashpot as the viscous element in an attempt to model the behavior of fibers. Likewise, Haward and Thackray [194] proposed one of the first models for thermoplastic polymers below the glass transition temperature. The elastic element in the Maxwell branch is still a linear spring. However, the elastic element parallel to it is a Langevin spring, while the viscous element is an Eyring dashpot. The model is formulated assuming small strains and is restricted to one-dimensional loading.

Later, Boyce, Argon, and Parks [133] generalized this model, now known as the BPA model, to three dimensions, among other additions. A multiplicative kinematic split between the elastic and inelastic deformation is enforced, as described in Section 6.4. The linear spring is generalized to three dimensions and large deformation using the Hencky model (see Eq. (83)), with the shear and bulk moduli temperature-dependent. The thermally activated process is now nucleation controlled by employing the model proposed by Argon [106] (see Eq. (10)) with the addition that the athermal strength $\hat{\tau}_0$ is replaced by an internal variable, $\tilde{\tau}$, which is given by $\tilde{\tau} = \hat{\tau} + \alpha p$ and α is a material property. The rate equation for the athermal strength, $\hat{\tau}$, is chosen according to Eq. (35), such that the distinctive strain softening of glassy polymers is captured. The model does not account for volumetric flow. Lastly, the three-chain model gives the stress in the other elastic element (see Eq. (88)), responsible for the strain hardening. For other contributions exploring this model while employing different rubber-like elasticity models, see, e.g., [163, 164, 195, 196, 197]. In fact, the most widely used model of this type is the so-called Arruda-Boyce model [163, 164], which employs an eight-chain model for the rubber-elastic element.

Arruda et al. [164] extended the BPA model to the moderate strain rate domain, by considering a thermomechanical coupled framework with isotropic thermal expansion, and by incorporating an internal state variable associated with the temperature-evolution of

the density of the weak entanglements. Bergström and Boyce [128, 198] also modified the BPA model to describe the response of elastomeric materials and filled elastomers. Their modification is based on a rheological decomposition into two parallel polymer networks: one capturing the equilibrium response, the branch containing the elastic spring, and the other describing the time-dependent deviation from equilibrium, the Maxwell branch. The flow rule adopted for the dashpot is given by Eq. (25), inspired by the reptation theory of polymer dynamics [127], with both elastic elements modeled employing the eight-chain model (see Eq. (86)). The influence of filler particles is modeled by amplifying the scalar equivalent values of stretch and shear stress, effectively providing adjusted measures of matrix stretch and matrix shear stress.

Also expanding on the BPA model [133], Chowdhury and coworkers [138] propose a very similar model in the context of manufacturing-induced voids in polymer-based composites, formulated, however, hypoelastically. The model was later validated on epoxy resins by Poulain and coworkers [199]. As in the BPA model, the athermal strength (Eq. (10)) is taken as an internal variable following a different rate equation (Eq. (38)). This choice allows a smoother strain softening. Also, the response of the rubber-elastic element is now a linear combination of the response obtained from a three-chain model (Eq. (88)) and an eight-chain model (Eq. (86)). Hao and coworkers [107] propose a very similar model, where the rate equation for the athermal strength is given by Eq. (40), rendering a model able to capture the double yield phenomenon in semicrystalline polymers. The last authors also consider the thermomechanical aspects of polymer modeling, including self-heating, thermal softening, and temperature-dependent properties. They validate their model against experimental results obtained for epoxy, nylon101, and PA6.

Richeton and coworkers [121] also present a model based on the standard linear solid. Where the hardening spring is modeled employing the eight-chain model (see Eq. (86)) and the flow rule is adopted as Eq. (20) for flow below the glass transition temperature and Eq. (21) above it. The authors compare their model against experimental results for PMMA and PC samples subject to compression tests at different strain rates and temperatures.

Employing a similar arrangement of rheological elements as the BPA model, Mirkhalaf et al. [200] proposed a finite strain elasto-visco-plastic constitutive model to predict the

nonlinear behavior of amorphous polymers. Although the model operates within a finite strain framework, it is implemented using a formulation based on the functional structure of the infinitesimal strain regime. Within this context, the state update procedure and the consistent tangent operator are pre- and post-processed by a purely kinematic finite strain extension [201]. Besides its simplicity, this type of extension preserves the most important properties of the infinitesimal strains formulation, namely volume-preserving plastic deformations and finite plastic incompressibility. In this context, instead of adopting the left Cauchy-Green strain tensor as the strain measure, the logarithmic strain tensor is used, $\boldsymbol{\varepsilon} = \frac{1}{2} \ln \boldsymbol{B}$. It is worth highlighting that the use of the additive approximation of the logarithmic strains, also known as Green plasticity, significantly simplifies the computational implementation of this constitutive model. Moreover, this approximation is associated with a negligible error under moderately small elastic strains [202]. Note that an alternative formulation based on elastic corrector rates has been recently proposed [203, 204, 205] to handle this additive update. In the work developed by Mirkhalaf et al. [7], this model was further extended to capture the material's behavior under different triaxial states. Within this context, the strain-softening and strain-hardening constitutive laws have been modified to account for the stress triaxiality and the lode angle.

Recently, the model proposed by Mirkhalaf et al. [200] was extended to account for visco-elasticity [148]. In this context, the elastic spring parallel to the Maxwell branch is replaced by a generalized Maxwell model, where the shear relaxation modulus follows a Prony series as given in Eq. (A.42). Since this falls under the umbrella of Finite Linear Visco-elasticity theory, which is based on a single stored energy [170, 206, 207], this choice alone does not lead to strain rate dependency. This is accounted for through the material parameters in the Prony series. As a result, the visco-elastic relaxation times are considered dependent on the strain rate, following the evolution law introduced by Yu et al. [208]:

$$\theta_i(\dot{\varepsilon}^{\mathrm{eq}}) = \theta_{i,T} \, (\dot{\varepsilon}^{\mathrm{eq}})^{-\lambda_{g,i}} \,, \qquad i = 1, \, \ldots, \, n_{\mathrm{V}} \,, \tag{120}$$

where $\theta_{i,T}$ is constant, $\lambda_{g,i}$ represents the shear relaxation time strain rate sensitivity, and the spatial logarithmic equivalent strain rate is given by $\dot{\varepsilon}^{\mathrm{eq}} = \sqrt{\frac{2}{3}} \overline{\| \boldsymbol{\varepsilon} \|}$, with $\overline{(\bullet)}$ denoting the time derivative.

Holopainen et al. [209, 210] extended the BPA model to propose a thermodynamically consistent approach that describes the isothermal ductile fatigue damage in amorphous polymers. Wang et al. [211] extended the effective temperature model proposed by Xiao and Nguyen [212] to develop a large deformation model that accurately captures the temperature-dependent and strain rate-dependent post-yielding strain hardening behavior as well as the Bauschinger effect under reversed loading. In this model, the Eyring model is applied to characterize the temperature-dependence and strain rate-dependence of the viscous resistance to network deformation, and the Arruda-Boyce eight-chain model [163] is used to describe the internal energy associated with network deformation to account for the limiting stretch of the network structure.

Uchida et al. [213] developed a visco-elastic visco-plastic model grounded in the physics of polymer chain deformation. Building on their earlier work [214], they extended the model to incorporate the temperature- and strain rate-dependent mechanical behavior observed below the glass transition temperature.

Another significant contribution to the constitutive modeling of amorphous polymers was proposed by Leonov [215], now based on the Maxwell representation of the standard linear solid. This model was later extended to a compressible version by Baaijens [216], and later derived within a thermodynamically consistent framework by Tveroort et al. [217]. In addition, to capture the typical behavior of the post-yield region of amorphous polymers, namely the phenomenon of strain-softening and strain hardening, this model was extended by Timmermans and Govaert [218, 219], leading to the generalized compressible Leonov model, currently known as the Eindhoven Glassy Polymer (EGP) model.

Khaleghi et al. [220] extended the EGP model with a thermodynamically consistent damage model based on the damage evolution law introduced by Lemaitre [221]. The Oxford Glass Rubber (OGR) model [196] is structurally similar to the EGP model, but the resistance to entropy-elastic chain stretch is described by the Edwards-Vilgis free energy function [165]. In the work of van Breemen et al. [222], the single-mode EGP model is extended to a multi-mode constitutive model. This extension assumes that the pre-yield response is governed by a spectrum of linear relaxation times, which shift to shorter timescales under the influence of applied stress.

Models originally developed for polymers have also been further extended and adapted for composite materials. For instance, in the work developed by Amiri-Rad et al. [223], the EGP model is extended to establish an anisotropic visco-elastic visco-plastic macromechanical framework specifically tailored for short-fiber reinforced polymers, capturing the direction-dependent behavior introduced by fiber orientation. In a related effort, Nciri et al. [224] proposed a continuum model for short-fiber-reinforced composites that incorporates visco-elastic and visco-plastic behavior of the amorphous polymer matrix, with particular emphasis on complex fiber orientation distributions and rate-dependent effects.

Although not explicitly making reference to a rheological model, Anand and Gurtin [139] present a constitutive model for glassy polymers that can also be interpreted as a generalization of the standard linear solid in its Kelvin-Voigt representation. The elastic element in series is modeled employing the Saint-Venant-Kirchhoff model (see Eq. (84)), while the flow rule is by a power law (Eq. (22)), employing internal variables to capture strain softening and hardening (see Eq. (44)). The corresponding backstress is modeled for small to moderate strains employing a Neo-Hookean model (see Eq. (85)), and a non-Gaussian network model (see Eq. (86)) for large strains. The authors validate their model against experimental data in uniaxial compression for PC.

Some of the same authors [140, 141] propose an improvement on this model, now with the rheological representation depicted in Fig. 18. A flow rule based on the cooperative model (see Eq. (20)) is now adopted for the viscous element, while the internal variables follow the evolution laws in Eq. (48), capturing strain softening and hardening. Bouvard et al. [225] proposed a finite strain thermomechanical visco-plastic model with thermal expansion to predict the behavior of amorphous polymers. The model is derived adopting a formulation based on internal variables very similar to that of Anand and coworkers [140, 141]. This model was recently extended by Lan et al. [226], by dividing the molecular entanglements into permanent entanglements and dynamic entanglements, as introduced by Jiang et al. [227, 228].

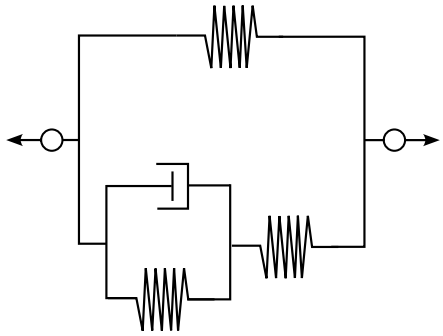

Figure 18: Rheological model for the Anand-Ames model [140, 141].

7.3. Burgers material

Another common material model in infinitesimal viscoelasticity is the so-called Burgers material, which incorporates viscous flow into the standard linear solid model. It also accepts two equivalent descriptions as

$$\sigma + \left(\frac{\eta_1}{E_1} + \frac{\eta_2}{E_2}\right)\dot{\sigma} + \frac{\eta_1\eta_2}{E_1E_2}\ddot{\sigma} = (\eta_1+\eta_2)\,\dot{\varepsilon} + \frac{\eta_1\eta_2\,(E_1+E_2)}{E_1E_2}\ddot{\varepsilon} \quad \text{(Maxwell representation)}, \tag{121}$$

$$\sigma + \left(\frac{\eta_1}{E_1} + \frac{\eta_2}{E_1} + \frac{\eta_2}{E_2}\right)\dot{\sigma} + \frac{\eta_1\eta_2}{E_1E_2}\ddot{\sigma} = \eta_2\dot{\varepsilon} + \frac{\eta_1\eta_2}{E_1}\ddot{\varepsilon} \quad \text{(Kelvin-Voigt representation)}, \tag{122}$$

in the context of small strains. See Fig. 19 for the corresponding rheological models.

Bardenhagen and coworkers [229] propose a three-dimensional viscoplastic model for polymeric materials, which is a generalization of the Maxwell representation of the Burgers material. One of the branches is a three-dimensional, large-strain hypoelastic generalization of the Maxwell model. The other branch employs an associative hypoelastic elastoplastic model with the von Mises criterion as the yield criterion, including an isotropic hardening

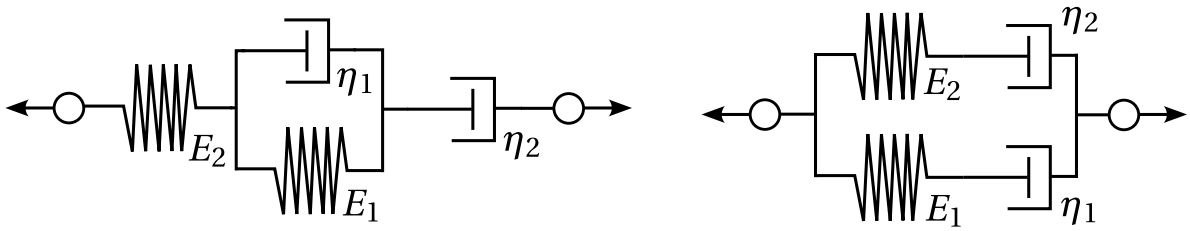

(a) (b)

Figure 19: Rheological model for the Burgers material. a Maxwell representation. b Voigt representation.

function. The authors provide a comparison with experimental results.

Boyce and coworkers [230] also present a model generalizing the Maxwell representation of the Burgers material. One of the branches contains an elastic element following Hencky's model (see Eq. (83)) and an Eyring dashpot, in the same way as the model already described in [133]. In the other branch, the elastic element follows the eight-chain model (see Eq. (86)), while the dashpot is similar to the Bergström-Boyce model (see Eq. (25)). It is used by the authors to model poly(ethylene terephthalate) above the glass transition temperature, accounting for strain-induced crystallization. This is achieved by neglecting the last dashpot if the stretch is larger than a given value, which depends on the plastic strain rate and the temperature.

Kletschkowski and coworkers [231] present another description fitting into this class of material models. One of the Maxwell branches is made of a linear elastic spring, and its viscous element follows the cooperative model (see Eq. (20)) for the strain rate. The other branch employs the endochronic viscoplasticity theory [232]. It resembles viscoelasticity with the caveat that time is replaced by an 'inner' time, a function of the strain, hence the name endochronic. The authors employ this model in the description of filled PTFE.

Pouriayevali and coworkers [33] present a constitutive model to describe the quasi-static and high strain rate, large deformation response of semicrystalline polymers, which can be seen as a generalization of the Kelvin-Voigt representation of the Burgers material. The elastic elements are hyperelastic, and their stress response is obtained from Eq. (A.20), given a suitable free energy potential. Regarding the viscous elements, element one obeys von Mises yield criterion with the strain rate also given by Eq. (23), and the other obeys Newton's viscosity law (see Eq. (68)), neglecting the volumetric contribution. The corresponding free energy, including the dependency on the temperature, is also supplied. The authors validate their model through comparisons with Nylon 6.

The dual network fluoropolymer model is presented in [130] as an extension of the Bergström and Boyce [128] and Arruda and Boyce [164] models, generalizing the Kelvin-Voigt representation of the Burgers material. The Arruda-Boyce eight-chain model gives the response of both springs (see Eq. (86)), with the response of the second element taken as a scalar factor $s^{(2)}$, a specified material parameter, times the expression employed to

describe the response of the first evaluated according to the deformation gradient across element 2. The kinematic decomposition is as expected from the discussion in Sections 6.4 and 6.5, including a thermal deformation gradient. The rate equations for $\dot{\gamma}^{(1)}_{\text{dev}}$ and $\dot{\gamma}^{(1)}_{\text{vol}}$ in Eq. (106) in the viscous element one are given similarly to the Bergström-Boyce model (see Eq. (25)) multiplied by a power law, function of the stress and the temperature. The volumetric strain rate is given by Eq. (70). The strain rate for the viscous element 2, $\dot{\gamma}^{(2)}_{\text{dev}}$, is given by Eq. (27).

7.4. Generalized Maxwell model

A generalized Maxwell model is one that contains n Maxwell branches in parallel. In addition, a single branch with only an elastic element may also be considered. See Fig. 20 for the corresponding rheological model. This framework includes Maxwell representations for the standard linear solid model and the Burgers material. Models with more than two branches are considered in the following section.

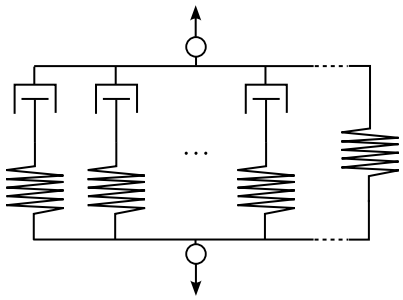

Figure 20: Rheological model for the generalized Maxwell model.

Holmes and coworkers [233] present a large strain deformation elasto-viscoplastic material model for modeling semicrystalline polymers. According to the authors, each of the branches in the model coincides with a mode of deformation: elastic, viscoelastic, and viscoplastic. Each of the elastic elements' response follows from the free energy chosen and the constitutive relation in Eq. (A.20). The authors suggest employing an Ogden free energy for the elastic and viscoelastic branches and a Saint Venant-Kirchhoff free energy (see Eq. (84)) for the viscoplastic contribution. The flow rule adopted follows the work of Brussele-Dupend and coworkers [234, 235] for semicrystalline polypropylene, accounting for the inadequacies

of the Eyring equation (see Eq. (2)). Regarding the viscoplastic branch of the model, the strain rate is given by Equations (73) and (23).

Anand and Ames [236] proposed a one-dimensional constitutive model to describe the localized visco-elastic visco-plastic mechanical response of amorphous polymers under micro-indentation. It considers several of Voigt spring-damper units (a spring and a damper in parallel) in series. One of these units captures the macroscopic response, and the others model the microscopic response. There are also two extra springs, one in series with all the Voigt units and another in parallel with them, similar to the standard linear solid model. The flow rules selected for the viscous elements are of the power law type (see Eq. (22)), with only the scalar internal variables related to the macroscopic response evolving according to Eq. (48). Building directly on this thermodynamically consistent framework, Lele and Anand [237] developed a strain-gradient framework to capture the behavior of isotropic visco-plastic materials undergoing large deformations. The theory incorporates strain gradients into the constitutive formulation, which allows for the modeling of size-dependent effects and localized deformation phenomena, such as those occurring in shear bands.

Regarding another model by some of the same authors [140, 141], an extension was proposed by Srivastava et al. [238] to accurately capture the mechanical response of amorphous polymers over a temperature range that includes the glass transition. They propose the addition of two Maxwell branches in parallel to capture the contribution of microscopic mechanisms, in addition to the appropriate temperature-dependent evolution laws for the internal variables, given the temperature range of interest. Wang et al. [239] proposed a similar variation where new branches are added to capture the contributions of entangled chains and non-entangled chains to the intermolecular resistance to deformation.

Zeng and coworkers [30] developed an elastoplastic constitutive model for semicrystalline polymers under isothermal conditions between the glass transition temperature and the melting temperature under low-level strain rates, neglecting viscous effects. Each of the branches in the rheological model is based on physical considerations concerning the mesoscopic semicrystalline structure. The foundational idea is a three-phase morphology depending on the average distance between crystalline blocks. The interaction is modeled as elastoplastic with linear hardening when the distance is small. For medium distances, the

behavior is elastoplastic with perfect plasticity, and for large distances, the material is modeled following the eight-chain model (see Eq. (86)). The authors validate the model against the results of uniaxial and biaxial experiments on PA6 and PE at different strain rates. The model parameters are easily calibrated using these uniaxial stress–strain experimental curves.

The model developed by Bergström and Boyce [128] based on the BPA model was later extended to the high-strain-rate domain by Mulliken and Boyce [240, 51] by adding a new polymer network in parallel with the existing ones, enabling the model to capture the β-transition accurately. Subsequent modifications were introduced to enhance the model's predictive capability and broaden its applicability across different loading conditions and material behaviors — for instance, by introducing additional polymer networks, coupling the model with a thermo-mechanical adiabatic framework, and modifying the softening evolution laws of the polymer networks [241, 242, 243, 244]. Inspired by the developments of Mulliken and Boyce [240, 51], a finite strain visco-elastic visco-plastic constitutive model is proposed by Carvalho Alves et al. [245]. This model extended the model in [148] to predict the response of amorphous polymers across low and high strain rates by accounting for the distinct molecular processes that govern the material's mechanical behavior at these strain rates.

Okereke and Akpoyomare [142] propose a model based on an elastic-viscoelastic-viscoplastic framework to predict the temperature and rate-dependent response of an incompressible semicrystalline polymer. Three branches materialize it in a rheological model, two containing a viscous and an elastic element corresponding to the contribution of the mobile amorphous fraction, and the crystalline and rigid amorphous fractions, and another branch containing only an elastic element, representing the contribution of the entangled molecular network. The basis of this model is a one-process glass-rubber model for amorphous polymers [196], adapted to the description of semicrystalline polymers, which considers the α- and β-processes, making it a two-process model. The authors connect these processes to the glass transition of the rigid amorphous and the mobile amorphous phases, respectively. The flow rule for both branches containing the viscous elements is given according to Eq. (73), where the volumetric contribution is neglected, and the deviatoric strain rate is given by

Eq. (54), capturing the significant post-yield strain-softening observed in high-rate compression of propylene. The elastic elements in the branches contain viscous elements according to the Saint-Venant-Kirchhoff model (see Eq. (84)), while the other elastic element follows the Edwards-Vilgis model (see Eq. (90)).

The three-network model is presented in [16] and is very similar to the models already presented based on a generalized Maxwell model. The springs follow the Arruda-Boyce eight-chain model (see Eq. (86)) and the dashpot power laws (similar to Eq. (22)). The effective shear stress is taken as an internal variable with a corresponding rate equation. A linear dependence on temperature is also included for the stress response of the elastic elements. The same author also explores a parallel network model that adds more Maxwell branches, each following similar constitutive equations.

Hao and coworkers [174] propose a model containing three branches to study the double yield phenomenon as well as the rate- and temperature-dependent thermomechanical response below the glass transition temperature of semicrystalline polymers. The first branch contains an elastic element whose stress response follows Hencky's model (see Eq. (83)). The corresponding viscous element obeys Equations (2) and (10) following the work of Boyce and coworkers [133]. The athermal strength is taken as an internal variable, and its rate equation is shown in Eq. (38), following Chowdhury and coworkers [138]. The behavior of the elastoplastic branch coincides with rate-independent plasticity, and it is made up of an elastic element, also following Hencky's model (see Eq. (83)), and a viscous element respecting a paraboloidal yield criterion. The yield criterion describing the yielding in the crystalline region is similar to the Drucker-Prager yield criterion with the strain rate/plastic multiplier $\dot{\gamma}$ found by taking into account the Kuhn-Tucker's loading-unloading consistency conditions. The same law as Chowdhury and coworkers [138] is adopted for the rubber-like elastic responsible for the hardening response, combining a four-chain model (see Eq. (88)) and an eight-chain model (see Eq. (86)).

The hybrid model has been developed to model UHWPE [246, 247] and employs the rheological model shown in Fig. 21. The spring E is linear, following the Hencky model (Eq. (83)), springs A and B follow the Arruda-Boyce eight-chain model (Eq. (86)), employing the same expression except for a multiplicative constant s_B. This constant is treated in the

model as an internal variable that evolves according to an equation similar to Eq. (31). The rate of viscoplastic flow in element P, $\dot{\gamma}^p$, is given by a power law (Eq. (22)), as is the flow rate in element B.

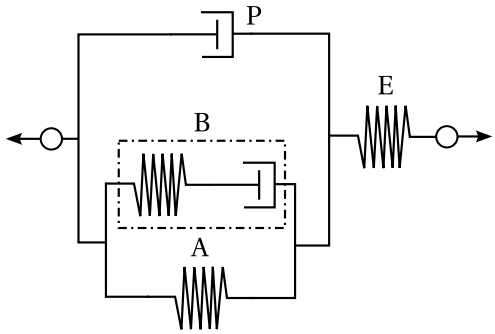

Figure 21: Rheological model for the Hybrid model [246, 247].

7.5. Models considering bulk crystallinity

The following set of models considers different phases in semicrystalline polymers, a crystalline phase, and an amorphous phase. These adopt simple geometric considerations that mostly focus on bulk crystallinity and overlap with mean-field approaches, as discussed in Section 5.2.

The work of Takayanagi and coworkers [248] was one of the first to consider such an approach to model semicrystalline polymers. The employed mixture rule is neither the Voigt nor the Reuss rule, but instead depends on an additional parameter that attempts to capture the spatial distribution of the crystalline phase. In [249], the authors employ similar techniques to model drawn samples of polyethylene (PE) and isotactic propylene (iPP), among other crystalline polymers.

G'sell, Dahoun, and coworkers [13, 250] employ a mixture model using the Voigt composite model to combine the contributions from the amorphous (rubber-like) and the crystalline (viscoplastic) portions of the polymer. They assume a temperature above the glass transition temperature and attempt to describe HDPE and PEEK subject to uniaxial tension and pure shear. The response of the amorphous portion of the polymer is given according to the elastic rubber model in [195]. In contrast, the behavior of the crystalline phase is modeled following Parks and Ahzi [251]. It is based on a local-global interaction model established

for polycrystalline metals [252], accounting for the kinematically indeterminate component of stress in a rigid-viscoplastic crystal due to the locally inextensible direction. They consider a fully crystalline HDPE and make predictions for the large-deformation texture and the macroscopic stress-strain response.

Ahzi and coworkers [137] model PET at large strains, including strain-induced polymer crystallization above the glass transition temperature. The model is based on [230], considering two distinct resistances, an intermolecular (A) and network resistance (B). As in the base model, the network stress is captured by the Arruda-Boyce eight-chain model (see Eq. (86)), and the viscous element follows the Bergström-Boyce model (see Eq. (25)). The intermolecular resistance, however, is treated in a composite framework in which the crystalline and amorphous phases are treated as two separate resistances coupled via a Voigt or Reuss-like mixture rule, yielding upper and lower bounds for the stiffness, respectively. The elastic elements corresponding to the crystalline and amorphous phases follow the Hencky model (see Eq. (83)), and the viscous elements follow a model similar to the one proposed by Argon (see Eq. (10)), where the athermal strength s_i in each phase evolves according to Eq. (37).

Regarding applying the mixture rules to the intermolecular resistance, contributions come from the crystalline part, denoted by c, and the amorphous part, a, of the semicrystalline polymer. These are combined according to the degree of crystallinity, χ, in two ways: in parallel, such that the gradient acting in each element is equal, and the Cauchy stress is supplied by

$$\boldsymbol{\sigma}_A = \chi \boldsymbol{\sigma}_A^c + (1-\chi)\boldsymbol{\sigma}_A^a; \tag{123}$$

in series, such that the stress acting on both elements is the same, and the plastic rate of deformation is given by

$$\boldsymbol{D}_A^p = \chi \boldsymbol{D}_A^{p,\,c} + (1-\chi)\boldsymbol{D}_A^{p,\,a}. \tag{124}$$

The crystallization rate is expressed following a non-isothermal phenomenological expression based on the modified Avrami equation

$$\dot{\chi} = \chi_\infty \frac{\dot{\varepsilon}_{\text{eq}}}{\dot{\varepsilon}_{\text{ref}}} m K_{\text{av}}(T)(-\ln(1-y))^{(m-1)/m}(1-y)\exp\left(\xi \frac{\operatorname{tr}\boldsymbol{\sigma}}{G_{\text{comp}}}\right), \tag{125}$$

where χ_∞ is the maximum degree of crystallinity, m is the Avrami, ξ is a dimensionless model parameter, G_{comp} is the composite bulk modulus, $\dot{\varepsilon}_{\text{eq}}$ is the applied equivalent strain rate and $\dot{\varepsilon}_{\text{ref}}$ is taken as the maximum strain rate for which experimental results are available for the calibration of the model parameters. K_{av} is the transformation rate function, which is defined in the case of PET as

$$K_{\text{av}}(T) = 1.47 \times 10^{-3} \left[\frac{4\pi \text{Nu}}{3\chi_\infty}\right]^{1/3} \exp\left[-\left(\frac{T-141}{47.33}\right)\right] \quad (\text{s}^{-1},\, T \text{ in } ^\circ\text{C}), \tag{126}$$

with Nu the number density of nuclei initially present within the amorphous phase.

Strobl and coworkers [73, 73, 62] propose a somewhat similar description for polyethylene. They also consider two branches in a rheological model. The first is a Maxwell branch with a linear spring and an Eyring dashpot in series. The second is obtained via a Voigt mixture rule between rubber-elastic and elastoplastic elements. Extensive experimental results on PEVA and PE support these choices.

Makradi and coworkers [253] extend this model by considering a self-consistent approach based on the Eshelby result. It amounts to the use of a Maxwell branch as the intermolecular resistance, where the properties of the elastic and viscous elements are appropriate equivalent properties computed from the self-consistent scheme. The authors employ the same description of the evolution of crystallinity as [137], in addition to Flory's theory, to predict the onset of crystallization as a function of processing temperature and the extension of polymer molecules. Later, Regrain and coworkers [254] extended the DID models to semicrystalline models, employing a self-consistent scheme to consider the contribution of both phases.

Dusunceli and Colak [255] extend the viscoplasticity theory based on overstress (VBO) to include crystallinity. This is achieved by describing both phases employing the VBO model and considering their contributions using a Voigt or a Reuss mixture rule. The authors validate their model using polyethylenes (UHWPE and XLPE) and PTFE. Ayoub and coworkers [256, 27] present a model very similar to [137] and [230] to describe the mechanical behavior of HDPE. The inelastic mechanisms involve two parallel elements: a visco-hyperelastic network resistance in parallel with a viscoelastic–viscoplastic intermolecular resistance, with the amorphous and crystalline phases explicitly accounted for. The

semicrystalline polymer is considered a two-phase composite, similar to that already described. In the first contribution, both the crystalline and amorphous resistances are modeled employing the VBO model. Their contributions to the intermolecular resistance are incorporated through a Voigt mixture rule. In the second contribution, the elastic and viscous elements in crystalline and amorphous resistances are modeled employing Hencky's model (see Eq. (83)) and a simplified version of Argon's model (see Eq. (10)). They employ a modified Voigt mixture rule, where the contribution to the intermolecular resistance coming from the crystalline and amorphous phases is combined through

$$\boldsymbol{\sigma}_A = \chi^{\beta}\boldsymbol{\sigma}_c + (1-\chi)^{\beta}\boldsymbol{\sigma}_a, \tag{127}$$

where β is an appropriate exponent. Such an exponent is found from a fit of the Young modulus as a function of the degree of crystallinity, as shown in Fig. 11a. When compared with the experimental results obtained for polyethylene samples with degrees of crystallinity between 15% and 72%, the model accurately captures the change in response with increasing crystallinity before strain hardening becomes evident. Different material parameters for each crystallinity level are needed to capture strain hardening at large strains (¿1). A similar model can be found in [257], where the major difference is the substitution of the Maxwell branch in the network resistance for two branches, one corresponding to the amorphous contribution and the other to the crystalline contribution. They are combined as shown in Eq. (127). This constitutive model aims to generalize strain-hardening behavior across different degrees of crystallinity, so that the same material parameters apply to all degrees. Very recently, Cundiff and coworkers [258] proposed another model where the inclusion of the crystallinity is achieved through the modified Voigt mixture rule (see Eq. (127)). Regarding the constitutive description of each phase, it employs many of the same laws found in [137] and [138]. It describes strain-rate crystallization using a rate equation similar to Eq. (125).

Lastly, the two-phase model of Cangemi and Meimon for semicrystalline polymers [18] accounts for bulk crystallinity differently. It is based on the continuum mixture theory, such that, according to the microstructure of semicrystalline polymers, the free amorphous phase is assumed to be comparable to a fluid that saturates the complementary space to the solid

structure, the crystalline phase plus the rigid amorphous phase.

Remark 2 (Model complexity and parameter identification). *Due to the large number of constitutive models proposed in the literature, Carvalho et al. recently conducted a comparative study of different formulations for amorphous polymers in a wide range of strain rates [259]. In this work, a simple and modular computational framework was developed to implement and evaluate various constitutive equations. Specifically, the study compares the models proposed by Mulliken [51], Varghese and Batra [241], Richeton et al. [121], and Wang et al. [243]. This framework also enables efficient testing and development of new constitutive formulations by allowing flexible integration of alternative laws or modifications.*

Moreover, one of the main downsides of these complex models is that non-standard or several experiments are often required to determine the extensive number of material parameters, resulting in a high-dimensional parameter space that must be explored during model calibration. Furthermore, the physical meaning of some material properties is often challenging to grasp. On top of all this, the identification of the material parameters is typically performed using trial-and-error approaches based on visual assessment of the experimental data, which is highly time-consuming [260, 7]. In light of the aforementioned limitations, optimization techniques have been explored to accelerate parameter identification [261]. In this context, Coelho et al. [8] conducted a systematic and critical comparison of different optimization algorithms. The results showcase the superior performance of the Composite Bayesian Optimization. This strategy, available as a `Python` *package [262], employs a dynamic, adaptive sampling approach to efficiently explore the optimization space, thereby significantly reducing the number of required experiments.*

8. Concluding remarks

This paper provides an in-depth review of the theoretical foundations, deformation mechanisms, and constitutive models for thermoplastic polymers. Within this setting, the fundamental aspects of polymer science are presented, understanding the unique characteristics of amorphous and semicrystalline polymers, and the deformation mechanisms that govern their thermomechanical behavior, namely shear yielding, crazing, and internal particle

cavitation. A focus on the typical behavior of solid polymers, including their mechanical response and transitions, lays the groundwork for the modeling demands of these materials. Continuum models, micro-mechanical models, and multi-scale approaches are highlighted, each contributing valuable insights into the mechanical behavior of amorphous polymers under various loading conditions.

In the context of continuum models, we highlight the nearly ubiquitous use of one-dimensional rheological models with their originin linear viscoelasticity as a basis for non-linear constitutive formulations. A detailed account of the most relevant flow rules and free energy functions is provided, along with common choices for the internal variables employed to capture transient effects. This contribution also collects the different models proposed in the literature based on the arrangment of rheological elements, as this choice alone accounts for a significant difference in the predicted response. The extensions necessary to also describe the thermomechanical behavior of thermoplastic polymers is also discussed, ranging from the temperature dependence of the mechanical properties, to the dissipation of mechanical work into heat. For semicrystalline polymers, in particular, we also breach the class of two-phase models that explicitly account for the degree of crystallinity in the constitutive description, still based on rheological models.

Micro-mechanical and multi-scale models are also briefly reviewed, highlighting their advantages and limitations compared to continuum models.

Acknowledgment

The authors acknowledge the support provided by Fundação para a Ciência e a Tecnologia through the scholarship with reference 2021.07345.BD (José L. P. Vila-Chã). This work is also partly supported by the ERC advanced grant INELASTIC-101141273. (Funded by the European Union). Views and opinions expressed are those of the authors only and do not necessarily reflect those of the European Union or the European Research Council Executive Agency. Neither the European Union nor the granting authority can be held responsible for them. This research has also been supported by Instituto de Ciência e Inovação em Engenharia Mecânica e Engenharia Industrial (INEGI).

References

[1] EIN Presswire. Polymers market size to worth around usd 1078.5 billion by 2030. https://www.einpresswire.com/article/597978035/polymers-market-size-to-worth-around-usd-1078-5-billion-by-2030, 2022. Accessed: 2025-04-17.

[2] R. N. Haward and R. J. Young. *The Physics of Glassy Polymers*. Springer Netherlands, Dordrecht, 1997.

[3] William Callister and David Rethwisch. Materials Science and Engineering: An Introduction, 10th Edition — Wiley. *Wiley.com*, 2018.

[4] Sabana Ara Begum, Ajay Vasudeo Rane, and Krishnan Kanny. Chapter 20 - applications of compatibilized polymer blends in automobile industry. In Ajitha A.R. and Sabu Thomas, editors, *Compatibilization of Polymer Blends*, pages 563–593. Elsevier, 2020.

[5] Bingchun Jiang, Quan Chen, and Jiang Yang. Advances in joining technology of carbon fiber-reinforced thermoplastic composite materials and aluminum alloys. *The International Journal of Advanced Manufacturing Technology*, 110:1–19, 10 2020.

[6] Gregory B. Olson. Designing a new material world. *Science*, 288(5468):993–998, May 2000.

[7] S.M. Mirkhalaf, F.M. Andrade Pires, and Ricardo Simoes. Modelling of the post yield response of amorphous polymers under different stress states. *International Journal of Plasticity*, 88:159–187, January 2017.

[8] R.P. Cardoso Coelho, A. Francisca Carvalho Alves, and F.M. Andrade Pires. Efficient constitutive parameter identification through optimisation-based techniques: A comparative analysis and novel composite bayesian optimisation strategy. *Computer Methods in Applied Mechanics and Engineering*, 427:117039, 2024.

[9] S.M. Mirkhalaf, F.M. Andrade Pires, and Ricardo Simoes. Determination of the size of the representative volume element (rve) for the simulation of heterogeneous polymers at finite strains. *Finite Elements in Analysis and Design*, 119:30–44, 2016.

[10] Mohsen Mirkhalaf and Rahele Vadizadeh. Micro-mechanical modeling of semi-crystalline polymers: A review. *International Journal of Solids and Structures*, 290:112691, 2024.

[11] Ali Gooneie, Stephan Schuschnigg, and Clemens Holzer. A review of multiscale computational methods in polymeric materials. *Polymers*, 9:16, 01 2017.

[12] I. M. Ward and J. Sweeney. *An introduction to the mechanical properties of solid polymers*. Wiley, Chichester, West Sussex, England, 2nd ed edition, 2004.

[13] C. G'sell and A. Dahoun. Evolution of microstructure in semi-crystalline polymers under large plastic deformation. *Materials Science and Engineering: A*, 175(1-2):183–199, February 1994.

[14] Ali Argon. *The Physics of Deformation and Fracture of Polymers*. Cambridge University Press, 2013.

[15] S Nikolov and I Doghri. A micro/macro constitutive model for the small-deformation behavior of polyethylene. *Polymer*, 41(5):1883–1891, March 2000.

[16] J.S. Bergström. *Mechanics of Solid Polymers : Theory and Computational Modeling*. Plastics Design Library. Elsevier Science, 2015.

[17] F. Khoury and E. Passaglia. The Morphology of Crystalline Synthetic Polymers. In N. B. Hannay, editor, *Treatise on Solid State Chemistry*, pages 335–496. Springer US, Boston, MA, 1976. tex.ids= khouryMorphologyCrystallineSynthetic1976a.

[18] L. Cangemi and Y. Meimon. A Two-Phase Model for the Mechanical Behavior of Semicrystalline Polymers. *Oil & Gas Science and Technology*, 56(6):555–580, November 2001. tex.ids= cangemiTwoPhaseModelMechanical2001a.

[19] S. Fakirov and B. Krasteva. On the Glass Transition Temperature of Polyethylene as Revealed by Microhardness Measurements. *Journal of Macromolecular Science, Part B*, 39(2):297–301, March 2000.

[20] John D. Hoffman, G. Williams, and E. Passaglia. Analysis of the alpha, beta, and gamma relaxations in polychlorotrifluoroethylene and polyethylene: Dielectric and mechanical properties. *Journal of Polymer Science Part C: Polymer Symposia*, 14(1):173–235, March 2007.

[21] E. N. Brown, R. B. Willms, G. T. Gray, P. J. Rae, C. M. Cady, K. S. Vecchio, J. Flowers, and M. Y. Martinez. Influence of Molecular Conformation on the Constitutive Response of Polyethylene: A Comparison of HDPE, UHMWPE, and PEX. *Experimental Mechanics*, 47(3):381–393, June 2007.

[22] I.J. Rao and K.R. Rajagopal. A study of strain-induced crystallization of polymers. *International Journal of Solids and Structures*, 38(6-7):1149–1167, February 2001.

[23] Bernard A. G. Schrauwen, Roel P. M. Janssen, Leon E. Govaert, and Han E. H. Meijer. Intrinsic Deformation Behavior of Semicrystalline Polymers. *Macromolecules*, 37(16):6069–6078, August 2004. tex.ids= schrauwenIntrinsicDeformationBehavior2004a publisher: American Chemical Society.

[24] Qamer Zia, Daniela Mileva, and René Androsch. Rigid Amorphous Fraction in Isotactic Polypropylene. *Macromolecules*, 41(21):8095–8102, November 2008.

[25] J van Dommelen, D Parks, M Boyce, W Brekelmans, and F Baaijens. Micromechanical modeling of the elasto-viscoplastic behavior of semi-crystalline polymers. *Journal of the Mechanics and Physics of Solids*, 51(3):519–541, March 2003.

[26] S. Hobeika, Y. Men, and G. Strobl. Temperature and Strain Rate Independence of Critical Strains in Polyethylene and Poly(ethylene-co-vinyl acetate). *Macromolecules*, 33(5):1827–1833, March 2000. Publisher: American Chemical Society.

[27] G. Ayoub, F. Zaïri, C. Fréderix, J.M. Gloaguen, M. Naït-Abdelaziz, R. Seguela, and J.M. Lefebvre. Effects of crystal content on the mechanical behaviour of polyethylene

under finite strains: Experiments and constitutive modelling. *International Journal of Plasticity*, 27(4):492–511, April 2011.

[28] Z. Bartczak, R. E. Cohen, and A. S. Argon. Evolution of the crystalline texture of high-density polyethylene during uniaxial compression. *Macromolecules*, 25(18):4692–4704, August 1992.

[29] Leo Mandelkern. Crystalline polymer: Some reminiscences over the years. *Thermochimica Acta*, 442(1):31–34, March 2006.

[30] Fanfei Zeng, Philippe Le Grognec, Marie-France Lacrampe, and Patricia Krawczak. A constitutive model for semi-crystalline polymers at high temperature and finite plastic strain: Application to PA6 and PE biaxial stretching. *Mechanics of Materials*, 42(7):686–697, July 2010.

[31] Andrew Peacock. *Handbook of Polyethylene: Structures: Properties, and Applications*. CRC Press, Boca Raton, April 2014.

[32] Cédric Regrain, Lucien Laiarinandrasana, and Sophie Toillon. Experimental and numerical study of creep and creep rupture behavior of PA6. *Engineering Fracture Mechanics*, 76(18):2656–2665, 2009.

[33] H. Pouriayevali, S. Arabnejad, Y.B. Guo, and V.P.W. Shim. A constitutive description of the rate-sensitive response of semi-crystalline polymers. *International Journal of Impact Engineering*, 62:35–47, December 2013.

[34] Stanislav Patlazhan and Yves Remond. Structural mechanics of semicrystalline polymers prior to the yield point: a review. *Journal of Materials Science*, 47(19):6749–6767, October 2012.

[35] John R. Collier. Polymer Structure. *Industrial & Engineering Chemistry*, 61(9):50–65, 1969.

[36] R. Hill. *The Mathematical Theory of Plasticity*. Oxford classic texts in the physical sciences. Clarendon Press, 1998.

[37] A. A. Collyer. *Rubber Toughened Engineering Plastics*. Springer Netherlands, Dordrecht, 1994.

[38] B. J. Lee, D. M. Parks, and S. Ahzi. Micromechanical modeling of large plastic deformation and texture evolution in semi-crystalline polymers. *Journal of the Mechanics and Physics of Solids*, 41(10):1651–1687, October 1993.

[39] B.J Lee, A.S Argon, D.M Parks, S Ahzi, and Z Bartczak. Simulation of large strain plastic deformation and texture evolution in high density polyethylene. *Polymer*, 34(17):3555–3575, September 1993.

[40] N. G. McCrum, C. P. Buckley, C. B. Bucknall, Clive B. Bucknall, and C. B. Bucknall. *Principles of Polymer Engineering*. Oxford University Press, 1997.

[41] G. H. Michler. Correlation between craze formation and mechanical behaviour of amorphous polymers. *Journal of Materials Science*, 25(5):2321–2334, 1990.

[42] D.S. Dugdale. Yielding of steel sheets containing slits. *Journal of the Mechanics and Physics of Solids*, 8(2):100–104, 1960.

[43] R. J. Fields and M. F. Ashby. Finger-like crack growth in solids and liquids. *Philosophical Magazine*, 33(1):33–48, 1976.

[44] Athene M. Donald and Edward J. Kramer. The mechanism for craze-tip advance in glassy polymers. *Philosophical Magazine A*, 43(4):857–870, 1981.

[45] Athene M. Donald and Edward J. Kramer. The competition between shear deformation and crazing in glassy polymers. *Journal of Materials Science*, 17(7):1871–1879, 1982.

[46] Ferry. *Viscoelastic Properties of Polymers*. Wiley, 1980.

[47] H. Ben Hadj Hamouda, L. Laiarinandrasana, and R. Piques. Viscoplastic behaviour of a medium density polyethylene (MDPE): Constitutive equations based on double nonlinear deformation model. *International Journal of Plasticity*, 23(8):1307–1327, August 2007.

[48] Maxim Arzhakov. *Relaxation in Physical and Mechanical Behavior of Polymers*. CRC Press, 1 edition, January 2019.

[49] Yash P. Khanna, Edith A. Turi, Thomas J. Taylor, Virgil V. Vickroy, and Richard F. Abbott. Dynamic mechanical relaxations in polyethylene. *Macromolecules*, 18(6):1302–1309, June 1985.

[50] R.M. Christensen. *Theory of viscoelasticity*. Dover civil and mechanical engineering. Dover Publications, 2nd edition edition, 2013.

[51] A. Mulliken. *Mechanics of Amorphous Polymers and Polymer Nanocomposites during High Rate Deformation*. PhD Thesis, Massachusetts Institute of Technology, 2006.

[52] L.R.G. Treloar. *The Physics of Rubber Elasticity*. Oxford Classic Texts in the Physical Sciences. Oxford University Press, USA, 1975.

[53] A Khan and B Farrokh. Thermo-mechanical response of nylon 101 under uniaxial and multi-axial loadings: Part I, Experimental results over wide ranges of temperatures and strain rates. *International Journal of Plasticity*, 22(8):1506–1529, August 2006.

[54] Frederik Van Loock and Norman Fleck. Deformation and failure maps for PMMA in uniaxial tension. *Polymer*, 148, June 2018.

[55] C. F. Popelar, C. H. Popelar, and V. H. Kenner. Viscoelastic material characterization and modeling for polyethylene. *Polymer Engineering and Science*, 30(10):577–586, May 1990.

[56] R. W. Truss, R. A. Duckett, and I. M. Ward. Effect of hydrostatic pressure on the yield and fracture of polyethylene in torsion. *Journal of Materials Science*, 16(6):1689–1699, June 1981.

[57] C. Bauwens-Crowet. The compression yield behaviour of polymethyl methacrylate over a wide range of temperatures and strain-rates. *Journal of Materials Science*, 8(7):968–979, July 1973.

[58] Zakaria El-Qoubaa and Ramzi Othman. Strain rate sensitivity of polyetheretherketone's compressive yield stress at low and high temperatures. *Mechanics of Materials*, 95:15–27, April 2016.

[59] Ellen M. Arruda, Mary C. Boyce, and Harald Quintus-Bosz. Effects of initial anisotropy on the finite strain deformation behavior of glassy polymers. *International Journal of Plasticity*, 9(7):783–811, 1993.

[60] F Bedoui, J Diani, G Regnier, and W Seiler. Micromechanical modeling of isotropic elastic behavior of semicrystalline polymers. *Acta Materialia*, 54(6):1513–1523, April 2006.

[61] S.M Kurtz, M.L Villarraga, M.P Herr, J.S Bergström, C.M Rimnac, and A.A Edidin. Thermomechanical behavior of virgin and highly crosslinked ultra-high molecular weight polyethylene used in total joint replacements. *Biomaterials*, 23(17):3681–3697, September 2002.

[62] Bing Na, Qin Zhang, Qiang Fu, Yongfeng Men, Ke Hong, and Gert Strobl. Viscous-Force-Dominated Tensile Deformation Behavior of Oriented Polyethylene. *Macromolecules*, 39(7):2584–2591, April 2006. Publisher: American Chemical Society.

[63] A. C. Steenbrink and E. van der Giessen. On cavitation, post-cavitation and yield in amorphous polymer-rubber blends. *Journal of the Mechanics and Physics of Solids*, 47(4):843–876, 1999.

[64] C. Fond. Cavitation criterion for rubber materials: A review of void-growth models. *Journal of Polymer Science Part B: Polymer Physics*, 39(17):2081–2096, 2001.

[65] Christian G'Sell, Serge Boni, and Suresh Shrivastava. Application of the plane simple shear test for determination of the plastic behaviour of solid polymers at large strains. *Journal of Materials Science*, 18(3):903–918, March 1983.

[66] Jevan Furmanski, Carl M. Cady, and Eric N. Brown. Time–temperature equivalence and adiabatic heating at large strains in high density polyethylene and ultrahigh molecular weight polyethylene. *Polymer*, 54(1):381–390, January 2013.

[67] C. G'Sell, J. M. Hiver, A. Dahoun, and A. Souahi. Video-controlled tensile testing of polymers and metals beyond the necking point. *Journal of Materials Science*, 27(18):5031–5039, September 1992.

[68] F. Lauro, B. Bennani, D. Morin, and A. F. Epee. The SE$\dot{\text{E}}$ method for determination of behaviour laws for strain rate dependent material: Application to polymer material. *International Journal of Impact Engineering*, 37(6):715–722, June 2010.

[69] R. Balieu, F. Lauro, B. Bennani, G. Haugou, F. Chaari, T. Matsumoto, and E. Mottola. Damage at high strain rates in semi-crystalline polymers. *International Journal of Impact Engineering*, 76:1–8, February 2015.

[70] Mario Polanco-Loria, Arild H. Clausen, Torodd Berstad, and Odd Sture Hopperstad. Constitutive model for thermoplastics with structural applications. *International Journal of Impact Engineering*, 37(12):1207–1219, December 2010.

[71] Masayoshi Kitagawa and Takeshi Yoneyama. Plastic dilatation due to compression in polymer solids. *Journal of Polymer Science Part C: Polymer Letters*, 26(4):207–212, 1988. _eprint: https://onlinelibrary.wiley.com/doi/pdf/10.1002/pol.1988.140260407.

[72] R. Hiss, S. Hobeika, C. Lynn, and G. Strobl. Network Stretching, Slip Processes, and Fragmentation of Crystallites during Uniaxial Drawing of Polyethylene and Related Copolymers. A Comparative Study. *Macromolecules*, 32(13):4390–4403, June 1999. Publisher: American Chemical Society.

[73] K. Hong, A. Rastogi, and G. Strobl. A Model Treating Tensile Deformation of Semicrystalline Polymers: Quasi-Static Stress-Strain Relationship and Viscous Stress Determined for a Sample of Polyethylene. *Macromolecules*, 37(26):10165–10173, December 2004. tex.ids= hongModelTreatingTensile2004a publisher: American Chemical Society.

[74] J. Blumm, A. Lindemann, M. Meyer, and C. Strasser. Characterization of PTFE Using Advanced Thermal Analysis Techniques. *International Journal of Thermophysics*, 31(10):1919–1927, October 2010.

[75] L. Olasz and P. Gudmundson. Viscoelastic Model of Cross-Linked Polyethylene Including Effects of Temperature and Crystallinity. *Mechanics of Time-Dependent Materials*, 9(4):23–44, December 2005.

[76] D. P. Pope. Characterization of oriented low-density polyethylene samples by differential scanning calorimetry. *Journal of Polymer Science: Polymer Physics Edition*, 14(5):811–820, 1976. _eprint: https://onlinelibrary.wiley.com/doi/pdf/10.1002/pol.1976.180140504.

[77] F. J. Zoepfl, V. Marković, and Joseph Silverman. Differential scanning calorimetry studies of irradiated polyethylene: I. Melting temperatures and fusion endotherms. *Journal of Polymer Science: Polymer Chemistry Edition*, 22(9):2017–2032, 1984. _eprint: https://onlinelibrary.wiley.com/doi/pdf/10.1002/pol.1984.170220907.

[78] Kevin Lukas and Peter K. LeMaire. Differential scanning calorimetry: Fundamental overview. *Resonance*, 14(8):807–817, August 2009.

[79] Robert Panowicz, Marcin Konarzewski, Tomasz Durejko, Mateusz Szala, Magdalena Łazińska, Magdalena Czerwińska, and Piotr Prasuła. Properties of Polyethylene Terephthalate (PET) after Thermo-Oxidative Aging. *Materials*, 14(14):3833, January 2021. Number: 14 Publisher: Multidisciplinary Digital Publishing Institute.

[80] M. F. Ashby. *Materials selection in mechanical design*. Butterworth-Heinemann, Oxford, OX ; Boston, MA, 2nd ed edition, 1999.

[81] Karel Matous, Marc Geers, Varvara Kouznetsova, and Andrew Gillman. A review of predictive nonlinear theories for multiscale modeling of heterogeneous materials. *Journal of Computational Physics*, 330, 11 2016.

[82] F. Zaïri, M. Naït-Abdelaziz, J.M. Gloaguen, and J.M. Lefebvre. Modelling of the elasto-viscoplastic damage behaviour of glassy polymers. *International Journal of Plasticity*, 24(6):945–965, 2008.

[83] F. Zaïri, M. Naït-Abdelaziz, J.M. Gloaguen, and J.M. Lefebvre. A physically-based constitutive model for anisotropic damage in rubber-toughened glassy polymers during finite deformation. *International Journal of Plasticity*, 27(1):25–51, 2011.

[84] Sami Holopainen. Influence of damage on inhomogeneous deformation behavior of amorphous glassy polymers. Modeling and algorithmic implementation in a finite element setting. *Engineering Fracture Mechanics*, 117:28–50, 2014.

[85] A. Francisca Carvalho Alves, Bernardo P. Ferreira, and F.M. Andrade Pires. On the modeling of cavitation and yielding in rubber-toughened amorphous polymers: Fully implicit implementation and optimization-based calibration. *International Journal of Solids and Structures*, 283:112488, 2023.

[86] K.G.W. Pijnenburg and E. Van der Giessen. Macroscopic yield in cavitated polymer blends. *International Journal of Solids and Structures*, 38(20):3575–3598, 2001.

[87] Mats Danielsson, David M. Parks, and Mary C. Boyce. Micromechanics, macromechanics and constitutive modeling of the elasto-viscoplastic deformation of rubber-toughened glassy polymers. *Journal of the Mechanics and Physics of Solids*, 55(3):533–561, 2007.

[88] Michael Rubinstein and Ralph H. Colby. *Polymer Physics*. Oxford University Press, Oxford, UK, 2003.

[89] H. Moulinec and P. Suquet. A numerical method for computing the overall response of nonlinear composites with complex microstructure. *Computer Methods in Applied Mechanics and Engineering*, 157(1):69–94, 1998.

[90] Amine Bahloul, Issam Doghri, and Laurent Adam. Linking a phase field model for polymer crystallization to full-field micromechanical simulations of semi-crystalline polymers. *Computational Materials Science*, 199:110685, 2021.

[91] Vinh Phu Nguyen, Martijn Stroeven, and Lambertus Sluys. Multiscale continuous and discontinuous modeling of heterogeneous materials: A review on recent developments. *Journal of Multiscale Modelling*, 3:1–42, 07 2012.

[92] Eduardo A. de Souza Neto and Raúl A. Feijóo. *Variational Foundations of Large Strain Multiscale Solid Constitutive Models: Kinematical Formulation*, chapter 9, pages 341–378. John Wiley & Sons, Ltd, 2010.

[93] António Rui de Oliveira Santos Silva Melro. *Analytical and numerical modelling of damage and fracture of advanced composites*. PhD thesis, University of Porto, 2011.

[94] Vladimir Salnikov, Daniel Choi, and Philippe Karamian-Surville. On efficient and reliable stochastic generation of rves for analysis of composites within the framework of homogenization. *Computational Mechanics*, 55, 08 2014.

[95] M. Herráez, J. Segurado, C. González, and C.S. Lopes. A microstructures generation tool for virtual ply property screening of hybrid composites with high volume fractions of non-circular fibers – viper. *Composites Part A: Applied Science and Manufacturing*, 129:105691, 2020.

[96] Ramin Bostanabad. Reconstruction of 3d microstructures from 2d images via transfer learning. *Computer-Aided Design*, 128:102906, 2020.

[97] José L.P. Vila-Chã, Bernardo P. Ferreira, and F.M. Andrade Pires. An adaptive multi-temperature isokinetic method for the rve generation of particle reinforced heterogeneous materials, part i: Theoretical formulation and computational framework. *Mechanics of Materials*, 163:104069, 2021.

[98] P.J. Blanco, P.J. Sánchez, E.A. de Souza Neto, and R.A. Feijóo. The method of multiscale virtual power for the derivation of a second order mechanical model. *Mechanics of Materials*, 99:53–67, 2016.

[99] H. J. Frost and M. F. Ashby. *Deformation-mechanism Maps: The Plasticity and Creep of Metals and Ceramics*. Elsevier Science Limited, 1982. Google-Books-ID: s9BRAAAAMAAJ.

[100] Henry Eyring. Viscosity, Plasticity, and Diffusion as Examples of Absolute Reaction Rates. *The Journal of Chemical Physics*, 4(4):283–291, April 1936.

[101] H. C. Brinkman and F. Schwarzl. A mechanical and thermodynamical theory of non-linear relaxation behaviour of solids. *Discussions of the Faraday Society*, 23:11, 1957.

[102] U.F. Kocks, A.S. Argon, and M.F. Ashby. *Thermodynamics and kinetics of slip*. Progress in materials science. Pergamon Press, 1975. tex.lccn: 75012519.

[103] Richard E. Robertson. Theory for the Plasticity of Glassy Polymers. *The Journal of Chemical Physics*, 44(10):3950–3956, May 1966. Publisher: American Institute of Physics.

[104] R. A. Duckett, S. Rabinowitz, and I. M. Ward. The strain-rate, temperature and pressure dependence of yield of isotropic poly(methylmethacrylate) and poly(ethylene terephthalate). *Journal of Materials Science*, 5(10):909–915, October 1970.

[105] D. G. Fotheringham and B. W. Cherry. The role of recovery forces in the deformation of linear polyethylene. *Journal of Materials Science*, 13(5):951–964, May 1978.

[106] A. S. Argon. A theory for the low-temperature plastic deformation of glassy polymers. *Philosophical Magazine*, 28(4):839–865, October 1973.

[107] P. Hao, Z. Dai, V. Laheri, and F. A. Gilabert. A unified amorphous–crystalline viscoplastic hardening law for non-isothermal modelling of thermoplastics and thermosets. *International Journal of Plasticity*, 159:103469, December 2022. tex.ids= haoUnifiedAmorphousCrystalline2022a.

[108] Dale Klahn, Amiya K Mukherjee, and John E Dorn. Strain-rate Effects. In *Proceedings of the 2nd International Conference on the Strength of Metals and Alloys*. California Univ., Berkeley. Lawrence Radiation Lab., 1970. Keynote paper. Also issued as Lawrence Radiation Laboratory Report UCRL-20320, University of California, Berkeley. AEC Contract No. W-7405-eng-48.

[109] C. G'Sell and J. J. Jonas. Yield and transient effects during the plastic deformation of solid polymers. *Journal of Materials Science*, 16(7):1956–1974, July 1981.

[110] John J. Gilman. THE PLASTIC WAVE MYTH. In S. C. Schmidt, R. D. Dick, J. W. Forbes, and D. G. Tasker, editors, *Shock Compression of Condensed Matter–1991*, pages 387–389. Elsevier, Amsterdam, January 1992.

[111] Taikyue Ree and Henry Eyring. Theory of Non-Newtonian Flow. I. Solid Plastic System. *Journal of Applied Physics*, 26(7):793–800, July 1955.

[112] J.A Roetling. Yield stress behaviour of poly(ethyl methacrylate) in the glass transition region. *Polymer*, 6(11):615–619, November 1965.

[113] J.A Roetling. Yield stress behaviour of isotactic polypropylene. *Polymer*, 7(7):303–306, July 1966.

[114] J. C. Bauwens, C. Bauwens-Crowet, and G. Homès. Tensile yield-stress behavior of poly(vinyl chloride) and polycarbonate in the glass transition region. *Journal of Polymer Science Part A-2: Polymer Physics*, 7(10):1745–1754, October 1969.

[115] J. C. Bauwens. Relation between the compression yield stress and the mechanical loss peak of bisphenol-A-polycarbonate in the ? transition range. *Journal of Materials Science*, 7(5):577–584, May 1972. tex.ids= bauwensRelationCompressionYield1972.

[116] J. Haussy, J. P. Cavrot, B. Escaig, and J. M. Lefebvre. Thermodynamic analysis of the plastic deformation of glassy poly(methyl methacrylate). *Journal of Polymer Science: Polymer Physics Edition*, 18(2):311–325, February 1980.

[117] B. W. Cherry and C. M. Holmes. Yield of adhesive joints. *Journal of Physics D: Applied Physics*, 2(6):821, June 1969.

[118] David Fotheringham, B. W. Cherry, and C. Bauwens-Crowet. Comment on "the compression yield behaviour of polymethyl methacrylate over a wide range of temperatures and strain-rates". *Journal of Materials Science*, 11(7):1368–1371, July 1976.

[119] J. Richeton, S. Ahzi, L. Daridon, and Y. Rémond. A formulation of the cooperative model for the yield stress of amorphous polymers for a wide range of strain rates and temperatures. *Polymer*, 46(16):6035–6043, July 2005.

[120] J. Richeton, S. Ahzi, K. S. Vecchio, F. C. Jiang, and R. R. Adharapurapu. Influence of temperature and strain rate on the mechanical behavior of three amorphous polymers: Characterization and modeling of the compressive yield stress. *International Journal of Solids and Structures*, 43(7):2318–2335, 2006.

[121] J. Richeton, S. Ahzi, K. S. Vecchio, F. C. Jiang, and A. Makradi. Modeling and validation of the large deformation inelastic response of amorphous polymers over a wide range of temperatures and strain rates. *International Journal of Solids and Structures*, 44(24):7938–7954, 2007.

[122] J. Richeton, S. Ahzi, and L. Daridon. Thermodynamic investigation of yield-stress models for amorphous polymers. *Philosophical Magazine*, 87(24):3629–3643, August 2007.

[123] A. M. Brown and M. F. Ashby. On the power-law creep equation. *Scripta Metallurgica*, 14(12):1297–1302, December 1980.

[124] P. Perzyna. The constitutive equations for rate sensitive plastic materials. *Quarterly of Applied Mathematics*, 20(4):321–332, 1963.

[125] James M. Kelly and Peter P. Gillis. The influence of a limiting dislocation flux on the mechanical response of polycrystalline metals. *International Journal of Solids and Structures*, 10(1):45–59, January 1974.

[126] S. R. Bodner and Y. Partom. A Large Deformation Elastic-Viscoplastic Analysis of a Thick-Walled Spherical Shell. *Journal of Applied Mechanics*, 39(3):751–757, September 1972.

[127] Masao Doi and S. F. Edwards. Dynamics of concentrated polymer systems. Part 1.—Brownian motion in the equilibrium state. *J. Chem. Soc., Faraday Trans. 2*, 74(0):1789–1801, 1978.

[128] J.S. Bergström and Mary C. Boyce. Constitutive modeling of the large strain time-dependent behavior of elastomers. *Journal of the Mechanics and Physics of Solids*, 46(5):931–954, May 1998.

[129] J.S. Bergström and M.C. Boyce. Constitutive modeling of the time-dependent and cyclic loading of elastomers and application to soft biological tissues. *Mechanics of Materials*, 33(9):523–530, September 2001. tex.ids= bergstromConstitutiveModeling-Timedependent2001a.

[130] J.S. Bergström and L.B. Hilbert. A constitutive model for predicting the large deformation thermomechanical behavior of fluoropolymers. *Mechanics of Materials*, 37(8):899–913, August 2005.

[131] E.A. de Souza Neto, D. Peric, and D.R.J. Owen. *Computational Methods for Plasticity: Theory and Applications*. Wiley, 2008.

[132] O. A. Hasan and M. C. Boyce. A constitutive model for the nonlinear viscoelastic viscoplastic behavior of glassy polymers. *Polymer Engineering & Science*, 35(4):331–344, 1995.

[133] Mary C. Boyce, David M. Parks, and Ali S. Argon. Large inelastic deformation of glassy polymers. part I: Rate dependent constitutive model. *Mechanics of Materials*, 7(1):15–33, 1988.

[134] S. R. Bodner and Y. Partom. Constitutive Equations for Elastic-Viscoplastic Strain-Hardening Materials. *Journal of Applied Mechanics*, 42(2):385–389, June 1975.

[135] Fahmi Zaïri, Moussa Naït-Abdelaziz, Krzysztof Woznica, and Jean-Michel Gloaguen. Elasto-viscoplastic constitutive equations for the description of glassy polymers behavior at constant strain rate. *Journal of Engineering Materials and Technology*, 129(1):29–35, January 2007.

[136] O. A. Hasan, M. C. Boyce, X. S. Li, and S. Berko. An investigation of the yield and postyield behavior and corresponding structure of poly(methyl methacrylate). *Journal of Polymer Science Part B: Polymer Physics*, 31(2):185–197, 1993.

[137] S. Ahzi, A. Makradi, R.V. Gregory, and D.D. Edie. Modeling of deformation behavior and strain-induced crystallization in poly(ethylene terephthalate) above the glass

transition temperature. *Mechanics of Materials*, 35(12):1139–1148, December 2003. tex.ids= ahziModelingDeformationBehavior2003a.

[138] K. A. Chowdhury, R. Talreja, and A. A. Benzerga. Effects of Manufacturing-Induced Voids on Local Failure in Polymer-Based Composites. *Journal of Engineering Materials and Technology*, 130(2), March 2008.

[139] Lallit Anand and Morton E. Gurtin. A theory of amorphous solids undergoing large deformations, with application to polymeric glasses. *International Journal of Solids and Structures*, 40(6):1465–1487, 2003.

[140] Lallit Anand, Nicoli M. Ames, Vikas Srivastava, and Shawn A. Chester. A thermo-mechanically coupled theory for large deformations of amorphous polymers. Part I: Formulation. *International Journal of Plasticity*, 25(8):1474–1494, August 2009.

[141] Nicoli M. Ames, Vikas Srivastava, Shawn A. Chester, and Lallit Anand. A thermo-mechanically coupled theory for large deformations of amorphous polymers. Part II: Applications. *International Journal of Plasticity*, 25(8):1495–1539, August 2009.

[142] Michael I. Okereke and Ambrose I. Akpoyomare. Two-process constitutive model for semicrystalline polymers across a wide range of strain rates. *Polymer*, 183:121818, November 2019.

[143] A. L. Gurson. Continuum theory of ductile rupture by void nucleation and growth. Part I. Yield criteria and flow rules for porous ductile media. Technical Report COO-3084/39, Brown Univ., Providence, R.I. (USA). Div. of Engineering, 1977.

[144] C. Chu and Alan Needleman. Void nucleation effects in biaxially stretched sheets. *Journal of Engineering Materials and Technology*, 102:249, 07 1980.

[145] X. Tvergaard. Influence of voids on shear band instabilities under plane strain conditions. *International Journal of Fracture*, 17:389–407, 1981.

[146] M. Gologanu, J.-B. Leblond, G. Perrin, and J. Devaux. *Recent Extensions of Gurson's Model for Porous Ductile Metals*, pages 61–130. Springer Vienna, Vienna, 1997.

[147] Zhu Yan, Qiang Guo, Fahmi Zaïri, and Ali Zaoui. A multi-scale plastic-damage model for strain-induced morphological anisotropy in semi-crystalline polyethylene. *International Journal of Non-Linear Mechanics*, 147:104238, 2022.

[148] Bernardo P. Ferreira, A. Francisca Carvalho Alves, and F.M. Andrade Pires. An efficient finite strain constitutive model for amorphous thermoplastics: Fully implicit computational implementation and optimization-based parameter calibration. *Computers & Structures*, 281:107007, 2023.

[149] C. B. Bucknall, A. Karpodinis, and X. C. Zhang. A model for particle cavitation in rubber-toughened plastics. *Journal of Materials Science*, 29(13):3377–3383, Jul 1994.

[150] B.P. Gearing and L. Anand. Notch-sensitive fracture of polycarbonate. *International Journal of Solids and Structures*, 41(3-4):827–845, 2004.

[151] M. G. A. Tijssens, E. van der Giessen, and L. J. Sluys. Modeling of crazing using a cohesive surface methodology. *Mechanics of Materials*, 32(1):19–35, 2000.

[152] R. Estevez, M. G. A. Tijssens, and E. van der Giessen. Modeling of the competition between shear yielding and crazing in glassy polymers. *Journal of the Mechanics and Physics of Solids*, 48(12):2585–2617, 2000.

[153] R. Estevez and E. Van der Giessen. Modeling and Computational Analysis of Fracture of Glassy Polymers. In Hans-Henning Kausch, editor, *Intrinsic Molecular Mobility and Toughness of Polymers II*, volume 188, pages 195–234. Springer Berlin Heidelberg, Berlin, Heidelberg, 2005.

[154] Thomas Seelig and Erik Giessen. Effects of microstructure on crack tip fields and fracture toughness in PC/ABS polymer blends. *International Journal of Fracture*, 145(3):205–222, 2007.

[155] B.P. Gearing and L. Anand. On modeling the deformation and fracture response of glassy polymers due to shear-yielding and crazing. *International Journal of Solids and Structures*, 41(11-12):3125–3150, 2004.

[156] A. S. Argon. Craze plasticity in low molecular weight diluent-toughened polystyrene. *Journal of Applied Polymer Science*, 72(1):13–33, 1999.

[157] Erik Van der Giessen and Thomas Seelig. Computational modeling of rubber-toughening in amorphous thermoplastic polymers: A review. *International Journal of Fracture*, 196(1-2):207–222, 2015.

[158] M. Helbig, E. van der Giessen, A. H. Clausen, and Th Seelig. Continuum-micromechanical modeling of distributed crazing in rubber-toughened polymers. *European Journal of Mechanics A-Solids*, 57:108–120, 2016.

[159] Han Jiang, Jianwei Zhang, Zhuoran Yang, Chengkai Jiang, and Guozheng Kang. Modeling of competition between shear yielding and crazing in amorphous polymers' scratch. *International Journal of Solids and Structures*, 124:215–228, 2017.

[160] Elhem Ghorbel. A viscoplastic constitutive model for polymeric materials. *International Journal of Plasticity*, 24(11):2032–2058, November 2008. tex.ids= ghorbelViscoplasticConstitutiveModel2008a.

[161] R. Balieu, F. Lauro, B. Bennani, T. Matsumoto, and E. Mottola. Non-associated viscoplasticity coupled with an integral-type nonlocal damage model for mineral filled semi-crystalline polymers. *Computers & Structures*, 134:18–31, April 2014.

[162] Ming Chen Wang and Eugene Guth. Statistical Theory of Networks of Non-Gaussian Flexible Chains. *The Journal of Chemical Physics*, 20(7):1144–1157, July 1952.

[163] Ellen M. Arruda and Mary C. Boyce. Evolution of plastic anisotropy in amorphous polymers during finite straining. *International Journal of Plasticity*, 9(6):697–720, 1993.

[164] Ellen M. Arruda, Mary C. Boyce, and R. Jayachandran. Effects of strain rate, temperature and thermomechanical coupling on the finite strain deformation of glassy polymers. *Mechanics of Materials*, 19(2-3):193–212, January 1995. tex.ids= arrudaEffectsStrainRate1995a.

[165] S. F. Edwards and Th. Vilgis. The effect of entanglements in rubber elasticity. *Polymer*, 27(4):483–492, April 1986.

[166] E. H. Lee and D. T. Liu. Finite-Strain Elastic—Plastic Theory with Application to Plane-Wave Analysis. *Journal of Applied Physics*, 38(1):19–27, January 1967.

[167] E. H. Lee. Elastic-Plastic Deformation at Finite Strains. *Journal of Applied Mechanics*, 36(1):1–6, March 1969.

[168] Stefanie Reese and Sanjay Govindjee. A theory of finite viscoelasticity and numerical aspects. *International Journal of Solids and Structures*, 35(26-27):3455–3482, September 1998.

[169] Bernard D. Coleman and Walter Noll. Foundations of Linear Viscoelasticity. *Reviews of Modern Physics*, 33(2):239–249, April 1961. Publisher: American Physical Society.

[170] J.C. Simo. On a fully three-dimensional finite-strain viscoelastic damage model: Formulation and computational aspects. *Computer Methods in Applied Mechanics and Engineering*, 60(2):153–173, February 1987.

[171] E. T. Onat. Representation of elastic-plastic behavior in the presence of finite deformations and anisotropy. *International Journal of Plasticity*, 1987.

[172] S. C. H. Lu and K. S. Pister. Decomposition of deformation and representation of the free energy function for isotropic thermoelastic solids. *International Journal of Solids and Structures*, 11(7):927–934, July 1975.

[173] J. C. Simo and C. Miehe. Associative coupled thermoplasticity at finite strains: Formulation, numerical analysis and implementation. *Computer Methods in Applied Mechanics and Engineering*, 98(1):41–104, July 1992.

[174] P. Hao, V. Laheri, Z. Dai, and F.A. Gilabert. A rate-dependent constitutive model predicting the double yield phenomenon, self-heating and thermal softening in semi-crystalline polymers. *International Journal of Plasticity*, 153:103233, June 2022.

[175] A. IA Malkin and Avraam I. Isayev. *Rheology: concepts methods, and applications*. ChemTec Publishing, Toronto, 3rd edition edition, 2017. OCLC: ocn963393005.

[176] Thor L. Smith. Nonlinear Viscoelastic Response of Amorphous Elastomers to Constant Strain Rates. *Transactions of the Society of Rheology*, 6(1):61–80, March 1962.

[177] Fahmi Zaïri, Krzysztof Woznica, and Moussa Naït-Abdelaziz. Phenomenological nonlinear modelling of glassy polymers. *Comptes Rendus Mécanique*, 333(4):359–364, April 2005.

[178] Chuntao Zhang and Ian D. Moore. Nonlinear mechanical response of high density polyethylene. Part II: Uniaxial constitutive modeling. *Polymer Engineering & Science*, 37(2):414–420, February 1997.

[179] Geoffrey J Frank and Robert A Brockman. A viscoelastic–viscoplastic constitutive model for glassy polymers. *International Journal of Solids and Structures*, 38(30):5149–5164, July 2001.

[180] G. Cailletaud and K. Saï. Study of plastic/viscoplastic models with various inelastic mechanisms. *International Journal of Plasticity*, 11(8):991–1005, January 1995.

[181] B. Miled, I. Doghri, and L. Delannay. Coupled viscoelastic–viscoplastic modeling of homogeneous and isotropic polymers: Numerical algorithm and analytical solutions. *Computer Methods in Applied Mechanics and Engineering*, 200(47):3381–3394, 2011.

[182] Anouar Krairi and Issam Doghri. A thermodynamically-based constitutive model for thermoplastic polymers coupling viscoelasticity, viscoplasticity and ductile damage. *International Journal of Plasticity*, 60:163–181, 2014.

[183] Muralidhar Reddy Gudimetla and Issam Doghri. A finite strain thermodynamically-based constitutive framework coupling viscoelasticity and viscoplasticity with application to glassy polymers. *International Journal of Plasticity*, 98:197–216, 2017.

[184] A. Krairi, I. Doghri, J. Schalnat, G. Robert, and W. Van Paepegem. Thermo-mechanical coupling of a viscoelastic-viscoplastic model for thermoplastic polymers:

Thermodynamical derivation and experimental assessment. *International Journal of Plasticity*, 115:154–177, 2019.

[185] E. P. Cernocky and E. Krempl. A theory of viscoplasticity based on infinitesimal total strain. *Acta Mechanica*, 36(3):263–289, September 1980.

[186] M. C. M. Liu and E. Krempl. A uniaxial viscoplastic model based on total strain and overstress. *Journal of the Mechanics and Physics of Solids*, 27(5):377–391, December 1979.

[187] D. Yao and E. Krempl. Viscoplasticity theory based on overstress. The prediction of monotonic and cyclic proportional and nonproportional loading paths of an aluminum alloy. *International Journal of Plasticity*, 1(3):259–274, January 1985.

[188] Masayoshi Kitagawa, Tatsuya Mori, and Tomohiko Matsutani. Rate-dependent nonlinear constitutive equation of polypropylene. *Journal of Polymer Science Part B: Polymer Physics*, 27(1):85–95, 1989.

[189] Masayoshi Kitagawa and Hideyuki Takagi. Nonlinear constitutive equation for polyethylene under combined tension and torsion. *Journal of Polymer Science Part B: Polymer Physics*, 28(11):1943–1953, 1990.

[190] Erhard Krempl and Kwangsoo Ho. An overstress model for solid polymer deformation behavior applied to Nylon 66. *ASTM special technical publication*, 1357:118–140, 2000.

[191] O Colak. Modeling deformation behavior of polymers with viscoplasticity theory based on overstress. *International Journal of Plasticity*, 21(1):145–160, January 2005.

[192] K. Ho and E. Krempl. Extension of the viscoplasticity theory based on overstress (VBO) to capture non-standard rate dependence in solids. *International Journal of Plasticity*, 18(7):851–872, July 2002.

[193] George Halsey, Howard J. White, and Henry Eyring. Mechanical Properties of Textiles, I. *Textile Research Journal*, 15(9):295–311, September 1945.

[194] R. N. Haward and G. Thackray. The Use of a Mathematical Model to Describe Isothermal Stress-Strain Curves in Glassy Thermoplastics. *Proceedings of the Royal Society of London. Series A, Mathematical and Physical Sciences*, 302(1471):453–472, 1968.

[195] P. D. Wu and E. Van Der Giessen. On improved network models for rubber elasticity and their applications to orientation hardening in glassy polymers. *Journal of the Mechanics and Physics of Solids*, 41(3):427–456, March 1993.

[196] C. P. Buckley and D. C. Jones. Glass-rubber constitutive model for amorphous polymers near the glass transition. *Polymer*, 36(17):3301–3312, January 1995.

[197] J. Sweeney and I. M. Ward. Rate dependent and network phenomena in the multiaxial drawing of poly(vinyl chloride). *Polymer*, 36(2):299–308, January 1995.

[198] J.S. Bergström and M.C. Boyce. Large strain time-dependent behaviour of filled elastomers. *Mechanics of Materials*, 32:627–644, 11 2000.

[199] X. Poulain, A. A. Benzerga, and R. K. Goldberg. Finite-strain elasto-viscoplastic behavior of an epoxy resin: Experiments and modeling in the glassy regime. *International Journal of Plasticity*, 62:138–161, November 2014.

[200] S. M. Mirkhalaf, F. M. Andrade Pires, and R. Simoes. An elasto-viscoplastic constitutive model for polymers at finite strains: Formulation and computational aspects. *Computers & Structures*, 166:60–74, April 2016.

[201] E.A. De Souza Neto, Djordje Perić, and D.R.J. Owen. A model for elastoplastic damage at finite strains: Algorithmicissues and applications. *Engineering Computations*, 11(3):257–281, January 1994.

[202] Adrian Luis Eterovic and Klaus-Jürgen Bathe. A hyperelastic-based large strain elasto-plastic constitutive formulation with combined isotropic-kinematic hardening using the logarithmic stress and strain measures. *International Journal for Numerical Methods in Engineering*, 30(6):1099–1114, 1990.

[203] Marcos Latorre and Francisco J. Montáns. A new class of plastic flow evolution equations for anisotropic multiplicative elastoplasticity based on the notion of a corrector elastic strain rate. *Applied Mathematical Modelling*, 55:716–740, 2018.

[204] Meijuan Zhang and Francisco J. Montáns. A simple formulation for large-strain cyclic hyperelasto-plasticity using elastic correctors. theory and algorithmic implementation. *International Journal of Plasticity*, 113:185–217, 2019.

[205] Meijuan Zhang, K. Nguyen, Javier Segurado, and Francisco J. Montáns. A multiplicative finite strain crystal plasticity formulation based on additive elastic corrector rates: Theory and numerical implementation. *International Journal of Plasticity*, 137:102899, 2021.

[206] J. C. Simo and T. J. R. Hughes. *Computational Inelasticity*. Interdisciplinary Applied Mathematics. Springer-Verlag, New York, 1998.

[207] Gerhard A. Holzapfel. *Nonlinear Solid Mechanics: A Continuum Approach for Engineering*. Wiley, April 2000.

[208] Peng Yu, Xiaohu Yao, Qiang Han, Shuguang Zang, and Yabei Gu. A viscoelastoplastic constitutive model for large deformation response of polycarbonate over a wide range of strain rates and temperatures. *Polymer*, 55(25):6577–6593, December 2014.

[209] Sami Holopainen, Thierry Barriere, Gang Cheng, and Reijo Kouhia. Continuum approach for modeling fatigue in amorphous glassy polymers. applications to the investigation of damage-ratcheting interaction in polycarbonate. *International Journal of Plasticity*, 91:109–133, 2017.

[210] Sami Holopainen and Thierry Barriere. Modeling of mechanical behavior of amorphous solids undergoing fatigue loadings, with application to polymers. *Computers & Structures*, 199:57–73, 2018.

[211] Zheliang Wang, Jingkai Guo, Jonathan E. Seppala, and Thao D. Nguyen. Extending the effective temperature model to the large strain hardening behavior of glassy polymers. *Journal of the Mechanics and Physics of Solids*, 146:104175, 2021.

[212] Rui Xiao and Thao D. Nguyen. An effective temperature theory for the nonequilibrium behavior of amorphous polymers. *Journal of the Mechanics and Physics of Solids*, 82:62–81, 2015.

[213] Makoto Uchida, Kouhei Kamimura, Toyoshi Yoshida, and Yoshihisa Kaneko. Viscoelastic-viscoplastic modeling of epoxy based on transient network theory. *International Journal of Plasticity*, 153:103262, 2022.

[214] Makoto Uchida, Ryohei Wakuda, and Yoshihisa Kaneko. Evaluation and modeling of mechanical behaviors of thermosetting polymer under monotonic and cyclic tensile tests. *Polymer*, 174:130–142, 2019.

[215] A. I. Leonov. Nonequilibrium thermodynamics and rheology of viscoelastic polymer media. *Rheologica Acta*, 15(2):85–98, 1976.

[216] F. Baaijens. Calculation of residual stresses in injection molded products. *Rheologica Acta*, 30:284–299, 1991.

[217] T.A. Tervoort, R.J.M. Smit, W.A.M. Brekelmans, and L.E. Govaert. A constitutive equation for the elasto-viscoplastic deformation of glassy polymers. *Mechanics of Time-Dependent Materials*, 1(3):269–291, 1998.

[218] P. H. M. Timmermans. *Evaluation of a Constitutive Model for Solid Polymeric Materials: Model Selection and Parameter Quantification.* PhD thesis, Eindhoven University of Technology, 1997.

[219] L. Govaert, Peter Timmermans, and W. Brekelmans. The Influence of Intrinsic Strain Softening on Strain Localization in Polycarbonate: Modeling and Experimental Validation. *Journal of Engineering Materials and Technology-transactions of The Asme - J. Eng. Mater. Technol.*, 122, April 2000.

[220] Hassan Khaleghi, Ahmad Amiri-Rad, and Mohammad Mashayekhi. A thermodynamically consistent continuum damage model for time-dependent failure of thermoplastic polymers. *International Journal of Plasticity*, 154:103278, 2022.

[221] Jean Lemaitre. *A Course on Damage Mechanics*. Springer Science & Business Media, 2013.

[222] L.C.A. van Breemen, E.T.J. Klompen, L.E. Govaert, and H.E.H. Meijer. Extending the egp constitutive model for polymer glasses to multiple relaxation times. *Journal of the Mechanics and Physics of Solids*, 59(10):2191–2207, 2011.

[223] A. Amiri-Rad, L.V. Pastukhov, L.E. Govaert, and J.A.W. van Dommelen. An anisotropic viscoelastic-viscoplastic model for short-fiber composites. *Mechanics of Materials*, 137:103141, 2019.

[224] Mariem Nciri, Delphine Notta-Cuvier, Franck Lauro, Fahmi Chaari, Yamen Maalej, and Bassem Zouari. Viscoelastic-viscoplastic model for short-fibre-reinforced composites with complex fibre orientation. *Mechanics of Advanced Materials and Structures*, 26, 01 2018.

[225] J.L. Bouvard, D.K. Francis, M.A. Tschopp, E.B. Marin, D.J. Bammann, and M.F. Horstemeyer. An internal state variable material model for predicting the time, thermomechanical, and stress state dependence of amorphous glassy polymers under large deformation. *International Journal of Plasticity*, 42:168–193, 2013.

[226] Tianxiang Lan, Yaodong Jiang, and Peidong Wu. A thermodynamically-based constitutive theory for amorphous glassy polymers at finite deformations. *International Journal of Plasticity*, 158:103415, 2022.

[227] Chengkai Jiang. Finite deformation constitutive model for macro-yield behavior of amorphous glassy polymers with a molecular entanglement-based internal-state variable. *International Journal of Mechanical Sciences*, 161-162:105064, 08 2019.

[228] Chengkai Jiang, Zhongmeng Zhu, Jianwei Zhang, and Zhuoran YANG. Constitutive modeling of the rate- and temperature-dependent macro-yield behavior of amorphous glassy polymers. *International Journal of Mechanical Sciences*, 179:105653, 04 2020.

[229] S.G. Bardenhagen, M.G. Stout, and G.T. Gray. Three-dimensional, finite deformation, viscoplastic constitutive models for polymeric materials. *Mechanics of Materials*, 25(4):235–253, May 1997.

[230] M.C. Boyce, S. Socrate, and P.G. Llana. Constitutive model for the finite deformation stress–strain behavior of poly(ethylene terephthalate) above the glass transition. *Polymer*, 41(6):2183–2201, March 2000.

[231] Thomas Kletschkowski, Uwe Schomburg, and Albrecht Bertram. Endochronic viscoplastic material models for filled PTFE. *Mechanics of Materials*, 34(12):795–808, December 2002.

[232] K. C. Valanis. A Theory of Viscoplasticity without a Yield Surface. Part 1. General Theory. Technical report, 1970.

[233] D. W. Holmes, J. G. Loughran, and H. Suehrcke. Constitutive model for large strain deformation of semicrystalline polymers. *Mechanics of Time-Dependent Materials*, 10(4):281–313, December 2006.

[234] N. Brusselle-Dupend, D. Lai, X. Feaugas, M. Guigon, and M. Clavel. Mechanical behavior of a semicrystalline polymer before necking. Part 1: Characterization of uniaxial behavior. *Polymer Engineering & Science*, 41(1):66–76, 2001.

[235] N. Brusselle-Dupend, D. Lai, X. Feaugas, M. Guigon, and M. Clavel. Mechanical behavior of a semicrystalline polymer before necking. Part II: Modeling of uniaxial behavior. *Polymer Engineering & Science*, 43(2):501–518, 2003.

[236] L. Anand and N.M. Ames. On modeling the micro-indentation response of an amorphous polymer. *International Journal of Plasticity*, 22(6):1123–1170, 2006.

[237] Suvrat P. Lele and Lallit Anand. A large-deformation strain-gradient theory for isotropic viscoplastic materials. *International Journal of Plasticity*, 25(3):420–453, 2009.

[238] Vikas Srivastava, Shawn A. Chester, Nicoli M. Ames, and Lallit Anand. A thermo-mechanically-coupled large-deformation theory for amorphous polymers in a temperature range which spans their glass transition. *International Journal of Plasticity*, 26(8):1138–1182, 2010. Special Issue In Honor of Lallit Anand.

[239] J. Wang, L.F. Peng, Y.J. Deng, X.M. Lai, M.W. Fu, and J. Ni. A finite strain thermodynamically-based constitutive modeling and analysis of viscoelastic-viscoplastic deformation behavior of glassy polymers. *International Journal of Plasticity*, 122:135–163, 2019.

[240] A. D. Mulliken and M. C. Boyce. Mechanics of the rate-dependent elastic–plastic deformation of glassy polymers from low to high strain rates. *International Journal of Solids and Structures*, 43(5):1331–1356, March 2006.

[241] A.G. Varghese and R.C. Batra. Constitutive equations for thermomechanical deformations of glassy polymers. *International Journal of Solids and Structures*, 46(22):4079–4094, 2009.

[242] Keivan H. Safari, Jamal Zamani, Fernando J. Ferreira, and Rui M. Guedes. Constitutive modeling of polycarbonate during high strain rate deformation. *Polymer Engineering & Science*, 53(4):752–761, 2013.

[243] Haitao Wang, Yun Zhang, Zhigao Huang, Zhongbin Tang, Yanpei Wang, and Huamin Zhou. Establishment and comparison of four constitutive relationships of pc/abs from low to high uniaxial strain rates. *Mechanics of Time-Dependent Materials*, 22, 11 2018.

[244] Joakim Johnsen, Arild Clausen, Frode Grytten, Ahmed Benallal, and Odd Hopperstad. A thermo-elasto-viscoplastic constitutive model for polymers. *Journal of the Mechanics and Physics of Solids*, 124, 11 2018.

[245] A. Francisca Carvalho Alves, Bernardo P. Ferreira, and F.M. Andrade Pires. A constitutive model for amorphous thermoplastics from low to high strain rates: Formulation and computational aspects. *International Journal of Plasticity*, 169:103712, 2023.

[246] J Bergström. Constitutive modeling of ultra-high molecular weight polyethylene under large-deformation and cyclic loading conditions. *Biomaterials*, 23(11):2329–2343, June 2002.

[247] Jörgen S. Bergström, C.M. Rimnac, and S.M. Kurtz. Prediction of multiaxial mechanical behavior for conventional and highly crosslinked UHMWPE using a hybrid constitutive model. *Biomaterials*, 24(8):1365–1380, April 2003.

[248] Motowo Takayanagi, Shinsaku Uemura, and Shunsuke Minami. Application of equivalent model method to dynamic rheo-optical properties of crystalline polymer. *Journal of Polymer Science Part C: Polymer Symposia*, 5(1):113–122, 1964. _eprint: https://onlinelibrary.wiley.com/doi/pdf/10.1002/polc.5070050111.

[249] Motowo Takayanagi, Kiyohisa Imada, and Tisato Kajiyama. Mechanical properties and fine structure of drawn polymers. *Journal of Polymer Science Part C: Polymer Symposia*, 15(1):263–281, January 1967. Publisher: John Wiley & Sons, Ltd.

[250] A. Dahoun, M. Aboulfaraj, C. G'Sell, A. Molinari, and G. R. Canova. Plastic behavior and deformation textures of poly(etherether ketone) under uniaxial tension and simple shear. *Polymer Engineering and Science*, 35(4):317–330, February 1995.

[251] D. M. Parks and S. Ahzi. Polycrystalline plastic deformation and texture evolution for crystals lacking five independent slip systems. *Journal of the Mechanics and Physics of Solids*, 38(5):701–724, January 1990.

[252] A. Molinari, G. R. Canova, and S. Ahzi. A self consistent approach of the large deformation polycrystal viscoplasticity. *Acta Metallurgica*, 35(12):2983–2994, December 1987.

[253] A. Makradi, S. Ahzi, R.V. Gregory, and D.D. Edie. A two-phase self-consistent model for the deformation and phase transformation behavior of polymers above the

glass transition temperature: application to PET. *International Journal of Plasticity*, 21(4):741–758, April 2005.

[254] Cedric Regrain, Lucien Laiarinandrasana, Sophie Toillon, and Kacem Saï. Multi-mechanism models for semi-crystalline polymer: Constitutive relations and finite element implementation. *International Journal of Plasticity*, 25(7):1253–1279, July 2009.

[255] Necmi Dusunceli and Ozgen U. Colak. Modelling effects of degree of crystallinity on mechanical behavior of semicrystalline polymers. *International Journal of Plasticity*, 24(7):1224–1242, July 2008.

[256] G. Ayoub, F. Zaïri, M. Naït-Abdelaziz, and J.M. Gloaguen. Modelling large deformation behaviour under loading–unloading of semicrystalline polymers: Application to a high density polyethylene. *International Journal of Plasticity*, 26(3):329–347, March 2010. tex.ids= ayoubModellingLargeDeformation2010a.

[257] H. Abdul-Hameed, T. Messager, G. Ayoub, F. Zaïri, M. Naït-Abdelaziz, Z. Qu, and F. Zaïri. A two-phase hyperelastic-viscoplastic constitutive model for semi-crystalline polymers: Application to polyethylene materials with a variable range of crystal fractions. *Journal of the Mechanical Behavior of Biomedical Materials*, 37:323–332, September 2014.

[258] K.N. Cundiff, G. Ayoub, and A.A. Benzerga. Modeling the viscoplastic behavior of a semicrystalline polymer. *International Journal of Solids and Structures*, 254-255:111920, November 2022.

[259] A. Francisca Carvalho Alves, B. P. Ferreira, and F. M. Andrade Pires. Constitutive modeling of amorphous thermoplastics from low to high strain rates: Formulation and critical comparison employing an optimization-based parameter identification. *International Journal of Solids and Structures*, page 112258, 2023.

[260] H. G. H. van Melick, L. E. Govaert, and H. E. H. Meijer. Localisation phenomena in glassy polymers: Influence of thermal and mechanical history. *Polymer*, 44(12):3579–3591, June 2003.

[261] Tomonari Furukawa, Tomohiro Sugata, Shinobu Yoshimura, and Mark Hoffman. An automated system for simulation and parameter identification of inelastic constitutive models. *Computer Methods in Applied Mechanics and Engineering*, 191(21):2235–2260, 2002.

[262] R. P. Cardoso Coelho, A. Francisca Carvalho Alves, T. M. Nogueira Pires, and F. M. Andrade Pires. piglot: an open-source package for derivative-free optimisation of numerical responses. *Journal of Open Source Software*, 9(99):6652, 2024.

[263] B.H. Lavenda. *Thermodynamics of irreversible processes*. Wiley, 1978. tex.lccn: 76022604.

[264] G. A. Maugin. *The Thermomechanics of Nonlinear Irreversible Behaviours*, volume 27 of *World Scientific Series on Nonlinear Science*. World Scientific, 1999.

[265] Gerhard A. Holzapfel. *Nonlinear Solid Mechanics: A Continuum Approach for Engineering*. Wiley, April 2000.

[266] M. Ciampa, M. Franciosi, and M. Poletti. Linear Differential Equations and Related Continuous LTI Systems. *Circuits, Systems, and Signal Processing*, 38(10):4465–4503, October 2019.

[267] S. Matsuoka. Thermodynamic theory of viscoelasticity. *Journal of Thermal Analysis*, 46(3-4):985–1010, March 1996.

Appendix A. Thermomechanical problem

This section provides a brief overview of the thermomechanical problem in the context of continuum mechanics, which serves as the foundation for the constitutive modeling approaches discussed in the body of the manuscript. To provide a common vocabulary for the discussion of the thermomechanical behavior of solid polymers observed in experiments, we also introduce the linear thermo-viscoelastic model, which captures the essential features of polymer response under various loading conditions. The failures of this simple model to accurately represent the complex behavior of amorphous polymers motivate the development of more advanced constitutive models, which are reviewed in Section 7.

Appendix A.1. Kinematics of deformation

Let a deformable body $\mathscr{B}$ occupy an open region Ω_0 of the tridimensional Euclidean space $\mathscr{E}$ with a regular boundary $\partial\Omega_0$ in its reference configuration. A smooth one-to-one function defines its motion $\boldsymbol{\varphi}\colon \Omega \times \mathbb{R} \to \mathscr{E}$, mapping each material particle of coordinates $\boldsymbol{X}$ in the reference configuration to its position $\boldsymbol{x}$ in the deformed configuration. Accordingly, the displacement is defined as $\boldsymbol{u} \equiv \boldsymbol{x} - \boldsymbol{X}$. The well-known deformation gradient second-order tensor is defined as

$$\boldsymbol{F}(\boldsymbol{X}, t) \equiv \nabla_0 \boldsymbol{\varphi}(\boldsymbol{X}, t), \tag{A.1}$$

and its determinant, denoted as $J \equiv \det \boldsymbol{F} \geq 0$, represents the local unit volume change, where ∇_0 is the gradient operator with respect to the material coordinates $\boldsymbol{X}$. The polar decomposition theorem, yields two unique multiplicative decompositions of the deformation gradient as

$$\boldsymbol{F} = \boldsymbol{R}\boldsymbol{U} = \boldsymbol{V}\boldsymbol{R}, \tag{A.2}$$

where $\boldsymbol{R}$ is a proper orthogonal tensor representing the rigid body rotation, $\boldsymbol{U}$ is the right stretch tensor, and $\boldsymbol{V}$ is the left stretch tensor, the unique symmetric and positive definite square roots of the right and left Cauchy-Green deformation tensors, defined as

$$\boldsymbol{C} \equiv \boldsymbol{F}^T\boldsymbol{F} = \boldsymbol{U}^2, \quad \boldsymbol{B} \equiv \boldsymbol{F}\boldsymbol{F}^T = \boldsymbol{V}^2, \tag{A.3}$$

respectively. The principal stretches λ_i $(i = 1, 2, 3)$ are defined as the eigenvalues of the right or left stretch tensors.

A commonly used family of strain measures is the Seth-Hill family of generalized strain tensors, defined as

$$\boldsymbol{E}^{(m)} \equiv \begin{cases} \frac{1}{2m}(\boldsymbol{C}^m - \boldsymbol{I}), & m \neq 0, \\ \frac{1}{2}\ln \boldsymbol{C}, & m = 0, \end{cases}, \tag{A.4}$$

where m is a real number and $\boldsymbol{I}$ is the second-order identity tensor. The infinitesimal strain tensor $\boldsymbol{\varepsilon}$ is recovered as the first order approximation of $\boldsymbol{E}^{(m)}$, valid for small deformations. Isochoric and volumetric versions of these strain measures are also commonly used in the modeling of incompressible or nearly incompressible materials, such as polymers, trough a multiplicative decomposition of the deformation gradient into volumetric and isochoric parts as

$$\boldsymbol{F} = J^{1/3}\boldsymbol{F}^*, \tag{A.5}$$

where $\boldsymbol{F}^* \equiv J^{-1/3}\boldsymbol{F}$ is the isochoric part of the deformation gradient, satisfying $\det \boldsymbol{F}^* = 1$ [207, 16].

Also relevant to the present work is the spatial velocity gradient

$$\boldsymbol{L} \equiv \dot{\boldsymbol{F}}\boldsymbol{F}^{-1}, \tag{A.6}$$

where $\dot{\boldsymbol{F}}$ denotes the time derivative of the deformation gradient and the dependence of the spatial coordinates and time is omitted. This tensor can be additively decomposed into its symmetric and skew-symmetric parts as

$$\boldsymbol{L} = \boldsymbol{D} + \boldsymbol{W}, \tag{A.7}$$

where $\boldsymbol{D} \equiv \frac{1}{2}(\boldsymbol{L} + \boldsymbol{L}^T)$ is the rate of deformation tensor and $\boldsymbol{W} \equiv \frac{1}{2}(\boldsymbol{L} - \boldsymbol{L}^T)$ is the spin tensor.

Appendix A.2. Stress measures

In continuum mechanics, several stress measures are used to describe the internal forces within a deformable body. The Cauchy stress tensor $\boldsymbol{\sigma}$ is the most commonly used stress measure, representing the true stress in the current configuration of the body. However, for large deformations, it is often more convenient to use stress measures defined in the reference configuration. The first Piola-Kirchhoff stress tensor $\boldsymbol{P}$ relates forces in the current

configuration to areas in the reference configuration, while the second Piola-Kirchhoff stress tensor $\boldsymbol{S}$ relates forces and areas both in the reference configuration. These stress measures are related through

$$\boldsymbol{P} = J\boldsymbol{\sigma}\boldsymbol{F}^{-T}, \quad \boldsymbol{S} = \boldsymbol{F}^{-1}\boldsymbol{P}. \tag{A.8}$$

Other stress measures include the Kirchhoff stress tensor $\boldsymbol{\tau} = J\boldsymbol{\sigma}$ and the Mandel stress tensor $\boldsymbol{M} = J\boldsymbol{F}^T\boldsymbol{\sigma}\boldsymbol{F}^{-T}$. Each stress measure is paired with a specific strain measure, defining the work-conjugate pairs used in constitutive modeling. In effect, the mechanical power can be expressed equivalently in terms of any of these stress-strain pairs as

$$\boldsymbol{P} : \dot{\boldsymbol{F}} = J(\boldsymbol{\sigma} : \boldsymbol{D}) = \boldsymbol{S} : \dot{\boldsymbol{E}}^{(1)} = \boldsymbol{\tau} : \boldsymbol{D} = (\boldsymbol{R}^T\boldsymbol{\tau}\boldsymbol{R}) : \dot{\boldsymbol{\varepsilon}}^{(0)} = \boldsymbol{M} : \dot{\boldsymbol{E}}^{(0)}, \tag{A.9}$$

where the colon operator $(\bullet) : (\bullet)$ denotes the double contraction between two second-order tensors, and $\boldsymbol{\varepsilon}^{(0)} \equiv \ln \boldsymbol{V}$ is the logarithmic strain tensor.

When modeling polymer behavior, it is common to consider the deviatoric and volumetric components of the stress tensors separately. The deviatoric part of a second-order tensor $\boldsymbol{A}$ is defined as

$$\boldsymbol{A}_{\text{dev}} \equiv \boldsymbol{A} - A_m\boldsymbol{I}, \tag{A.10}$$

where $A_m = \text{tr}\,\boldsymbol{A}/3$ is the mean normal component and tr $(\bullet)$ denotes the trace operator. p is the hydrostatic pressure, defined as $p \equiv -\sigma_m$.

Appendix A.3. Fundamental conservation principles

In continuum thermomechanics, there is a set of conservation principles and thermodynamic laws that, irrespective of the quantities used to describe the mechanical behavior of a body undergoing large deformations, must always be satisfied, namely,

$$\text{div}_0\,\boldsymbol{P} + \boldsymbol{b}_0 = \rho_0\ddot{\boldsymbol{u}}, \quad \text{(balance of momentum)}; \tag{A.11}$$

$$\boldsymbol{F}^{-1}\boldsymbol{P} = \boldsymbol{P}^T\boldsymbol{F}^{-T}, \quad \text{(balance of moment of momentum)}; \tag{A.12}$$

$$\rho_0\dot{e} = \boldsymbol{P} : \dot{\boldsymbol{F}} + \rho_0 r - \text{div}_0\,\boldsymbol{q}_0, \quad \text{(balance of energy)}; \tag{A.13}$$

$$\rho_0\dot{s} + \text{div}_0\left[\frac{\boldsymbol{q}_0}{T}\right] - \frac{\rho_0 r}{T} \geq 0, \quad \text{(entropy production inequality)}, \tag{A.14}$$

where $\boldsymbol{b}_0$ is the body force field, measured in force per unit undeformed volume; ρ_0 is the material density, measured in mass per unit undeformed volume; e is the internal energy

per unit mass; r is the heat supply per unit mass; $\boldsymbol{q}_0$ is the heat flux vector, measured in heat power per unit undeformed surface; T is the absolute temperature; and s is the specific entropy per unit mass.

Appendix A.4. Thermodynamically consistent constitutive modeling

Eqs. (A.11-A.14) do not constitute a well-posed problem, as they contain more unknowns than equations. The stresses, entropies and heat fluxes in the governing equations need to be connected with the deformations and temperatures via constitutive laws that represent the physical behavior of the material. Following our physical intuition, it is standard to assume that the stresses, entropies and heat fluxes depend on the history of deformation and temperature, adopting the axiom of *thermodynamic determinism* [131], and thus symbolically represented as

$$\boldsymbol{P} = \mathcal{H}({}^t\boldsymbol{F}, {}^tT), \tag{A.15}$$

$$s = \mathcal{J}({}^t\boldsymbol{F}, {}^tT), \tag{A.16}$$

$$\boldsymbol{q}_0 = \mathcal{G}({}^t\boldsymbol{F}, {}^tT, {}^t\boldsymbol{g}_0), \tag{A.17}$$

where $\boldsymbol{g}_0 \equiv \nabla_0 T$ is the material gradient of the temperature and the notation ${}^t\boldsymbol{F}$, ${}^tT$ and ${}^t\boldsymbol{g}_0$ denote the history of deformation gradient, temperature, and temperature gradient up to time t, respectively. However, such general functional dependencies are sometimes not practical for constitutive modeling, e.g., in the FEM context. A subset of models which satisfies thermodynamic determinism are those based on the concept of internal variables, in fact, for a so-called simple material, the thermodynamic state is assumed to be completely defined by the instantaneous values of a finite number of state variables, i.e., $\{\boldsymbol{F}, T, \boldsymbol{g}_0, \boldsymbol{\alpha}\}$, where $\boldsymbol{\alpha} \equiv \{\alpha_k\}$ is a set of internal variables, scalar or tensorial, associated with dissipative mechanisms, i.e.,

$$\dot{\boldsymbol{\alpha}} = \boldsymbol{f}(\boldsymbol{F}, T, \boldsymbol{g}_0, \boldsymbol{\alpha}), \tag{A.18}$$

$$s = j(\boldsymbol{F}, T, \boldsymbol{\alpha}), \tag{A.19}$$

$$\boldsymbol{P} = \boldsymbol{h}(\boldsymbol{F}, T, \boldsymbol{\alpha}), \tag{A.20}$$

$$\boldsymbol{q}_0 = \boldsymbol{g}(\boldsymbol{F}, T, \boldsymbol{g}_0, \boldsymbol{\alpha}). \tag{A.21}$$

It is a framework broad enough to describe thermodynamically irreversible processes, i.e., processes involving dissipation, thus allowing the modeling of physical phenomena relevant in terms of engineering practice. A thorough review of the different approaches to the thermodynamics of irreversible processes can be found in [263] and [264].

The constitutive description of the material must be consistent with the principles established by eqs. (A.11-A.14). Assuming that there is a function ψ depending on the deformation gradient $\boldsymbol{F}$, temperature T, and internal variables $\boldsymbol{\alpha}$ describing the Helmholtz free energy, i.e.,

$$\psi(\boldsymbol{F}, T, \boldsymbol{\alpha}) \equiv e(\boldsymbol{F}, T, \boldsymbol{\alpha}) - Ts(\boldsymbol{F}, T, \boldsymbol{\alpha}), \tag{A.22}$$

from the Clausius-Duhem inequality, it follows that the constitutive equations for the stress and entropy must be of the form

$$\boldsymbol{P} = \boldsymbol{h}(\boldsymbol{F}, T, \boldsymbol{\alpha}) = \rho_0 \frac{\partial \psi}{\partial \boldsymbol{F}}, \tag{A.23}$$

$$s = j(\boldsymbol{F}, T, \boldsymbol{\alpha}) = -\frac{\partial \psi}{\partial T}, \tag{A.24}$$

The constitutive function for the heat flux and the evolution equations for the internal variables may be postulated in various forms, however, these still need to comply with the second law of thermodynamics (Eq. (A.14)), which places constraints on the evolution equations for the internal variables and the constitutive equation for the heat flux.

Further constraints on the constitutive equations may be imposed by material symmetries, such as isotropy, transverse isotropy, orthotropy, among others, as well as by the principle of material frame indifference (or objectivity), which requires that the constitutive equations remain invariant under superposed rigid body motions [265].

The development of concrete models that are framed within such a constitutive theory can be achieved by postulating suitable functions for the Helmholtz free energy, or supplying directly the functions for the stress, entropy and heat and other ingredients, such as dissipation potentials and yield surfaces, and the evolution equations for the internal variables.

Appendix A.5. Heat conduction equation

In the context of thermomechanics, the most common form of the energy balance equation (Eq. (A.13)) is the heat conduction equation. Let $C_{\boldsymbol{F}}$ denote the specific heat at constant deformation, i.e., the amount of heat required to change a unit mass of a substance by one degree in temperature at fixed deformation, defined as

$$C_{\boldsymbol{F}} \equiv \left.\frac{\partial e}{\partial T}\right|_{\boldsymbol{F}} = -\frac{\partial^2 \psi}{\partial T^2} T = \frac{\partial s}{\partial T} T. \tag{A.25}$$

Taking Eq. (A.25), introducing the so-called Gough-Joule effect or thermoelastoplastic heating (or cooling) effect, $\mathcal{H}^{\mathrm{ep}}$, as

$$\mathcal{H}^{\mathrm{ep}} = -\rho_0 T \left(\frac{\partial^2 \psi}{\partial \boldsymbol{F} \partial T} : \dot{\boldsymbol{F}} + \frac{\partial^2 \psi}{\partial \boldsymbol{\alpha} \partial T} : \dot{\boldsymbol{\alpha}} \right), \tag{A.26}$$

and the internal dissipation $\mathcal{D}_{\mathrm{int}}$, given by

$$\mathcal{D}_{\mathrm{int}} = \boldsymbol{P} : \dot{\boldsymbol{F}} - \rho_0 (\dot{\psi} + \dot{T} s), \tag{A.27}$$

the energy balance equation can be recast as

$$\rho_0 C_{\boldsymbol{F}} \dot{T} = \rho_0 r - \mathrm{div}_0 \, \boldsymbol{q}_0 + \mathcal{D}_{\mathrm{int}} + \mathcal{H}^{\mathrm{ep}}. \tag{A.28}$$

The first term of Eq. (A.28) can be reinterpreted as

$$\frac{\partial^2 \psi}{\partial \boldsymbol{F} \partial T} = \frac{\partial \boldsymbol{P}}{\partial T} = \frac{\partial^2 \psi}{\partial T \partial \boldsymbol{F}} = \frac{\partial \boldsymbol{h}}{\partial T} = \boldsymbol{\beta}_{\boldsymbol{P}}, \tag{A.29}$$

assuming sufficient smoothness of the free energy function, where $\boldsymbol{\beta}_{\boldsymbol{P}}$ is the nonlinear counterpart of the coefficient of thermal stress, which will shortly be discussed in the context of infinitesimal thermo-viscoelasticity.

Appendix A.6. Fourier's law

Regarding the constitutive model for the heat flux (Eq. (A.21)), the second law of thermodynamics essentially requires the heat flow to occur in the opposite direction of the temperature gradient. The Fourier heat conduction law for isotropic conduction in the deformed volume is one of the simplest and most popular alternatives, defining the heat flux as

$$\boldsymbol{q}_0 = -k_0 \boldsymbol{C}^{-1} \boldsymbol{g}_0, \tag{A.30}$$

where k_0 is the thermal conductivity.

Appendix A.7. Infinitesimal thermo-viscoelasticity

Infinitesimal thermo-viscoelasticity, as presented in [50], fits into the framework of materials with fading memory framework (see Appendix A.4). It is assumed that strains, $\boldsymbol{\varepsilon}$, are small, as well as the temperature difference with respect to some reference temperature, $\Delta T = T - T_0$. This implies a small perturbation away from thermodynamic equilibrium. The constitutive relations found concerning stress and entropy, coinciding with the description of a linear time-invariant (LTI) system, are

$$\boldsymbol{\sigma}(t) = \int_{-\infty}^{t} \mathbf{G}(t-\tau) : \frac{\partial \boldsymbol{\varepsilon}}{\partial \tau} d\tau - \int_{-\infty}^{t} \boldsymbol{\beta}(t-\tau) \frac{\partial \Delta T(\tau)}{\partial \tau} d\tau, \tag{A.31}$$

$$\rho s(t) = \int_{-\infty}^{t} \boldsymbol{\beta}(t-\tau) : \frac{\partial \boldsymbol{\varepsilon}}{\partial \tau} d\tau + \int_{-\infty}^{t} m(t-\tau) \frac{\partial \Delta T(\tau)}{\partial \tau} d\tau, \tag{A.32}$$

assuming a quadratic free energy[50], where $\mathbf{G}$ denotes the time-dependent fourth-order relaxation modulus tensor, $\boldsymbol{\beta}$ is the time-dependent second-order thermal stress coefficient tensor, and m is a time-dependent material property related to the specific heat at constant deformation, i.e., $C_{\boldsymbol{F}} = Tm$. The constitutive equations above are linear in the sense that they satisfy the principle of superposition, i.e., the response to a sum of inputs is the sum of the responses to each individual input (see Fig. A.22). In the context of viscoelasticity, this principle is called the Boltzmann-Volterra superposition principle [12]. This is intrinsically connected to the fact that as a material property, the relaxation modulus is only a function of time and not of strain, strain rate or stress.

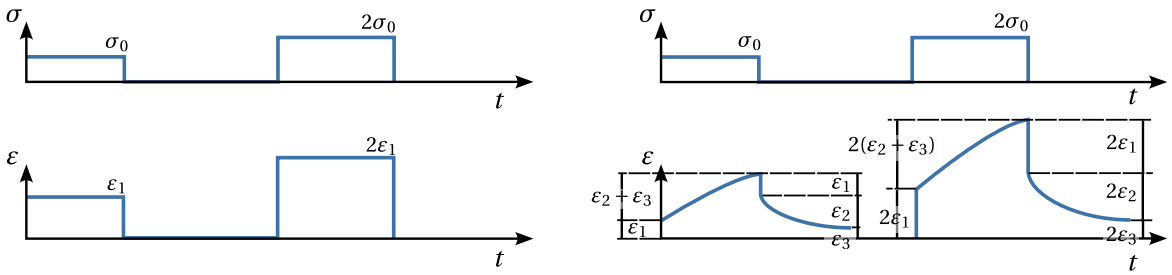

Figure A.22: Stress-driven linear response of a an elastic, and b a viscoelastic material. Adapted from [12].

The strain-stress relationship may also be expressed employing the stress as the inde-

pendent variable, leading to the so-called creep compliance formulation, as

$$\boldsymbol{\varepsilon}(t) = \int_{-\infty}^{t} \mathbf{J}(t-\tau) : \frac{\partial \boldsymbol{\sigma}(\tau)}{\partial \tau}\, d\tau + \int_{-\infty}^{t} \boldsymbol{\alpha}(t-\tau)\frac{\partial \Delta T(\tau)}{\partial \tau} d\tau, \tag{A.33}$$

where $\mathbf{J}$ is the creep compliance of the material and $\boldsymbol{\alpha}$ is the thermal expansion coefficient tensor.

In some cases, these descriptions are equivalent to a system of linear ordinary differential equations governing the evolution of the internal variables[5]. Thus, Eq. (A.31) is the solution of the system of equations

$$\dot{\boldsymbol{\alpha}}(t) = \mathbf{D} : \boldsymbol{\sigma}(t) + \boldsymbol{\varphi}\Delta T(t) + \mathbb{D} : \boldsymbol{\alpha}(t), \tag{A.34}$$

$$\boldsymbol{\sigma}(t) = \mathbf{G} : \boldsymbol{\varepsilon}(t) + \boldsymbol{\beta}\Delta T(t) + \mathbb{G} : \boldsymbol{\alpha}(t), \tag{A.35}$$

$$s(t) = \boldsymbol{\beta} : \boldsymbol{\varepsilon}(t) + m\Delta T(t) + \mathbb{B} : \boldsymbol{\alpha}(t), \tag{A.36}$$

where the matrices in the equations above are related to those in Eqs. (A.18) to (A.20) through

$$\mathbf{D} = \frac{\partial \boldsymbol{f}}{\partial \boldsymbol{F}}(\boldsymbol{I}, T, \boldsymbol{\alpha}_0), \quad \boldsymbol{\varphi} = \frac{\partial \boldsymbol{f}}{\partial T}(\boldsymbol{I}, T, \boldsymbol{\alpha}_0), \quad \mathbb{D} = \frac{\partial \boldsymbol{f}}{\partial \boldsymbol{\alpha}}(\boldsymbol{I}, T, \boldsymbol{\alpha}_0), \tag{A.37}$$

$$\mathbf{C} = \frac{\partial \boldsymbol{h}}{\partial \boldsymbol{F}}(\boldsymbol{I}, T, \boldsymbol{\alpha}_0), \quad \boldsymbol{\beta} = \frac{\partial \boldsymbol{h}}{\partial T}(\boldsymbol{I}, T, \boldsymbol{\alpha}_0), \quad \mathbb{G} = \frac{\partial \boldsymbol{h}}{\partial \boldsymbol{\alpha}}(\boldsymbol{I}, T, \boldsymbol{\alpha}_0), \tag{A.38}$$

$$\boldsymbol{\beta} = \frac{\partial j}{\partial \boldsymbol{F}}(\boldsymbol{I}, T, \boldsymbol{\alpha}_0), \quad m = \frac{\partial j}{\partial T}(\boldsymbol{I}, T, \boldsymbol{\alpha}_0), \quad \mathbb{B} = \frac{\partial j}{\partial \boldsymbol{\alpha}}(\boldsymbol{I}, T, \boldsymbol{\alpha}_0), \tag{A.39}$$

Often, these can be identified with the behavior of linear rheological models, which provide a visual counterpart and help in the interpretation of the model. These are one-dimensional mechanical models containing diverse arrangements of linear springs and dashpots. For an in-depth discussion on the connection between LTIs and ordinary differential equations, see [266].

There are other equivalent representations of the time-dependent material properties. In particular, when the loading is periodic, it is common to express the constitutive equations in the frequency domain, leading to the complex modulus representation [12]. The storage modulus, $\mathbf{G}'$, and the loss modulus, $\mathbf{G}''$, represent the elastic and viscous behavior of the

[5]The convolution and and the internal variables formulation are equivalent when the relaxation modulus is chosen as a Prony series, i.e., as a sum of exponential functions. See Eq. (A.42).

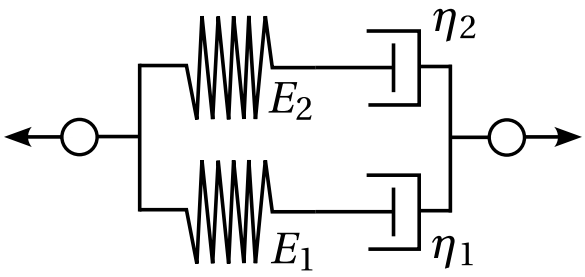

Figure A.23: Rheological model for the Burgers material (Maxwell representation).

material, respectively. They are defined as the real and imaginary parts of the complex modulus, $\mathbf{G}^*$, given by

$$\mathbf{G}^*(\omega) = \mathbf{G}'(\omega) + i\mathbf{G}''(\omega), \tag{A.40}$$

where ω is the angular frequency of the loading. The loss factor, δ, is as the phase-shift strain loading and stress response.

To better show what is the typical behavior of a viscoelastic material, we consider a so-called one-dimensional Burgers material, the relaxation modulus, G, is given by [175]

$$G(t) = G_1 e^{-t/\theta_1} + G_2 e^{-t/\theta_2}, \tag{A.41}$$

where $\theta_i = \eta_i/G_i$ is the ith relaxation time. See Fig. A.23 for the corresponding rheological model, that consists of two Maxwell elements (spring and dashpot in series) in parallel. If a spring in parallel is added to the Burgers model, and more Maxwell branches are considered, the so-called generalized Maxwell model is obtained. A representation of its relaxation modulus is given by the so-called Prony series [50, 12], expressed as

$$G(t) = G_\infty + \sum_{i=1}^{n_\mathrm{V}} G_i e^{-t/\theta_i}, \tag{A.42}$$

where G_∞ is the long-term modulus, G_i are the moduli of each Maxwell element, θ_i are the corresponding relaxation times, and n_V is the number of Maxwell elements in the model.

Also, for a Burgers material, an equivalent description can be established as

$$\dot{\varepsilon}_1^p(t) = \frac{1}{\theta_1}(\varepsilon(t) - \varepsilon_1^p(t)), \tag{A.43}$$

$$\dot{\varepsilon}_2^p(t) = \frac{1}{\theta_2}(\varepsilon(t) - \varepsilon_2^p(t)), \tag{A.44}$$

$$\sigma(t) = G_1(\varepsilon(t) - \varepsilon_1^p(t)) + G_2(\varepsilon(t) - \varepsilon_2^p(t)), \tag{A.45}$$

where ε_i^p is the strain in the i-th dashpot, $i = 1, 2$, the internal variables of the constitutive model. In a set of constant strain rate experiments at different strain rates, their evolution can be tied to transient effects, such as the ones observed at the beginning of the monotonic loading at a constant strain rate in the case of a Burger material (see Fig. A.24a). At some point (see Fig. A.25a), a steady state will be reached, ($\dot{\boldsymbol{\alpha}} = \text{constant}$), and the corresponding response of the Burgers material model is constant. Furthermore, for a given strain, the steady-state stress varies linearly with the strain rate and is proportional to the relaxation time, corresponding to so-called Newtonian viscosity [267] (see Fig. A.25a). An infinitesimal viscoelastic material will not show strain-rate dependence in the steady-state stress-strain curve, or be able to capture different transient effects at different strain rates, as shown in Fig. A.25b.

Figs. A.24b and A.24c illustrate the response of the Burgers material to a constant strain and constant stress, respectively, followed by release illustrating the ability of the model to capture the phenomena of strain recovery, creep, and recovery. The expected linear behavior in a stress relaxation experiment is to obtain the same stress response up to a multiplicative constant, which is the initial strain. Likewise, in a creep experiment, the strain response divided by the stress is equal for experiments at different stress levels. Both of these facts are not always observed in practice.

Note that, the response of this very simple model is already quite rich, indicating that the choice in the arrangement of springs and dashpots in the rheological model is crucial to capture the relevant physics of the material under study, even before considering nonlinear effects (compare the two hypothetical responses shown in Fig. A.25). As such, a grouping of nonlinear models based on different arrangments of springs and dashpots is pursued in Section 7. Also note that in addition to being independent of the deformation, the thermo-mechanical properties in infinitesimal viscoelasticity are also independent of temperature. This is not the case in practice, where the relaxation modulus and creep compliance are highly dependent on temperature, as discussed in Section 4.1.

The sections that follow aim to show that experimentally these linear assumptions are frequently violated. These results can now be discussed in light of the expected linear behavior, highlighting the necessary nonlinear additions for a more accurate constitutive model.

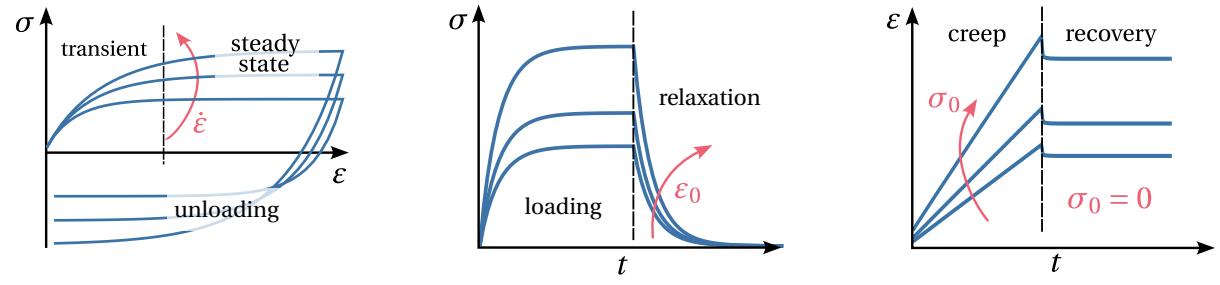

(a) (b) (c)

Figure A.24: Schematic response of the Burgers material in a a constant strain rate experiment followed by unloading at the same strain rate, b a stress relaxation experiment and a c creep experiment with recovery.

The advances in that direction suggested in the literature will be reviewed in Section 7.

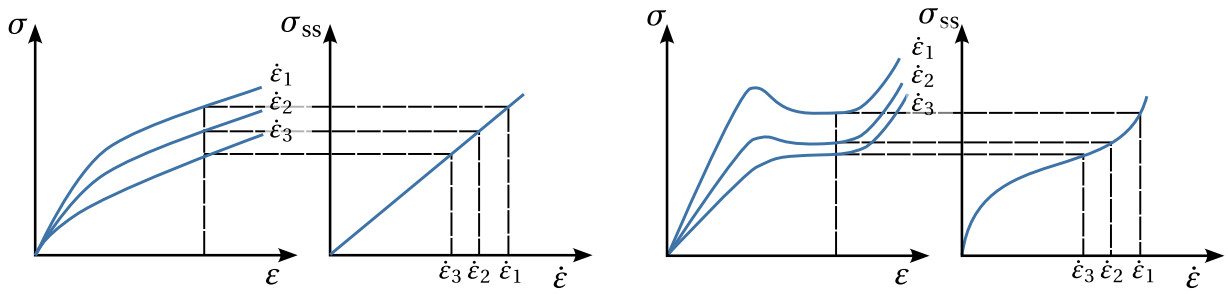

(a) (b)

Figure A.25: Stress-strain curve and steady-state stress-strain rate curve for a an infinitesimal viscoelastic material (linear) and a b a nonlinear material.